

71

Functional Magnetic Resonance Imaging of the Frequency Organization of Human Auditory Cortex

by

Thomas Michael Talavage

B.S.C.E.E, Purdue University (1992)

M.S.E.E., Purdue University (1993)

Submitted to the Harvard-MIT Division of Health Sciences and Technology
in partial fulfillment of the requirements for the degree of

Doctor of Philosophy

at the

MASSACHUSETTS INSTITUTE OF TECHNOLOGY

June 1998

MIT LIBRARIES
JUL 16 1998
SCHERING

© Massachusetts Institute of Technology 1998. All rights reserved.

(Handwritten scribbles)

Author.....
Harvard-MIT Division of Health Sciences and Technology
1998

Certified by.....
Bruce R. Rosen, M.D., Ph.D.
Visiting Associate Professor of Nuclear Engineering, MIT
Thesis Supervisor

Certified by.....
Jennifer R. Melcher, Ph.D.
Assistant Professor of Otology and Laryngology, HMS
Supervisor

Certified by.....
M. Christian Brown, Ph.D.
Associate Professor of Otology and Laryngology, HMS
Thesis Committee Chairman

Certified by.....
Albert M. Galaburda, M.D.
Emily Fisher Landau Professor of Neurology and Neuroscience, HMS
Thesis Committee Member

Accepted by.....
Martha L. Gray, Ph.D.
J.W. Kieckhefer Associate Professor of Electrical Engineering
Co-director, Division of Health Sciences and Technology

MASSACHUSETTS INSTITUTE
OF TECHNOLOGY
JUL 07 1998
LIBRARIES

SCHERING-PLOUGH

Functional Magnetic Resonance Imaging of the Frequency Organization of Human Auditory Cortex

by

Thomas Michael Talavage

Submitted to the Harvard-MIT Division of Health Sciences and Technology
on June 1, 1998, in partial fulfillment of the
requirements for the degree of
Doctor of Philosophy

Abstract

The topographical organization of frequency sensitivity in the human auditory cortex was examined through functional magnetic resonance imaging, and used to propose tonotopic organizations within five anatomically defined auditory areas. Two studies were conducted using non-linguistic acoustic stimuli (tones, noise, instrumental music) revealing (1) the location of higher- (above 2490 Hz) and lower-frequency (below 660 Hz) sensitive regions within auditory cortex, and (2) the location of progressions of frequency sensitivity from higher- to lower-frequencies. The first study identified eight frequency sensitive regions in the superior temporal plane, on and near Heschl's gyrus, the site of primary auditory cortex. Four of the eight regions were particularly sensitive to lower-frequencies, and four to higher-frequencies. A correspondence between these eight frequency sensitive regions and the known anatomically defined auditory areas was established based upon the average Talairach co-ordinates of the regions. A tonotopic organization was then proposed for those anatomically defined auditory areas containing both a higher- and a lower-frequency sensitive region. The second study revealed the presence of seven continuous, monotonic variations (progressions) in frequency sensitivity across the surface of the auditory cortex by examining the temporal responses to downward or upward frequency-swept stimuli. Higher- and lower-frequency ends of the progressions were found to contain seven of the eight previously established frequency sensitive regions, confirming the localization established in the first study. Smooth progressions of frequency sensitivity were observed to connect many of the higher- and lower-frequency sensitive regions to each other. The tonotopic organization proposed in the first study was tested and revised based upon the observation of progressions between pairs of higher- and lower-frequency sensitive regions that correspond to the same anatomical auditory area. It is concluded that the following anatomical areas are tonotopically organized: the medial and lateral divisions of primary auditory cortex (KAm and KAlt), the medial auditory area (ProA), anterior and posterior divisions of the lateral auditory area (PaAi), and two divisions of the superior temporal auditory area (PaAe).

Thesis Supervisor: Bruce R. Rosen, M.D., Ph.D.

Title: Visiting Associate Professor of Nuclear Engineering, MIT

Thesis Supervisor: Jennifer R. Melcher, Ph.D.

Title: Assistant Professor of Otology and Laryngology, HMS

Acknowledgments

I would like to take this opportunity to offer my most sincere gratitude to the entire staff and graduate student population of the MGH NMR Center. To a large extent this unmatched group of personalities and experience has served as a community mentor to me, with every individual teaching me lessons regarding science and the pursuit of knowledge that were invaluable in my research. From Dr. Bruce Rosen and Dr. Thomas Brady, the co-directors who encouraged me every step of the way, to Dr. Kenneth Kwong, Dr. Robert Weisskoff, Dr. Hans Breiter and Dr. Anders Dale, who always managed to provide that nugget of information I could find nowhere else, to Terrance Campbell, who always found an open slot for me, to fellow graduate students and collaborators including Patrick Ledden and Whitney Edmister, the support and collegiality were constant. To the many others at the lab who took part in my life over the past five years with friendship, enthusiasm for my work, and ever-present encouragement, I offer great thanks and acknowledge a debt that I can never repay.

Similarly, I must offer great thanks to the members of my thesis committee. All of the individuals on the committee invested a tremendous amount of their time in my work over the past three years. Their efforts and their willingness to share their unparalleled expertise are sincerely appreciated.

A special debt of gratitude is owed Dr. Randall Benson, my first mentor at the lab. Randy's willingness to teach me functional MRI and to investigate questions that were outside his own realm of interest was a gift that was second only to his instruction in the art of pitching. One of these days I'm going to manage to throw a curveball—and I'll have Randy to thank for it.

No research of this type can be conducted without volunteers who are willing to give up that Friday or Saturday night to help out a friend's research. I deeply thank those who gave so freely of their time, weekend after weekend.

Finally, I must offer my most heartfelt thanks to my family. The support of my parents and, most importantly of all, my wife, has been a rock to which I could anchor my spirit whenever the going looked dim. I can never fully thank my wife, Jennifer Talavage, for her encouragement over the past five years. Without her constant presence at my side, the MIT and Boston experiences would long ago have overwhelmed me.

Dedication

I dedicate this thesis to my loving wife

Jennifer Talavage

for her support, wisdom, and never-ending patience,

all of which are vital to every day of my life.

Contents

1	Overview	11
2	Regions of Frequency Sensitivity	14
2.1	Introduction	14
2.1.1	Human Auditory Cortex	15
2.1.2	Investigation of Frequency Sensitivity	16
2.2	Materials and Methods	18
2.2.1	Subjects	18
2.2.2	Acoustic Stimulation	18
2.2.3	Imaging	20
2.2.4	Imaging Coils	21
2.2.5	Data Analysis	22
2.3	Experimental Results	25
2.4	Discussion	35
2.4.1	Human Anatomical Studies	39
2.4.2	Correspondence Between Classified Regions and Anatomical Areas	40
2.4.3	Proposed Frequency Organization of Cytoarchitectural Areas	47
2.4.4	Comparison to Human Functional Studies	48
2.4.5	Comparison to Animal Studies	50
2.4.6	Implications of Tonotopy	51
3	Progressions of Frequency Sensitivity	55
3.1	Introduction	55
3.2	Materials and Methods	56
3.2.1	Subjects	56

3.2.2	Acoustic Stimulation	56
3.2.3	Imaging	57
3.2.4	Data Processing	58
3.3	Experimental Results	63
3.3.1	Identification of Frequency Sensitivity in Response to Swept Stimuli	63
3.3.2	Intra-Subject Comparison of Frequency Sensitive Regions	66
3.3.3	Inter-Subject Comparison of Frequency Sensitive Regions	74
3.3.4	Observed Frequency Sensitive Progressions	81
3.4	Discussion	82
3.4.1	Tonotopic Organizations in Human Auditory Cortex	85
3.4.2	Comparison to Non-human Primate Auditory Cortex	87
3.4.3	Extensions and Applications	91

A Improved Auditory Cortex Imaging Using Clustered Volume Acquisitions **93**

A.1	Abstract	93
A.2	Introduction	94
A.3	Methods	96
A.3.1	Imaging Sequence	96
A.3.2	Imaging Parameters	99
A.3.3	Experiments	100
A.3.4	Data Analysis	100
A.4	Results	101
A.4.1	Spatial Extent of Responses	101
A.4.2	Strength of Responses	102
A.5	Discussion	105
A.5.1	Analysis of Functional Effect	108
A.5.2	Benefits of Clustered Volume Acquisition	109
A.5.3	Extension of Paradigms	110
A.5.4	Conclusions	110
A.6	Acknowledgments	111

B Quantitative Assessment of Auditory Cortex Responses Induced by Im-	
ager Acoustic Noise	112
B.1 Abstract	112
B.2 Introduction	113
B.3 Methods	115
B.3.1 Imaging Sequence	115
B.3.2 Steady-State Imaging Conditions in Sledgehammer	120
B.3.3 Imaging Parameters	121
B.3.4 Experiments	122
B.3.5 Data Analysis	122
B.4 Results	124
B.4.1 Noise-Induced Response Localization	124
B.4.2 Noise-Induced Response Strength	124
B.5 Discussion	129
B.5.1 Response Characteristics	129
B.5.2 Implications for Auditory fMRI	130
B.5.3 Implications for Clustered Volume Acquisitions	131
B.6 Conclusions	131
B.7 Acknowledgments	132

List of Figures

2-1	Three frequency sensitive regions in the immediate vicinity of Heschl’s gyrus (session 1).	27
2-2	Summaries of three classified frequency sensitive regions (Regions 1–3) in the immediate vicinity of Heschl’s gyrus (left hemisphere), as imaged in the coronal plane, for all eight sessions.	29
2-3	Summaries of lower- and higher-frequency sensitive activation foci in the Talairach axial plane for Sessions 2, 5 and 8.	31
2-4	Comparison of location of the activation foci of frequency sensitive regions to the centers of cytoarchitecturally defined auditory areas of Rivier and Clarke [82].	42
3-1	Generation of a flat patch of left auditory cortex (Subject 1) [18].	60
3-2	Spatial progression of iso-angle contour “wavefronts” on flattened patch of the left superior temporal plane for Subject 1.	64
3-3	Spatial progression of iso-angle contour “wavefronts” and pseudo-color map of phase angle overlaid on left superior temporal plane patch for Subject 1.	67
3-4	Comparison of frequency sensitivity in the left superior temporal plane as assessed by presentation of two sustained, non-swept stimuli with different center-frequencies and average time of response to swept stimuli.	69
3-5	Comparison of frequency sensitivity at the locations of the eight classified frequency sensitive regions (Regions 1–8) from Chapter 2.	72
3-6	Flattened cortical patches of the left superior temporal plane for Subjects 1–6 overlaid with pseudo-color maps of relative frequency sensitivity.	76
3-7	Flattened cortical patches of the left superior temporal plane for Subjects 1–6.	78

3-8	Summary of wavefront progressions (A–G) in Subject 1 that were observed in the left superior temporal plane in at least three of six subjects.	83
A-1	Comparison of temporal acquisition of eight slices with TR = 4 s for (a) distributed volume acquisition (DVA) sequence and (b) clustered volume acquisition (CVA) sequence.	97
A-2	Comparison of the spatial extent and statistical significance of auditory cortex activation, in response to instrumental music, as a function of imaging sequence and TR.	103
A-3	Graphs of (a) mean percent signal change and (b) mean statistical power per unit imaging time.	106
B-1	A clustered volume acquisition (CVA) sequence shown for TR = 4 s and using a reverse-centric acquisition order.	116
B-2	Example of the Sledgehammer sequence (TR = 7 s).	118
B-3	Sledgehammer results for seven subjects using odd epoch stimulation of 2 s (16 slice volume) and even epoch stimulation of 4 s (16 slice volume with 16 extra beeps).	125
B-4	Graph of Intra-Acquisition Response percent signal changes observed for 12 and 16 slice volumes as a function of the net duration of the beep train (slices plus extra beeps) in the activation condition of the Sledgehammer sequence.	127

List of Tables

2.1	Average Talairach co-ordinates and positional classification criteria for the eight classified frequency sensitive regions.	33
2.2	Spatial extent (in number of voxels) of frequency sensitive regions.	34
2.3	Average percent signal change over the spatial extent of each of the eight categories of frequency sensitive regions.	34
3.1	Rate of occurrence of progressions of frequency sensitivity	81
A.1	Spatial extent (number of voxels) of activation ($p < 0.01$) in auditory cortex	102
B.1	Duration of imager noise stimulus (beep train) generated by the Sledgehammer sequence	123
B.2	Average percent signal changes for Sledgehammer Sequence	129

Chapter 1

Overview

The organization of frequency sensitivity in the human auditory cortex is largely unknown. The anatomical organization of the human auditory cortex has been the subject of many studies (e.g. [29, 76, 82]), but direct, functional measurements of auditory cortex have been from intra-operative recordings in which elucidating the underlying physiological organization of the cortex has not been the primary goal (e.g. [11, 12]). As a consequence, much of what is believed regarding human auditory cortex is an extrapolation of electrophysiological results from experimental mammals (e.g. [41, 52, 53, 57, 75]). The organization of human auditory cortex may be different from that of experimental mammals, however, due to functional specializations such as language. Therefore, the extrapolation of animal data to the human may not be appropriate.

Recent advances in functional magnetic resonance imaging (fMRI) have offered non-invasive, *in vivo* methods for the investigation of cortical activity (e.g. [8, 89, 95, 96]). Our objective has been to implement these methods in functional studies of the human auditory cortex. In particular we have desired to understand how the spatial distribution of responses in the auditory cortex varies as a function of stimulus frequency. To this end, two primary studies and two supplementary investigations were conducted using functional magnetic resonance imaging to examine the response properties of human auditory cortex.

The first study, described in Chapter 2, investigated frequency sensitivity using two spectrally disparate stimuli, one containing “lower-frequencies” (below 660 Hz) and the other containing “higher-frequencies” (above 2490 Hz). The responses to each stimulus were compared and regions were assigned a “lower-” or “higher-frequency sensitive” label

dependent upon the presentation periods during which they exhibited significantly greater signal levels. Eight frequency sensitive regions were identified within the superior temporal plane that correspond to portions of cytoarchitecturally defined auditory areas, suggesting the existence of a tonotopic organization in many portions of the auditory cortex.

The second study (Chapter 3) used frequency-swept stimuli to extend the results of Chapter 2 by examining the expanse of the superior temporal plane for spatial variations in frequency sensitivity that were consistent with an underlying tonotopic organization. Seven of the previously identified frequency sensitive regions were consistently observed to be located at or near the ends of progressions of frequency sensitivity. For many of the regions located in the middle of the superior temporal plane, near Heschl's gyrus, the gradient of frequency sensitivity was observed to reverse at the ends of the progressions, with multiple progressions either "originating" from a single higher-frequency region or "terminating" at a single lower-frequency region. This "mirror" organization is a characteristic property of the tonotopic organization in the primate auditory cortex [43,57]. Our data, coupled with previous anatomical work, indicate that multiple anatomically defined areas within human auditory cortex are tonotopically organized and are bounded by many of the eight frequency sensitive response regions identified in the first study.

Two supplementary studies were conducted to examine the effect on auditory cortex of the noise inherent in echo-planar fMRI [16,79] by examining whether or not a noise-induced cortical response affects the desired stimulus-induced response. In Appendix A [23], two acoustically different echo-planar pulse sequences were used to functionally image cortical responses to instrumental music. Statistically significant differences were observed between measures of response strength resulting from acquisitions using the two pulse sequences, suggesting that the acoustic environment of fMRI induces responses in auditory cortex that reduce the magnitude of stimulus-induced signal changes by 20–30%. In Appendix B [94] the noise-induced response was measured using a novel pulse sequence that presented alternating durations of trains of imager noise. Statistically significant responses to the noise were localized to portions of Heschl's gyrus that had previously been observed to be higher-frequency sensitive regions (Chapter 2). The magnitude of the noise-induced response was observed to be equivalent to the magnitude of the response induced by instrumental music. If the fMRI response in auditory cortex can become saturated, the robust, localized responses to the imager noise may obscure specific portions of stimulus-induced

signal changes by reducing the available dynamic range. It was concluded that while the acoustic environment in which fMRI is conducted may reduce the strength of stimulus-induced responses in portions of auditory cortex, it will not lead to improper assignment of activation to cortical regions that are not involved in the stimulus-induced response.

Because the localization of frequency sensitive regions appears not to be affected by the noise levels inherent in functional MRI, the results of the first two studies indicate that as many as five anatomically defined areas in human auditory cortex each contain at least one tonotopic map.

Chapter 2

Regions of Frequency Sensitivity

2.1 Introduction

Tonotopy, an ordered mapping of neuronal frequency sensitivity to spatial location, has been demonstrated in experimental animals to be present in structures throughout the auditory pathway, including the cerebral cortex. The present study investigates the presence and organization of neuronal frequency sensitivity in the human auditory cortex as a first step in investigating whether human auditory cortex is tonotopically organized.

Neuronal frequency sensitivity can be characterized by measuring the response thresholds of neurons as a function of acoustic stimulus frequency. In the auditory nerve, neurons exhibit their greatest sensitivity (i.e. lowest response threshold) at a particular “characteristic frequency” (CF). Mid- and high-CF neurons in the auditory nerve are sharply tuned, exhibiting thresholds that rise sharply as frequency increasingly differs from the CF, while low-CF (e.g. below 500 Hz) neurons are more broadly tuned. Frequency tuning is preserved throughout much of the auditory pathway, but can be more complex in the cortex than in the periphery. For example, some neurons in the cortex exhibit multiple “characteristic frequencies” to which they are highly sensitive [92]. Even though the frequency tuning can be complex, a CF may be determined for most cortical neurons or limited volumes of cortex by depth electrode recordings during presentation of a wide range of acoustic stimulus frequencies and intensity levels (e.g. [41, 52, 54, 72, 75]). Such measurements of CF are observed to be relatively constant across layers of cortex [41, 54].

In some portions of auditory cortex, CF varies as a function of position across the cortical surface. When the positional CF variation is monotonic across a region of cortex,

that region is said to possess a “tonotopic map.” Electrophysiological studies of the variation of CF across the surface of the cortex in experimental mammals [41, 43, 52, 54, 57, 58, 75] have revealed multiple tonotopic maps. Many of these tonotopic maps share low- or high-frequency boundaries with adjacent tonotopic maps such that they “mirror” one another [43, 57, 75].

Each of the multiple tonotopic maps observed in the auditory cortex of experimental mammals may be related to an auditory field [41, 75]. The auditory fields (and corresponding tonotopic maps) may be differentiated based upon anatomical properties such as cell populations, projections to and from the field, or by physiological properties such as threshold, response latency, and the breadth of tuning (e.g. [26, 41, 57, 75]). For example, primary auditory cortex (AI) is differentiated from other auditory fields by having the shortest response latencies, receiving direct projections from the auditory midbrain, and by an enlarged layer IV (typical of primary sensory cortex). When tonotopic maps mirror one another, they often do so across the boundary between anatomically defined auditory areas. In these cases, each of the individual maps is found to be wholly contained within a single cytoarchitecturally defined auditory field.

2.1.1 Human Auditory Cortex

Intra-operative recordings from the surface of the human cortex during acoustic stimulation have demonstrated that auditory cortex is located on the superior surface of the temporal lobe [68]. When patients undergoing surgery were stimulated using clicks [47] or tone pips [11, 12], stimulus-induced responses were observed in the superior temporal plane in the vicinity of the transverse temporal gyrus (Heschl’s gyrus), on the superior temporal gyrus, and as far superiorly as the upper bank of the Sylvian fissure. The responses on the medial portion of Heschl’s gyrus were the greatest in amplitude and the shortest in latency, suggesting that this is the location of primary auditory cortex [12]. The localization of auditory cortex in the superior temporal plane is supported by cytoarchitectural studies of human brains [29, 76, 82] and comparison to the organization of the macaque auditory cortex [29, 30]. The studies of human brains, examining cell and axon populations, have revealed multiple anatomically differentiable areas. Among these areas is a region of koniocortex (characterized by an enlarged layer of granule cells in layer IV) that is located on the medial two-thirds of Heschl’s gyrus. Koniocortex, typically indicating primary sensory

cortex, marks this region as the probable location of primary auditory cortex [29, 76, 82]. This localization is in agreement with that observed in intra-operative evoked potential studies. The cytoarchitectural studies have supported and extended the results of the intra-operative studies by demonstrating that auditory cortex may extend inferiorly to the superior bank of the superior temporal sulcus and superiorly to the upper bank of the Sylvian fissure [29].

Functional studies of human auditory cortex have, however, revealed an incomplete picture of the mapping of neuronal frequency sensitivity to place. Studies examining the response of human auditory cortex to bandlimited stimuli have been conducted using surface recorded evoked potentials, evoked magnetic fields, positron emission tomography (PET) and functional magnetic resonance imaging (fMRI). Both evoked potential (e.g. [5, 97]) and magnetic field (e.g. [10, 65–67, 84]) studies have examined the relationship between the location of response generators (i.e. an equivalent dipole) and stimulus frequency. Some studies have demonstrated monotonic relationships between frequency and dipole location on Heschl’s gyrus and in surrounding regions, a result that would be expected if different frequencies excited different regions within a tonotopic map. While differences are observed in the location (depth from the scalp) of the response generator between any two stimulus frequencies, the absolute location of the source remains imprecise due to the uncertainties of the inverse solution [18]. A region responsive to “low” (500 Hz) and a region responsive to “high” (4000 Hz) frequency stimulation have been identified by PET [45], but most of auditory cortex did not exhibit a differential response in this study. A similar study conducted with fMRI [98] compared responses to two relatively low frequencies (55 Hz and 880 Hz), also revealing only one focus of activation (on Heschl’s gyrus) for each stimulus.

2.1.2 Investigation of Frequency Sensitivity

Functional magnetic resonance imaging (fMRI) provides a complement to previous techniques used to study the human auditory cortex by allowing direct anatomical localization of multiple response regions in the auditory cortex of individual subjects. By obtaining both functional and anatomical data in the same imaging session with a known registration, fMRI responses may be directly mapped to their anatomical locations. fMRI further offers the capability of making repeated measurements in individual subjects, permitting intra-subject averaging to improve signal-to-noise ratios and, thereby, improve response

detectability. The ability to average within a single subject precludes the need for inter-subject averaging that may obscure the frequency-specific organization of responses due to inter-individual variability.

In the present study we used fMRI to investigate the frequency organization of auditory cortex in humans. Specifically, we measured activation in the superior temporal plane in response to moderate intensity bandlimited acoustic stimuli, examining whether regions existed that were more responsive to lower- than higher-frequency stimulation (“lower-frequency sensitive regions”), and vice versa (“higher-frequency sensitive regions”). The locations of any observed frequency sensitive regions could be related to the underlying cortical anatomy for each subject and to a standardized co-ordinate system [93]. The anatomical locations of these frequency sensitive regions could then be compared across subjects to identify consistent patterns in the sensitivity maps, in order to eventually propose a frequency organization for human auditory cortex.

Two aspects of our methodology, the development of a special imaging coil and the selection of stimulus parameters, were key to the success of the present study. The surface coil was designed specifically for imaging the superior temporal plane, greatly improving our ability to detect activation over that achieved with standard surface and head coils. Stimulus bandwidth and presentation levels were selected based both upon the animal and human literature and experimental constraints. Increasing the bandwidth or the intensity might have made it more likely that we would observe a response, but excessive increases in either property might have compromised our ability to resolve distinct response regions for each of our two stimuli. The literature provided guidelines for selecting narrow-bandwidth stimuli [77] separated by two or more octaves. The use of a two octave separation, corresponding to approximately 6 mm in magnetoencephalography (MEG) studies of auditory cortex [84], assumed that the MEG localization of frequency sensitivity in human auditory cortex was accurate and that the distance between evoked magnetic field generators would be similar to the distance between fMRI response peaks.

We have identified eight frequency sensitive regions that are consistently localized in the superior temporal plane on or near Heschl’s gyrus. This suggests the presence of multiple tonotopic maps in the human auditory cortex.

2.2 Materials and Methods

2.2.1 Subjects

Six adult subjects (4 male, 2 female), ages 22–35, were imaged in 8 sessions. All subjects had normal hearing in the range from 100 Hz to 8000 Hz. Informed consent was obtained from all subjects prior to each imaging session. Experimental protocols were approved by human studies committees at the Massachusetts Institute of Technology, Massachusetts Eye and Ear Infirmary and the Massachusetts General Hospital.

2.2.2 Acoustic Stimulation

In each session, subjects were stimulated binaurally with two narrow-bandwidth, non-swept (i.e. fixed center-frequency) stimuli, one “lower-frequency” stimulus and one “higher-frequency” stimulus. The spectra of lower-frequency stimuli were restricted to frequencies below 660 Hz, while the spectra of higher-frequency stimuli were restricted to frequencies above 2490 Hz. These frequency bounds were selected for two reasons, (1) so the spectral content of the stimuli would not overlap the 1 kHz, 118 dB SPL fundamental of the noise generated by the imager [79] (see Appendix A [23] and Appendix B [94]), and (2) so the predicted separation between cortical regions activated by lower- vs. higher-frequency stimuli would be readily detectable. A separation of at least two octaves between the lower- and higher-frequency bands was selected based on data from magnetoencephalography (MEG) studies of humans indicating that, in certain cortical regions, the representation of two octaves covers 6 mm [84, 85], a distance that exceeds the 3 mm resolution of our functional images.

Four types of stimuli were used, with only a single stimulus type presented in any given imaging session: (1) amplitude-modulated (AM) tones with a modulation rate of 10 Hz and a modulation index of 0.7 (sessions 6–8), (2) tone bursts, 25 ms in duration with 5 ms rise and fall times, presented at a rate of 10 per s (session 2), (3) amplitude-modulated, bandpass-filtered white noise with a modulation rate of 10 Hz and a modulation index of 0.7 (sessions 3–5), and (4) bandpass filtered instrumental music (session 1). The filter bandwidth for the noise was one octave or less, except for the lower-frequency stimulus in sessions 4 and 5 (20–200 Hz). The bandwidth of the lower-frequency music stimulus was 20–100 Hz, and that of the higher-frequency music stimulus was 7–8 kHz. The stimulus

that would produce the best activation was not known *a priori*, and the multiple stimuli used were a consequence of our attempts to obtain stronger responses.

Stimuli were played from a digital source and presented via a pneumatic delivery system. Tone and noise stimuli were digitally generated in LabVIEW on a Macintosh Quadra computer outfitted with a D/A board (National Instruments A2100). Bandpass-filtered music was generated by passing the output of a CD player through a brickwall (115 dB per octave) bandpass filter (Rockland Model 751A). The output of the filter or D/A board was fed into an amplifier located in the control room, the output of which was connected to acoustic transducers located next to the imager. The output of the transducers passed through flexible plastic tubing (3 m length) to and through earmuffs. The sound emerged from the flexible tubing approximately at the surface of the external ear. The earmuffs were worn by the subject to reduce the amount of imager acoustic noise at the subject's ears.

Stimuli were presented in a "block paradigm" consisting of separate epochs of lower- and higher-frequency stimulation and epochs of no stimulation (Figure 2-1, parts d and e). One stimulus presentation cycle consisted of 16–40 s of lower-frequency stimulation, a period of 8–20 s of no stimulation, 16–40 s of higher-frequency stimulation, and a final period (8–20 s) of no stimulation. Between three and eight stimulus cycles were presented in each functional imaging "run" of this paradigm. Between two and seven runs were conducted in each imaging session.

In all sessions, stimulus presentation levels were set relative to behavioral hearing thresholds. For sessions 2–8 thresholds were measured under the same acoustic conditions as those present during the functional imaging run. For session 1 thresholds were obtained in quiet. In sessions 2–8 (AM tones, tone bursts, and bandpass-filtered noise) lower-frequency stimuli were presented 35 dB above threshold; higher-frequency stimuli were 35 dB above threshold (sessions 3, 5–8) or matched in loudness to the lower-frequency stimuli (sessions 2, 4, parts of session 5). In session 1 (bandpass-filtered music) the lower-frequency stimulus was presented at 50 dB above threshold while the higher-frequency stimulus was made comparable in loudness (42 dB above threshold).

Subjects were instructed to attend to the auditory stimulus throughout each run and to keep their eyes closed or to maintain fixation on an arbitrarily chosen point in their direct line of sight. Subject motion was limited through the use of a dental bite bar made immediately prior to each imaging session. In sessions 2–8, attention to the stimulus was

maintained by an intensity change detection task. Stimulus intensity was randomly adjusted by ± 4 dB for 2 s, with an intensity change presented every 5–8 s. Subject responses were monitored by the experimenter. All subjects consistently responded to the intensity changes and no runs were discarded on the basis of attention.

2.2.3 Imaging

Each imaging session consisted of five segments of data collection. All data were obtained using a 1.5 T Signa (General Electric, Milwaukee, WI) imager, retrofitted for echo-planar imaging (EPI) by Advanced NMR Systems, Inc. (Wilmington, MA). Each imaging session began with the acquisition of contiguous sagittal images covering the entire width of the brain. These images were used to select the “slices of interest” to be used in subsequent imaging segments. The second segment of each imaging session was shimming of the magnetic fields in the region of interest (superior temporal plane) to improve field-homogeneity [80]. Next, flow-weighted images of the slices of interest were acquired for subsequent use in the registration of the functional slices to the sagittal data set prior to reslicing in Talairach co-ordinates [93]. High-resolution (in-plane resolution = 1.5 mm \times 1.5 mm) T_1 -weighted anatomical images were then acquired of the same slices. Finally, multiple runs of T_2^* -weighted functional images (128–256 images per slice) of these slices were acquired using an asymmetric spin-echo echo-planar imaging sequence ($\tau = -25$ ms).

Functional imaging parameters were the same for imaging sessions 2–8. These sessions were conducted using an acquisition matrix of size 128 \times 64 (TE = 70 ms, in-plane resolution = 3.1 mm \times 3.1 mm, TR = 2 s), 3 mm thick slices, and a 1 mm gap between slices to reduce inter-slice interference. Session 1 was conducted using a matrix size of 256 \times 128 (TE = 77 ms, in-plane resolution = 1.5 mm \times 1.5 mm, TR = 4 s) and 4 mm thick, contiguous slices.

The slices of interest in each session were selected to encompass all or the majority of the transverse temporal gyrus (Heschl’s gyrus). In sessions 2–8, either eight (sessions 2–6) or five (sessions 7 and 8) slices were acquired using a slice plane approximately parallel to the superior temporal plane. Images were acquired of the left superior temporal plane in sessions 2–7, and of both hemispheres in session 8 (bilateral surface coils). For session 1, five slices were acquired perpendicular to the superior temporal plane. Images acquired in session 1 were of the left hemisphere.

2.2.4 Imaging Coils

We developed a surface coil designed specifically for imaging the human auditory cortex. Early experiments using a head coil exhibited a general lack of fMRI responses in the auditory cortex in both hemispheres, probably a consequence of the low signal-to-noise ratio (SNR)—typically 15—in the superior temporal plane near the transverse temporal gyrus (Heschl’s gyrus). To improve the SNR we switched to small surface coils (5” and 3” General Electric general purpose coils), but it was difficult to center the coils over the superior temporal plane and keep their position fixed throughout the duration of an imaging session (approximately two hours). The 5” coil interfered with the placement of our combination stimulus delivery and passive attenuation earmuffs while the 3” coil had a field-of-view that was too narrow for observation of the entire surface of the temporal lobe. These complications led to mixed results when using the surface coils. It was determined that for the peak sensitivity of our coil to be located in the superior temporal plane, our coil had to be centered just superior to the ear. We also determined that the anterior-posterior extent of our region of interest required field-of-view comparable to that provided by the 5” surface coil. It was known from previous attempts with the 5” surface coil that a coil centered just superior to the ear precluded the effective use of the attenuating earmuffs on the side with the imaging coil. With the eventual goal of imaging both hemispheres at the same time, we chose to develop a set of bilateral imaging coils that were integrated into the earmuffs. The resulting set of two coils consists of square loop coils centered at the top of a set of earmuffs that passively attenuate the noise of imaging by approximately 30 dB. The coils may be used individually or as a bilateral set. This coil design consistently yields high SNR values—greater than 35—in our desired region of interest, the superior portion of the temporal lobe.

A signal-to-noise ratio in auditory cortex of 35 was retrospectively determined to be necessary for us to observe consistent results across individual runs of the experimental paradigm. Therefore only imaging sessions in which the SNR was at least 35 (a total of eight) are described here. Seven of these sessions (sessions 2–8) used our specially designed surface coil and one session (session 1) utilized the 3” surface coil. The few results that were obtained in sessions with lower SNRs are generally consistent with the findings reported here.

2.2.5 Data Analysis

The functional imaging data for each session were processed following a standard procedure. First, all functional imaging data for a given session were aligned (SPM95 [28]) to the first images acquired in the first run (immediately following acquisition of the high-resolution anatomical images) except for session 5, in which the last images acquired were used as a reference because the high-resolution images were acquired as the last segment of the imaging session. Each run was scaled, on an individual voxel basis, to a fixed mean signal level to eliminate inter-run baseline signal variations. Each voxel was also drift corrected, using a quadratic fitting algorithm, to reduce artifactual activations. To improve the detectability of responses to the stimuli, functional imaging data for each session were combined across runs. The data were averaged across runs in seven of the eight sessions (sessions 1, 2, 4–8). The data from the six runs of session 3 were combined by concatenation because the order of lower- and higher-frequency stimulation varied from run to run.

Conversion to Fixed Co-ordinate System

To facilitate inter-session comparisons of the location of responses, both functional and anatomical data from seven of the eight sessions (sessions 2–8) were transformed to a Talairach atlas co-ordinate system [93] and resliced in both axial and coronal planes (3 mm \times 3 mm \times 3 mm voxel size) using in-house software. The slice prescription information contained in the flow-weighted images was not obtained for session 1, precluding registration and reslicing. Because session 1 had been acquired in a near-coronal plane, this plane was used for data analysis and axial images were generated for inter-session comparisons by reslicing the three-dimensional volume of slices in an orthogonal (axial oblique) plane. For the seven sessions (2–8) resliced in Talairach axial and coronal planes, a volume containing most of the superior temporal plane and centered on Heschl’s gyrus was selected for analysis. This volume was a rectangular box bounded by the points $(x,y,z) = (-72,-54,0)$ and $(x,y,z) = (-12,6,15)$ and containing voxels from six Talairach axial slices (centers at $z = +0$ mm, $+3$ mm, $+6$ mm, $+9$ mm, $+12$ mm and $+15$ mm).

Statistical Analysis

Sensitivity to higher- vs. lower-frequencies was assessed using an unpaired t -test. This statistical test was used to compare the normalized signal levels in images assigned to one of the conditions—higher-frequency stimulation or lower-frequency stimulation—to the other. An image was assigned to the higher-frequency (lower-frequency) stimulation condition if it was acquired at least 3 s after the onset of the higher-frequency (lower-frequency) stimulus and at most 4 s after the offset of the stimulus. This accounts for the onset and offset time of the blood oxygenation level dependent (BOLD) fMRI response which is approximately 4–10 s [2, 8, 44]. Observation of a greater average signal level during the presentation of one of the two stimuli was interpreted as a particular sensitivity for that stimulus and the voxel was said to be “activated” by the stimulus. The statistical significance of the t -statistic values were computed and superimposed as a color “activation map” upon the T_1 -weighted images of the brain to determine the anatomical locations of the fMRI responses to the stimuli.

To examine equivalent levels of physiological responses across imaging sessions, it was necessary to incorporate a normalization into the t -test for the variable signal-to-noise ratios resulting from the variable number of total images acquired in each stimulation condition. This statistical normalization was effected for the purpose of defining the presence and extent of frequency sensitive regions. Normalization was implemented by selecting a baseline t -statistic cutoff of $t > 1.98$ ($p < 0.05$) for the case of a total of 192 images acquired in the higher- and lower-frequency stimulation conditions and scaling the t -statistic threshold used for other sessions up or down depending on the total number of images obtained in the two stimulation conditions. This technique increases the false positive rate in those experiments utilizing fewer images, but yields activation maps that are qualitatively similar in spatial extent.

Identification of Frequency Sensitive Regions

Frequency sensitive regions were identified by an analysis of all voxels achieving the normalized threshold of $p < 0.05$ that were adjacent to at least one other significant voxel exhibiting the same frequency sensitivity. First, local (within a $3 \times 3 \times 3$ cube centered on the voxel) statistical maxima were identified from among all voxels in the six slice volume

of interest that achieved the $p < 0.05$ significance level. Each voxel that was a statistical maximum was deemed to be the “activation focus” of a frequency sensitive region. If, within two voxels (6 mm) of the activation focus, a frequency sensitive region extended into the ventricles, out of the brain (defined as a T_1 -weighted high-resolution image signal level greater than 100), or out of the temporal lobe (e.g. into the parietal cortex), the activation focus and corresponding frequency sensitive region were discarded from further analysis. Isolated activation foci, those without statistically significant neighbor voxels, were also discarded. The Talairach co-ordinates of the activation focus of each remaining frequency sensitive region were computed and catalogued. Session 8 was conducted using bilateral surface coils, revealing activation foci in both hemispheres. In this case, activation foci in the right hemisphere were identified within a corresponding right hemisphere volume of interest using the preceding criteria and the Talairach co-ordinates were reflected across the midline and combined with the left hemisphere data.

The activation foci (and corresponding frequency sensitive regions) were examined across sessions for trends and classified based on their frequency sensitivity, spatial relationship to each other and the anatomy (see Section 2.3 for specific criteria), or were left unclassified. In relating different frequency sensitive regions to each other (e.g. determining if one was medial to another) the activation focus and the three most statistically significant adjacent voxels were used (see Figure 2-3). The full spatial extent of the region, including all connected voxels achieving the statistical threshold for that session (normalized $p < 0.05$) was used to determine the relation of each frequency sensitive region to the anatomy. Some regions were left “unclassified” because they were not observed in at least five of eight imaging sessions. Right hemisphere frequency sensitive regions in session 8 were classified based upon the right hemisphere anatomy and combined with those of the left hemisphere for analysis and display.

Summary figures of the cortical activation were created for each session to permit inter-session comparison of the ensemble of frequency sensitive regions. To generate axial summaries of activation, the activation focus of each frequency sensitive region (defined above) was identified along with the three most significant voxels adjacent to it within a given Talairach axial slice. Note that the activation focus is not necessarily the center of the corresponding frequency sensitive region, it is simply the voxel exhibiting the most significant (unpaired t -statistic) response. The frequency sensitive regions (classified and unclassified)

from all six slices in the axial volume of interest were then overlaid upon resliced versions of the T_1 -weighted high-resolution anatomical images. The activation in the axial slices centered at Talairach $z = +15$, $+9$ and $+3$ mm were projected onto the slices at $z = +12$, $+6$ and $+0$ mm, respectively, to yield three slice summaries of the activation in the superior temporal plane. Coronal summary figures were also generated for a subset of the frequency sensitive regions observed on Heschl's gyrus. In this case, the maximal extent of the frequency sensitive regions of interest within a 9 mm anterior-posterior extent were projected onto a tracing of landmarks from the Talairach coronal slice centered at $y = -24$ mm (sessions 2-5, 7 and 8) or $y = -21$ mm (session 6). The anterior-posterior extent was chosen to include a portion of all three frequency sensitive regions. Landmarks included in the tracing were Heschl's gyrus, the ventricles, the edge of the brain and the midline. Each slice was registered to the tracing by aligning the landmarks in the tracing with those in the slice. As noted previously, the frequency sensitive regions observed in the right hemisphere of session 8 were reflected across the midline onto the anatomy of the left hemisphere and displayed along with the left hemisphere regions.

2.3 Experimental Results

Eight regions on the superior temporal lobe were repeatedly observed to exhibit preferential activation to lower-frequency or higher-frequency stimulation, independent of the type of stimulus being presented. These "classified" regions were observed in at least five of the eight imaging sessions. Other regions that were not observed as frequently were left "unclassified." The description of the classified frequency sensitive regions will begin with those situated on or adjacent to the medial two-thirds of Heschl's gyrus, the location of primary auditory cortex [29, 76, 82], and proceed to those in surrounding regions of cortex.

Three of the eight frequency sensitive regions (Regions 1-3, Table 2.1) were consistently observed in the immediate vicinity of Heschl's gyrus. These regions, as imaged in a coronal plane, are depicted in Figure 2-1. Region 1, located on the superior aspect of Heschl's gyrus in part c of the figure, exhibited significantly ($p < 0.05$) greater image signal levels ("activation") during periods of lower-frequency (low-pass music) stimulation than during periods of higher-frequency (high-pass music) stimulation (Figure 2-1, part d). Therefore, Region 1 is a "lower-frequency sensitive region." Region 2, located infero-medial to Region

1, and Region 3, located infero-lateral to Region 1, exhibited significantly greater signal levels during periods of higher-frequency stimulation (Figure 2-1, parts c and e) and are therefore “higher-frequency sensitive regions.”

The three frequency sensitive regions in Figure 2-1 were observed in all sessions and for all stimuli used. This reproducibility may be appreciated from the composite activation maps in Figures 2-2 and 2-3. The coronal summaries (Figure 2-2) were generated using all voxels in each frequency sensitive region that were significant to the $p < 0.05$ level, while generation of the axial summaries (Figure 2-3) only used the activation foci and three most significant neighboring voxels.

The axial summaries (e.g. Figure 2-3) were used to classify these three frequency sensitive regions within each imaging session. Region 1 (Figure 2-3, middle slice for all three sessions) was defined as the most medial lower-frequency sensitive region on the superior aspect of Heschl’s gyrus. Region 2 (Figure 2-3, middle slice) was defined to be the higher-frequency sensitive region on the antero-medial aspect of Heschl’s gyrus, located medial to Region 1. Region 3 (Figure 2-3, superior slice) was defined as the higher-frequency sensitive region observed on or near the postero-lateral aspect of Heschl’s gyrus, at least as lateral as Region 1. Region 3 was usually observed superior to Region 1 in the axial plane as a consequence of the oblique angle between the superior temporal plane and the anterior commissure-posterior commissure (AC-PC) line used to define the $z = +0$ mm axial plane.

Five additional frequency sensitive regions (Regions 4–8, Table 2.1) were identified using the axial summaries for all eight sessions. Region 4 was defined as the higher-frequency sensitive region on or near the postero-medial aspect of Heschl’s gyrus, posterior to Region 2 (Figure 2-3, superior slice). Region 4 was observed in seven of eight imaging sessions. Region 5 (Figure 2-3, inferior slice of sessions 2 and 5) was defined as the higher-frequency sensitive region located in the inferior third of the Talairach volume, on the postero-lateral aspect of Heschl’s gyrus where it begins to merge with the superior temporal gyrus. This region was observed in six of eight sessions. Region 6 was defined to be the most superior and lateral lower-frequency sensitive region located on or immediately lateral to Heschl’s gyrus, superior and/or lateral to Region 1 (Figure 2-3, middle slice of all three sessions and superior slice of session 8). This region was observed in seven of eight sessions. Region 7 was defined as the lower-frequency sensitive region situated on the antero-lateral aspect of Heschl’s gyrus, or just anterior to Heschl’s gyrus on the superior temporal gyrus. The

Figure 2-1: Three frequency sensitive regions in the immediate vicinity of Heschl's gyrus (session 1). (a) Sagittal anatomical image through Heschl's gyrus (center of black circle) with red line drawn to illustrate the coronal oblique functional imaging slice plane, almost perpendicular to the superior temporal plane. (b) Schematic of the coronal oblique slice indicated in (a), passing through the center of Heschl's gyrus (center of black box). (c) Activation map of statistically significant ($p < 0.05$, t -statistic) responses overlaid on section of T_1 -weighted anatomical image corresponding to boxed region in (b). Increasingly significant "lower-frequency sensitive region" voxels are colored blue to green. Increasingly significant "higher-frequency sensitive region" voxels are colored orange to yellow. Region 1, on the superior aspect of Heschl's gyrus, exhibited greater image signal levels during lower-frequency (20–100 Hz) stimulus presentation (d). Region 2 (medial) and Region 3 (lateral) exhibited greater image signal levels during higher-frequency (7–8 kHz) stimulus presentation (e). (d) Smoothed (5 point window), average time-course of signal level in voxels in the circle enclosing Region 1 that were significant to the $p < 0.05$ level. Light (dark) gray vertical bands indicate the periods during which the lower-frequency (higher-frequency) stimulus was presented. (e) Smoothed (5 point window), average time-course of signal level in voxels in the circles enclosing Regions 2 and 3 that were significant to the $p < 0.05$ level.

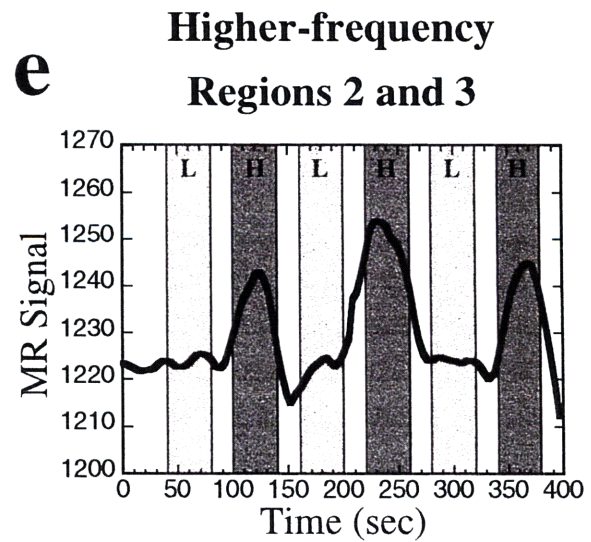
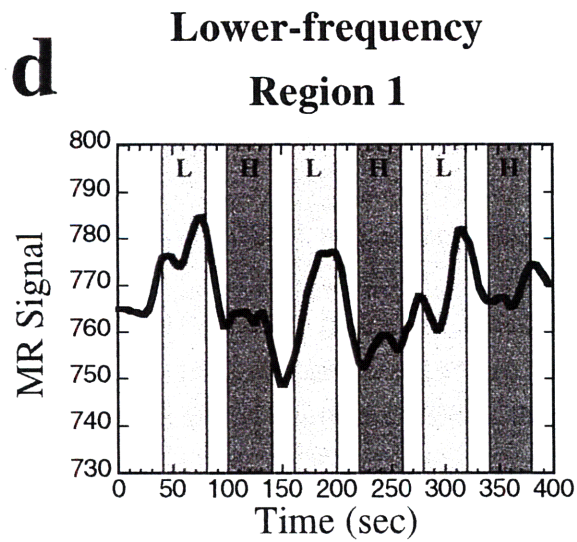
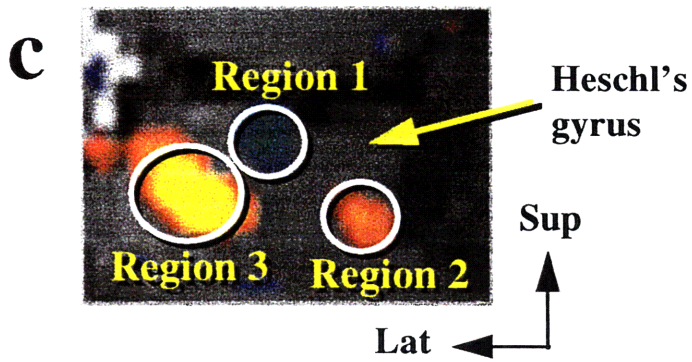
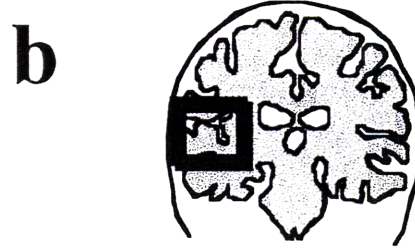
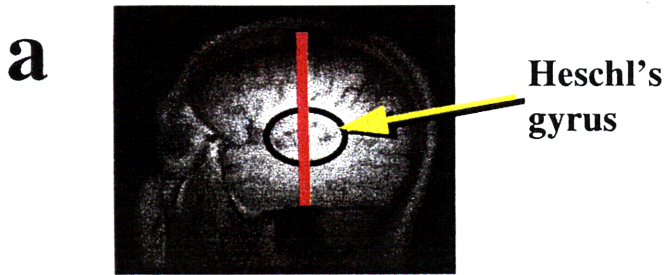
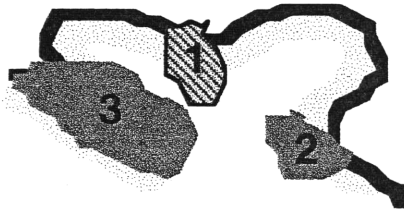
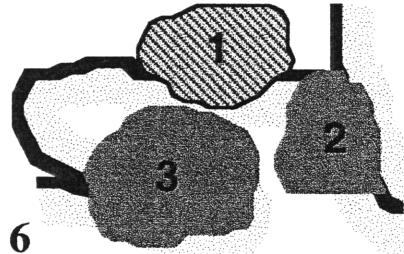


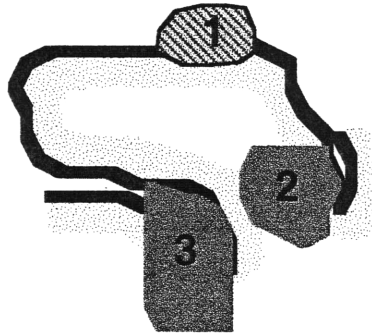
Figure 2-2: Summaries of three classified frequency sensitive regions (Regions 1–3) in the immediate vicinity of Heschl’s gyrus (left hemisphere), as imaged in the coronal plane, for all eight sessions. The full spatial extent of lower-frequency sensitive Region 1 is indicated by diagonally hatched, light gray regions. The full spatial extent of higher-frequency sensitive Regions 2 and 3 are indicated by solid, darker gray regions. Light gray speckled regions are stylistic representation of gray matter. Coronal summary figures were generated by projecting the spatial extent of Regions 1–3 in a 9 mm anterior-posterior volume (3 coronal slices) onto the outline of Heschl’s gyrus from the 3 mm slice centered at $y = -24$ mm (sessions 2–5, 7–8) or $y = -21$ mm (session 6). Session 1 could not be resliced into a Talairach coronal plane so the summary was generated from the single 4 mm thick slice containing the greatest medial-lateral extent of Heschl’s gyrus. Variations in imaging planes and identification of landmarks for the transformation to Talairach co-ordinate system contribute to the variable anatomy of Heschl’s gyrus for subject 2 in sessions 2, 4 and 8.



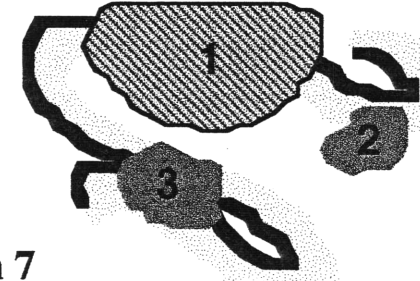
Session 1
Subject 1
Instrumental Music



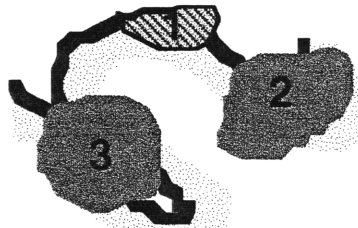
Session 6
Subject 5
AM Tones (10 Hz)



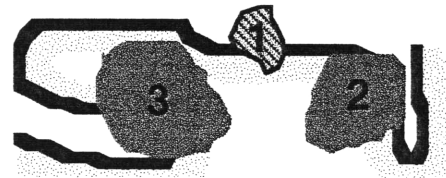
Session 2
Subject 2
Tone Bursts (10/s)



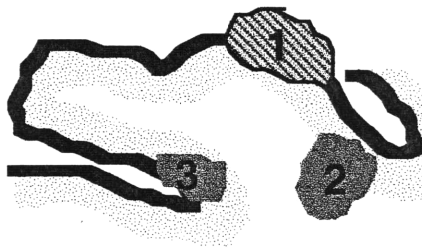
Session 7
Subject 6
AM Tones (10 Hz)



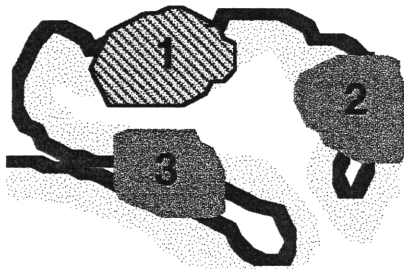
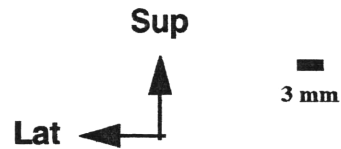
Session 3
Subject 3
AM Noise (10 Hz)



Session 8
Subject 2
AM Tones (10 Hz)



Session 4
Subject 2
AM Noise (10 Hz)



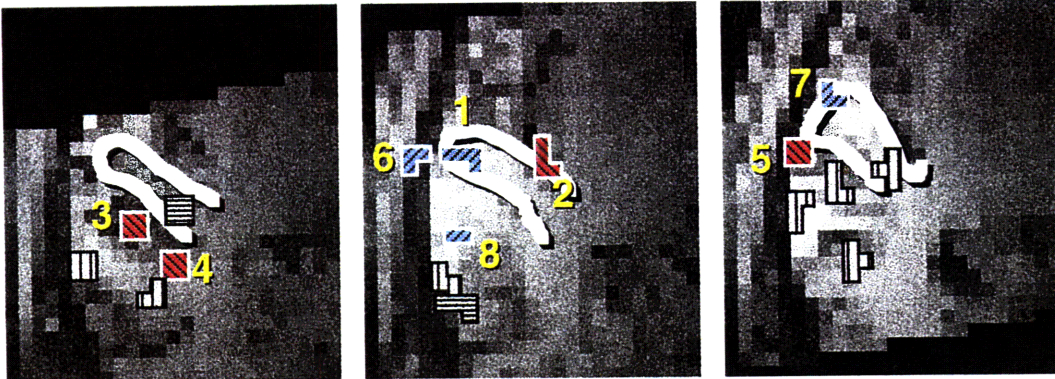
Session 5
Subject 4
AM Noise (10 Hz)



Figure 2-3: Summaries of lower- and higher-frequency sensitive activation foci in the Talairach axial plane for Sessions 2 (top), 5 (middle) and 8 (bottom). All three images in each row were generated by projecting the activation foci contained within a two slice (6 mm) volume onto the resliced T_1 -weighted anatomical image of the inferior slice. Slices represented in the figure are (left) $z = +15$ mm and $z = +12$ mm, (middle) $z = +9$ mm and $z = +6$ mm, (right) $z = +3$ mm and $z = +0$ mm. For each depicted slice, the limits of Heschl's gyrus are outlined in white. Regions are represented by their activation focus and the surrounding three most significant voxels. Diagonally hatched frequency sensitive regions indicate classified higher- (right downward, red; 2-5) and lower-frequency (left downward, blue; 1, 6-8) sensitive regions. Positional criteria for classification are provided in Table 2.1. Unclassified activation foci, those not observed in at least five of eight imaging sessions, are indicated by gray, vertically (higher-frequency) and horizontally (lower-frequency) hatched regions. The summary for session 8 was constructed using the data from both hemispheres, leading to the presence of multiple activation foci for Regions 1, 6 and 7.

Session 2

Subject 2
Tone Bursts (10/s)

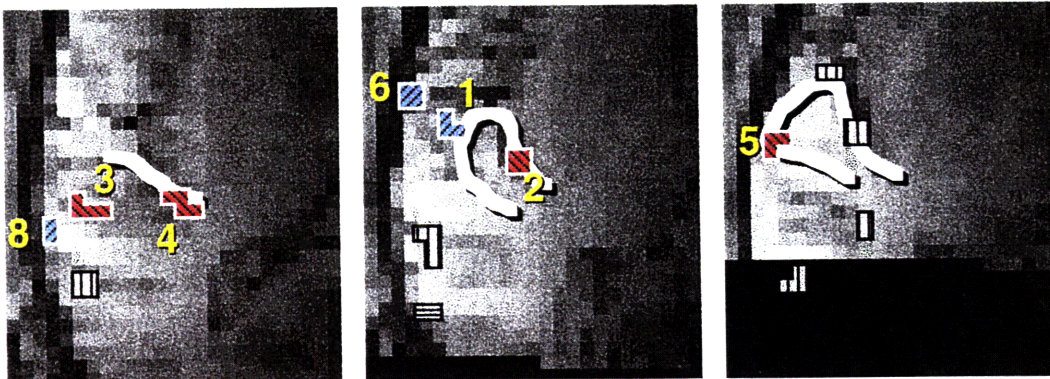


Superior

Inferior

Session 5

Subject 4
AM Noise (10 Hz)



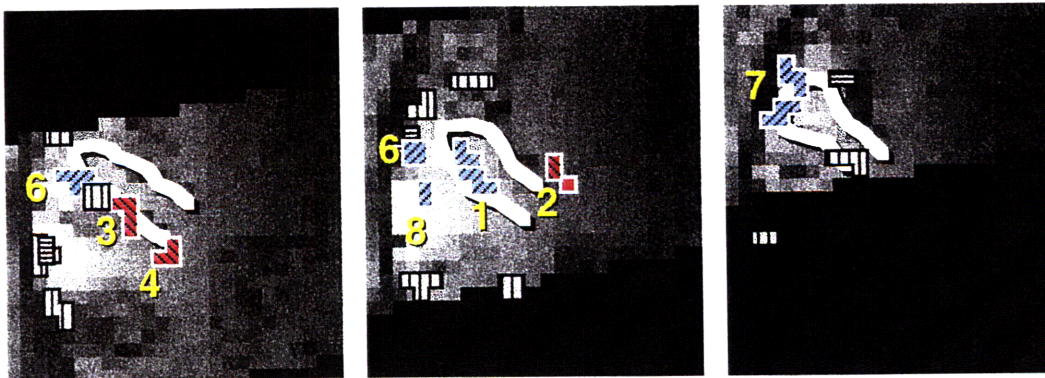
(z = +12, +15)

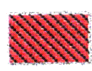
(z = +6, +9)


(z = +0, +3)

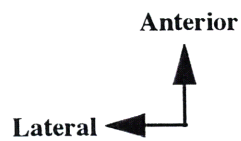
Session 8


Subject 2
AM Tones (10 Hz)




 Classified Higher-Frequency Region

 Unclassified Higher-Frequency Region



 Classified Lower-Frequency Region

 Unclassified Lower-Frequency Region

Region	Talairach Co-ordinates	Positional Criteria for Classification of Activation Foci	# of Sessions in which Region was Observed
1	x = -51.8 ± 1.1 y = -16.1 ± 1.7 z = 8.6 ± 0.7	Most medial lower-frequency activation focus on superior Heschl's gyrus (HG)	8/8
2	x = -35.1 ± 1.1 y = -18.9 ± 1.6 z = 8.6 ± 0.8	Higher-frequency focus on antero-medial aspect of HG, medial to Region 1	8/8
3	x = -51.9 ± 1.3 y = -25.7 ± 1.4 z = 10.3 ± 2.1	Higher-frequency focus on or near postero-lateral aspect of HG; at least as lateral as Region 1	8/8
4	x = -38.0 ± 1.3 y = -34.0 ± 2.3 z = 12.0 ± 1.3	Higher-frequency focus on or near postero-medial aspect of HG, posterior to Region 2	7/8
5	x = -63.0 ± 0.9 y = -14.4 ± 1.1 z = 2.4 ± 1.7	Higher-frequency focus in inferior third of volume, on postero-lateral aspect of HG where it merges with the superior temporal gyrus (STG)	6/8
6	x = -60.0 ± 1.4 y = -14.6 ± 2.1 z = 10.1 ± 1.3	Most superior and lateral lower-frequency focus on or immediately lateral to HG; superior and/or lateral to Region 1	7/8
7	x = -53.6 ± 2.7 y = -1.3 ± 2.2 z = 1.7 ± 0.9	Lower-frequency focus on antero-lateral aspect of HG or just anterior to HG on STG; inferior half of volume	6/7
8	x = -59.6 ± 1.2 y = -30.4 ± 1.0 z = 10.7 ± 1.3	Lower-frequency focus on STG, closest to HG, posterior to Regions 5 and 6, postero-lateral to Region 3; superior half of volume	8/8

Table 2.1: Average Talairach co-ordinates and positional classification criteria for the eight classified frequency sensitive regions.

anterior position also dictated that Region 7 was in the inferior half ($z \leq +6$ mm) of the volume of interest (Figure 2-3, inferior slice of sessions 2 and 8). Region 7 was observed in six of the seven sessions in which this portion of cortex was imaged (the coronal images obtained in session 1 did not include superior temporal cortex anterior to Heschl's gyrus). Region 8 (Figure 2-3, middle slices for sessions 2 and 8, superior slice for session 5) was defined as the lower-frequency sensitive region closest to Heschl's gyrus on the superior temporal gyrus, in the superior half ($z \geq +9$ mm) of the volume of interest, posterior to Regions 5 and 6 and postero-lateral to Region 3. This region was observed in all eight sessions. The mean and standard error of the Talairach co-ordinates of the classified activation foci are provided in Table 2.1. Some activation foci in the axial summaries were not observed in at least five of the eight sessions, and thus were left unclassified (vertically and horizontally

hatched regions in Figure 2-3).

Session	Size of Region (# voxels)							
	Lower-Frequency				Higher-Frequency			
	1	6	7	8	2	3	4	5
1	16	0	—	14	6	43	13	6
2	39	15	4	2	7	16	22	18
3	69	27	15	96	26	14	22	7
4	21	21	14	31	2	6	11	0
5	3	7	0	2	13	17	19	3
6	47	13	23	7	35	32	0	3
7	96	47	17	22	10	6	2	4
8	52	26	18	15	4	15	8	0

Table 2.2: Spatial extent (in number of voxels) of frequency sensitive regions. The spatial extent was computed as the number of voxels surrounding the activation focus with $p < 0.05$ (t -statistic). For each session, the largest region of each type of frequency sensitive regions (lower- or higher-frequency) is denoted by boldface numbers. Voxel dimensions were (session 1) 1.5 mm \times 1.5 mm \times 4 mm or (sessions 2–8) 3 mm \times 3 mm \times 3 mm.

Session	Strength of Response in Region (% Signal Change)							
	Lower-Frequency				Higher-Frequency			
	1	6	7	8	2	3	4	5
1	-0.93	—	—	-0.66	1.02	1.01	0.91	0.51
2	-0.41	-0.67	-0.47	-0.26	0.36	0.30	0.43	0.48
3	-0.29	-0.31	-0.20	-0.32	0.39	0.24	0.29	0.47
4	-0.24	-0.21	-0.20	-0.20	0.18	0.13	0.18	—
5	-0.18	-0.50	—	-0.17	0.22	0.26	0.28	0.19
6	-0.27	-0.19	-0.20	-0.15	0.26	0.36	—	0.23
7	-0.39	-0.47	-0.21	-0.36	0.19	0.16	0.20	0.18
8	-0.37	-0.48	-0.47	-0.38	0.41	0.29	0.33	—

Table 2.3: Average percent signal change over the spatial extent of each of the eight categories of frequency sensitive regions. For each session, the greatest percent signal change for each type of frequency sensitive region (lower- or higher-frequency) is denoted by boldface numbers.

The spatial extent (in voxels) and average percent signal change observed in the data were compared across frequency sensitive regions (Tables 2.2 and 2.3). Comparisons of the magnitude of these measures of response were not made across imaging sessions because of inter-session variability in the acoustic background noise arising from differences in the number and spatial resolution of the images acquired (see Section 2.2.3). Session-dependent noise-induced responses in auditory cortex (see Appendix B [94]) may have affected both

the spatial extent and percent signal changes observed in the classified frequency sensitive regions (Appendix A [23]). Therefore we will restrict ourselves to inter-session comparisons of the maximally activated regions within each session. Region 1 was the largest lower-frequency sensitive region in five of eight sessions. Regions 2 and 4 were each the largest higher-frequency sensitive region in three sessions. Region 6 exhibited the greatest percent signal change of the lower-frequency sensitive regions in four sessions, while Region 1 exhibited the greatest percent signal change in three sessions. As with spatial extent, each of Regions 2 and 4 had the greatest percent signal change of the higher-frequency sensitive regions in three sessions. Therefore, the regions with the greatest spatial extent were usually (13/16) on (Regions 1 and 2) or immediately proximal to (Regions 3 and 4) the medial two-thirds of Heschl's gyrus, the region in which koniocortex is located [29, 76, 82]. Regions with the greatest percent signal changes were less likely (9/16) to be located on or immediately proximal to the medial two-thirds of Heschl's gyrus. Regions exhibiting the greatest percent signal change were not necessarily those with the greatest spatial extent.

2.4 Discussion

We have observed consistent locations of higher- and lower-frequency sensitive regions in auditory cortex, suggesting that the frequency organization in some portions of human auditory cortex is consistent across subjects. Each of the observed frequency sensitive regions (classified and unclassified) exhibited greater signal levels during moderate intensity higher- or lower-frequency stimulation. Because signal increases are typically observed in functional MRI as a consequence of local increases in metabolic activity [38, 61], we may conclude that the frequency sensitive regions exhibited greater metabolic activity during the higher- or lower-frequency stimulation. This permits us to say that the observed frequency sensitivity is physiological in origin, being related to changes in the metabolic activity of neurons in auditory cortex. The eight classified regions (those observed in at least five of the eight imaging sessions) thus demonstrate that some of the frequency organization in auditory cortex is relatively invariant across individuals. The unclassified regions of cortex (those observed in fewer than five of the eight imaging sessions) may provide an indication of the inter-individual variability in the frequency organization of auditory cortex, or may reflect differential responses either to the various stimuli used in this study or to the variable

acoustic background.

Given our knowledge of the response properties of auditory cortex neurons in experimental mammals, the observed sensitivity to higher vs. lower stimulus frequencies suggests that the neurons in our eight classified frequency sensitive regions are tuned to either higher or lower frequencies. We propose that the increases in image signal level observed in response to a stimulus are a function of the overlap between the stimulus spectrum and the tuning curves of the neurons in the responding region. If our stimulus spectrum overlaps the tuning curve of a neuron, the neuron will increase its discharge rate unless it is inhibited by the portion of the stimulus spectrum away from CF (e.g. by “lateral inhibition” or by high-threshold inhibitory inputs [72, 73]). This increase in the discharge rate will induce metabolic changes, potentially including an increase in the consumption of oxygen [69, 74]. If a sufficiently large number of neurons in a given region increase their oxygen consumption, there will be an increase in the delivery of oxygen to that region [27, 51]. An increase in oxygen delivery that is sufficiently large relative to the oxygen consumption increase will lead to an increase in the signal level obtained from that region via fMRI [9, 38, 44, 61]. Under this simple model, significantly greater fMRI signal levels are expected when we present a band of frequencies to which the neurons in a region of cortex are most sensitive than when we present a band of frequencies to which the neurons are less sensitive.

The observation of multiple regions in human auditory cortex that are sensitive to higher or lower frequencies, coupled with the assumption that the organizing principles of animal auditory cortex are likely to be preserved in the human, suggests the existence of multiple areas in the human auditory cortex that are topographically organized by frequency sensitivity. We have observed multiple disjoint locations in the human cortex that appear to possess similar gross frequency sensitivity (below 660 Hz or above 2490 Hz). We know that animal auditory cortex is organized into multiple auditory areas (functionally and anatomically), each of which exhibits frequency sensitivity to some degree [26, 40, 41, 43, 52, 53, 57, 58, 71, 75]. It is reasonable to hypothesize that we are observing responses from analogous auditory areas in the human cortex. Under this hypothesis some auditory areas may be sensitive to both higher- and lower-frequency stimulation, with the presentation of higher- and lower-frequency stimuli providing two different samplings of the spatial organization of frequency sensitivity in auditory cortex. An alternate hypothesis is that all of the anatomically defined auditory areas that are responding to stimulation respond exclusively to either higher-

or lower-frequency stimulation. This hypothesis seems highly unlikely given the body of animal electrophysiological and anatomical data (e.g. [41, 43, 57, 75]).

We propose that multiple anatomical areas in the human auditory cortex may be tonotopically organized. This postulation is based upon the existence of multiple tonotopically organized anatomical auditory areas in experimental mammals (e.g. [58]), the presence of multiple anatomical auditory areas in human cortex (e.g. [29]), and our observation of multiple, regions of higher- and lower-frequency sensitivity. We have hypothesized that some pairs of our lower- and higher-frequency sensitive regions are contained partly within the same anatomical areas in the human auditory cortex. An anatomical area that contains both a higher- and a lower-frequency sensitive region necessarily exhibits some degree of spatial segregation of frequency sensitivity. If the sensitivity to stimulus frequency varies monotonically as a function of position between the higher- and lower-frequency sensitive regions, the anatomical area would be said to contain a tonotopic map. Therefore, the presence of both higher- and lower-frequency regions within an anatomical auditory area is necessary behavior for the prediction of the presence of a tonotopic map in that area.

We propose that our eight frequency sensitive regions consist of the highest and lowest CF “ends” of tonotopic maps, even though our stimuli do not include the highest and lowest CFs in the audible range. This proposition requires two assumptions regarding the response properties of auditory cortex. The first assumption is that our lower-frequency stimuli (below 660 Hz) will induce changes in the discharge patterns of the more broadly tuned low-CF (e.g. less than 500 Hz) neurons in cortex, potentially including the neurons with the lowest CFs. If this assumption is valid, a lower-frequency stimulus will produce an fMRI-observable response in those portions of the cortex containing the lowest CFs, even though the bandwidth of the stimulus does not include these frequencies. Second, we assume that our higher-frequency stimuli (above 2490 Hz) will induce fMRI-observable activation that is indistinguishable from activity in the sharply tuned high-CF (e.g above 10 kHz) neurons. Most neurons in primary auditory cortex are tuned such that the tip has a Q_{10} of 2–8 indicating that a neuron will only exhibit a response to frequencies within (at most) one-quarter octave of its CF at a level of 10 dB above the threshold at CF [70]. It is not unreasonable to assume that, at a stimulus level of 35 dB above threshold, we are likely to stimulate neurons with CFs that are at least one-half octave above the highest frequency contained in our stimulus spectrum. Because the higher-frequency stimuli in seven of eight

sessions included frequencies of 4.5 kHz and higher, this assumption would suggest that at least some neurons with CFs ranging from 7–10 kHz exhibited discharge rate increases as a consequence of acoustic stimulation. Given the previous assumption that two octaves will be represented over a 6 mm linear distance, our 3 mm resolution is likely make activation induced in neurons with CFs in the range of 7–10 kHz indistinguishable from activation induced in the neurons with the highest CFs (e.g. 15+ kHz). Therefore, our lower- and higher-frequency response regions are likely to include the lowest and highest CF ends of any tonotopic maps that are present.

Under the assumption that we are observing responses from the highest and lowest CF ends of tonotopic maps, we propose that some of our eight frequency sensitive regions consist of the higher- and lower-frequency ends of multiple tonotopic maps that are organized in a “mirror” fashion. Some of the tonotopic maps in animal auditory cortex exhibit a mirrored organization, with the highest frequency (lowest frequency) representation of one map adjacent to the highest frequency (lowest frequency) representation of a neighboring tonotopic map (e.g. the low frequency border of auditory areas R and AI in the monkey [43, 57]). Visual studies conducted using fMRI have revealed many neighboring areas in the human visual cortex to be organized retinotopically in a mirror fashion, similar to those observed in animal cortex [89]. By analogy, we assume that the mirror organization of tonotopic maps in animal cortex will be present in the human auditory cortex. If we are observing responses from the highest and lowest CF portions of tonotopic maps, the adjacency of the ends of mirror tonotopic maps will lead to the observation of multiple higher- and lower-frequency ends as a single higher- or lower-frequency sensitive region in our data. Therefore, we propose that some of our frequency sensitive regions are composed of responses from two or more mirror tonotopic maps (i.e. a single lower-frequency sensitive region may be connected to multiple higher-frequency sensitive regions, and vice versa).

A correspondence may be established between our higher- and lower-frequency sensitive regions and the anatomical areas of human auditory cortex, permitting us to propose a tonotopic organization for portions of the cortex. Assuming that each tonotopic map is wholly contained within a single anatomical auditory area, as observed in experimental animals (e.g. [41]), some of our frequency sensitive regions that have been proposed to represent portions of multiple tonotopic maps may further be interpreted to consist of responses from more than one anatomical auditory area. The presence of both higher- and

lower-frequency regions within an anatomical auditory area has already been presented as necessary behavior for the prediction of a tonotopic map in a given area. Possible correspondences between our frequency sensitive regions and the anatomical auditory areas will be addressed through comparison of our results to both the human and animal literature. These correspondences will then permit us to propose a tonotopic organization for some anatomically defined auditory areas.

2.4.1 Human Anatomical Studies

Anatomical studies have identified multiple cytoarchitectural areas in human auditory cortex. These architectonic studies (e.g. [29, 82]) have revealed multiple areas in the human auditory cortex based upon cell and axon populations.

Galaburda and Sanides [29] identified eight cytoarchitectural areas in the superior temporal plane of humans, including two divisions of koniocortex on Heschl's gyrus. The koniocortical area (primary auditory cortex) on Heschl's gyrus was surrounded by belt regions composed of parakonionicortex and prokonionicortex. The parakonionicortical and prokonionicortical cytoarchitectural areas are believed, based upon anatomical study of cell population and projections in the rhesus monkey [30], to represent secondary (functional) auditory areas. Galaburda and Sanides propose a division of the koniocortex on Heschl's gyrus into two cytoarchitectural divisions, one medial (KAm) and one lateral (KAlt), as was observed in the rhesus monkey. In the monkey KAm is richer in callosal projections suggesting a functional difference between the two koniocortical divisions, a distinction that may correspond to monkey auditory areas AI and R [57].

Recently, Rivier and Clarke [82] used multiple staining techniques to identify six cytoarchitectural auditory areas in part of the superior temporal plane. The organization proposed differs slightly from that proposed by Galaburda and Sanides, specifying only a single koniocortical area (primary auditory cortex, AI) on Heschl's gyrus and not describing any auditory areas on the lateral aspect of the gyrus.

The five non-primary cytoarchitectural auditory areas described by Rivier and Clarke may be easily related to similar areas described by Galaburda and Sanides based upon their position relative to the koniocortex on Heschl's gyrus. Rivier and Clarke propose two areas situated anterior to Heschl's gyrus. These are the anterior auditory area (AA), located antero-laterally on the superior temporal gyrus, and the medial auditory area (MA),

situated just anterior to Heschl's along its antero-medial extent. AA and MA probably correspond, respectively, to the rostral parakoniocortex (PaAr) and the prokoniocortex (ProA) of Galaburda and Sanides. Posterior to Heschl's gyrus and primary auditory cortex, Rivier and Clarke describe three further auditory areas. From lateral to medial, these three areas are the superior temporal auditory area (STA), the lateral auditory area (LA), and the posterior auditory area (PA). STA is located on the superior temporal gyrus, posterolateral to the lateral edge of Heschl's gyrus. LA is situated just postero-lateral to the gyrus and extending for approximately half its length. PA is located posterior to the medial portion of Heschl's gyrus. STA probably corresponds to the anterior portion of the external parakoniocortex (PaAe) of Galaburda and Sanides, LA likely corresponds to the posterior half of interior parakoniocortex (PaAi), and PA is located where posterior portion of the caudal/dorsal parakoniocortex (PaAc/d) was identified.

As a convention, we shall refer to each anatomical area by the designations of both studies, even in those cases where the area delimited by Rivier and Clarke does not correspond to the full extent of the area described by Galaburda and Sanides.

2.4.2 Correspondence Between Classified Regions and Anatomical Areas

We may propose a correspondence between the activation foci of our eight classified frequency sensitive regions and the centers of the anatomically defined auditory areas based upon a comparison of the distribution of these two sets of locations in the left superior temporal plane. The locations of the classified activation foci and the average location of the cytoarchitectural auditory areas of Rivier and Clarke [82] are shown in Figure 2-4, overlaid upon an image of the left superior temporal plane ($z = +9$ mm) from session 3. The distribution of the average Talairach positions [93] of the activation foci of the eight classified regions (Table 2.1) covers approximately the same extent of the superior temporal plane as the centers of the cytoarchitecturally defined auditory areas. It may also be observed that some activation foci are located almost equidistant from the center of two anatomically defined auditory areas (e.g. Region 3 with respect to AI and LA). Given the assumptions that our frequency sensitive regions include the highest and lowest CF ends of tonotopic maps and that each tonotopic map is wholly contained within a single anatomical auditory area, our frequency sensitive regions may be interpreted to correspond to the ends of tonotopic maps in multiple auditory areas. We use this interpretation to

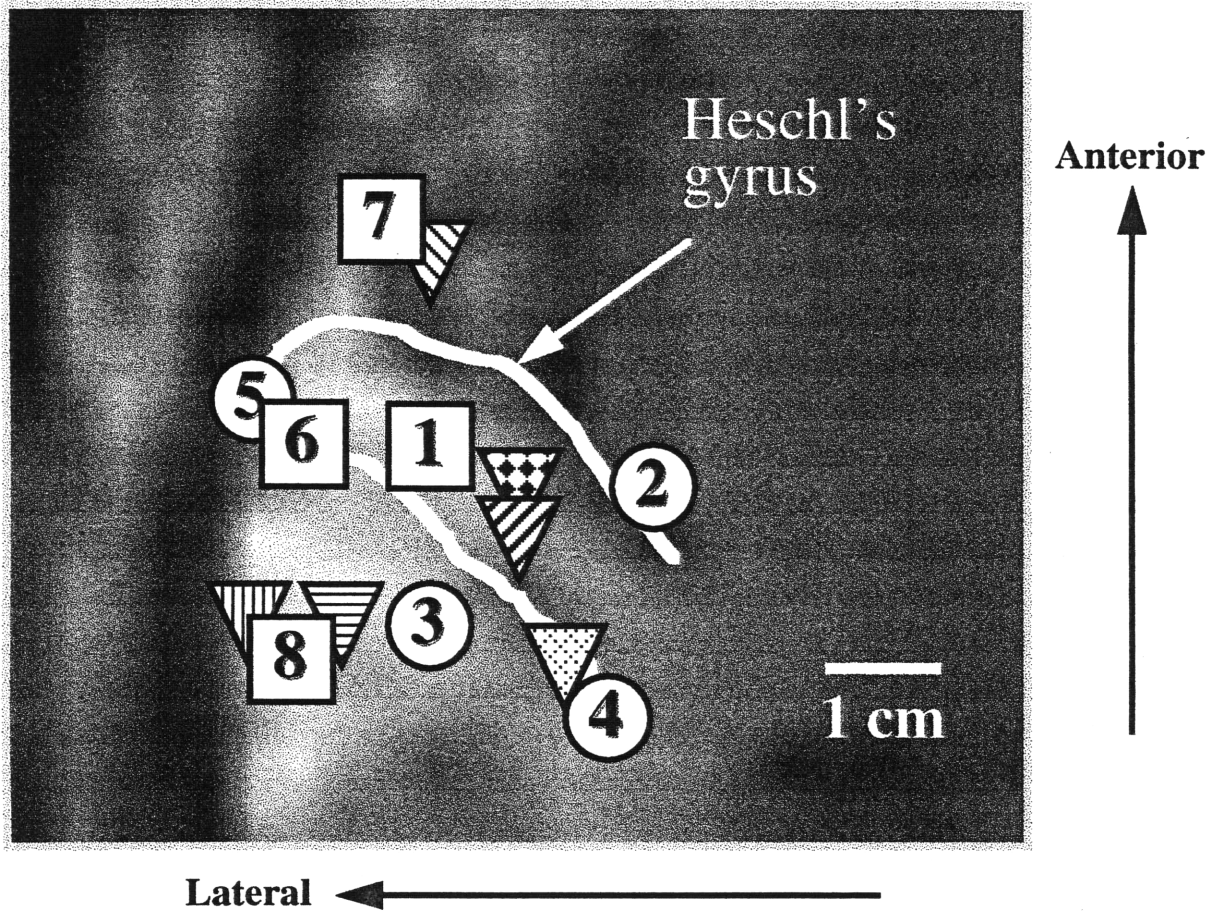
propose a correspondence between the eight classified frequency sensitive regions and the cytoarchitectural areas based upon arguments of proximity, anatomical extent of auditory areas, and the assumption that auditory cortex will exhibit mirror tonotopic maps.

We propose that portions of Regions 1–3 are comprised of responses from the primary auditory area (AI) of Rivier and Clarke and the koniocortical areas of Galaburda and Sanides (KAm and KAlt). These three classified regions are observed to be almost equidistant from the average center of AI and, along with Region 4, are the only classified regions in the immediate vicinity of the koniocortex—the medial two-thirds of Heschl’s gyrus [29, 76, 82]. Regions 4–8 are proposed to be located in non-koniocortical areas (outside the medial two-thirds of Heschl’s gyrus [76]), and are found to correspond well to possible limits of cytoarchitecturally defined auditory areas (Figure 2-4).

Region 1, located on the superior aspect of Heschl’s gyrus, is postulated to be wholly contained within the koniocortex—the medial two-thirds of Heschl’s gyrus [76]. Region 1 is located approximately two-thirds of the length of Heschl’s gyrus from the medial-most end of the gyrus (Figure 2-4), placing this classified region at the approximate lateral end of koniocortex. Region 1, located 9 mm antero-lateral of the average center of mass indicated for AI (KAm and KAlt) by Rivier and Clarke [82] is likely to mark the antero-lateral end of this area. We have previously noted that koniocortex consists of two cytoarchitecturally defined areas—medial AI (KAm) and lateral AI (KAlt). The boundary between these two areas runs almost parallel to the long axis of Heschl’s gyrus, from the postero-medial end of koniocortex to its antero-lateral end. Coupled with our assumption that tonotopic maps in auditory cortex may mirror one another, sharing higher- or lower-frequency sensitive borders, we propose that Region 1 represents a lower-frequency sensitive end of both medial AI (KAm) and lateral AI (KAlt). The superior position of Region 1 makes it unlikely that any portion of this classified lower-frequency sensitive region is shared with MA (ProA), because this anatomical area is observed to run along the inferior, antero-medial aspect of Heschl’s gyrus [29, 82].

Region 2 is postulated to span a border between medial AI (KAm) and the adjacent medial auditory area, MA (ProA). Region 2 is located on the antero-medial aspect of Heschl’s gyrus, equidistant from the centers of MA (ProA) and AI (KAm and KAlt)—approximately 9 mm medial of both (Figure 2-4). The proximity of Region 2 to areas MA (ProA) and AI (KAm and KAlt), under the assumption of mirror tonotopic maps, suggests that this classi-

Figure 2-4: Comparison of location of the activation foci of frequency sensitive regions to the centers of cytoarchitecturally defined auditory areas of Rivier and Clarke [82]. The average Talairach location of the activation foci of the four lower-frequency (squares) and four higher-frequency (circles) regions have been projected onto the anatomy of the $z = +9$ mm slice for session 3. The projected Talairach co-ordinates of the centers of the cytoarchitecturally defined auditory areas have been indicated as patterned triangles. Partially obscured symbols indicate a superior-inferior relationship. For example, area MA (ProA) is located on the antero-medial face of Heschl's gyrus where it folds back under the crown of the gyrus on which AI (KAm and KAlt) is located. The boundary of Heschl's gyrus within the $z = +9$ mm slice has been outlined in white to provide information about the relative anatomical position of each of the frequency sensitive regions.



□ Lower-frequency Sensitive Region

○ Higher-frequency Sensitive Region

▽ AA (PaAr)

▽ MA (ProA)

▽ AI (KAm and KAlt)

▽ STA (PaAe)

▽ LA (PaAi)

▽ PA (PaAc/d)

fied region represents a higher-frequency sensitive end of these two areas. Region 2 is likely to represent the antero-medial extent of koniocortex, and is most likely to be associated with medial AI (KAm). Region 2 is more distant from the centers of the other anatomically defined areas, the closest of which is PA (PaAc/d), 13 mm posterior of the activation focus. PA (PaAc/d) is sometimes observed to extend anteriorly across the medial end of Heschl's gyrus onto its antero-medial aspect [29]. Therefore, it is further possible that Region 2 may be associated with PA (PaAc/d) in addition to medial AI (KAm) and MA (ProA).

We propose that Region 3 spans a border between lateral AI (KAlt) and LA (PaAi). Region 3 is located almost directly posterior to Region 1, on or just posterior to Heschl's gyrus. Region 3 may be located in the sulcus just postero-lateral to Heschl's gyrus. We have previously noted that Region 1 is likely to be positioned at the antero-lateral end of koniocortex, approximately two-thirds of the length of the gyrus from its medial-most end. Koniocortex has been observed to extend into the sulcus posterior to Heschl's gyrus [29]. Therefore, the lateral and posterior limits of koniocortex coincide with the position of Region 3 leading us to propose that this classified region marks the postero-lateral extent of koniocortex, specifically lateral AI (KAlt). While Region 3 is located a distance (9 mm) from the center of AI that is consistent with the corresponding distances of Regions 1 and 2, Region 3 is actually closest (6 mm) to the center of LA (PaAi). LA (PaAi) is reported to run parallel to the posterior aspect of Heschl's gyrus, extending along the lateral half of the gyrus and onto the superior temporal gyrus immediately lateral to Heschl's gyrus [29]. As noted previously, Region 3 is located laterally, approximately two-thirds along the medial-lateral extent of Heschl's gyrus. This position suggests that Region 3 may represent the postero-medial extent of LA (PaAi). Under our assumption of mirrored frequency organization, we propose that Region 3 represents a higher-frequency sensitive end of both lateral AI (KAlt) and LA (PaAi).

It is possible that Region 3 also includes responses from two more auditory areas—PA (PaAc/d) and STA (PaAe). PA (PaAc/d) extends along the medial half of the posterior aspect of Heschl's gyrus, bordering laterally with LA (PaAi) [29, 82]. We have already proposed that Region 3 corresponds to the postero-medial end of LA (PaAi). This correspondence and the adjacency of LA (PaAi) and PA (PaAc/d) suggest that Region 3 may also represent a portion of PA (PaAc/d). STA (PaAe) runs parallel to LA (PaAi), bordering the latter anatomical area posteriorly in the superior temporal plane and laterally on

the superior temporal gyrus [29]. As with PA (PaAc/d), our proposed correspondence of Region 3 to the postero-medial end of LA (PaAi) and the adjacency of STA (PaAe) and LA (PaAi) argue for the possible inclusion of Region 3 at the postero-medial end of STA (PaAe).

We propose that Region 4, though located in the vicinity of koniocortex, only contains responses from PA (PaAc/d). The proximity of Region 4 to the center of PA (PaAc/d)—4.6 mm postero-medial of the center—makes it very likely that Region 4 represents a higher-frequency sensitive, postero-medial portion of this anatomical area (Figure 2-4). Two observations suggest that Region 4 is not adjacent to koniocortex, and thus does not represent the postero-medial extent of AI (KAm and KAlt). First, PA (PaAc/d) extends along the medial half of the posterior aspect of Heschl's gyrus and may extend over the medial-most end of the gyrus onto its antero-medial aspect (in the vicinity of Region 2) [29]. A significant portion of PA (PaAc/d) is, therefore, likely to be interposed between Region 4 and the center of AI (KAm and KAlt). Second, the distance of Region 4 from the center of AI (KAm and KAlt) is not consistent with the distance of other classified frequency sensitive regions that have been attributed to koniocortex. The activation focus of Region 4 is over 15 mm from the center of koniocortex, while the previously proposed antero-lateral (Region 1), antero-medial (Region 2) and postero-lateral (Region 3) extents were each only 9 mm from the center of AI (KAm and KAlt). Therefore, we only attribute Region 4 to PA (PaAc/d).

Region 5 is proposed to be shared by anatomical areas STA (PaAe) and LA (PaAi), possibly representing the anterior-most extent of each of these areas. Region 5 is located on the inferior, postero-lateral aspect of Heschl's gyrus, where Heschl's gyrus merges with the superior temporal gyrus. LA (PaAi) has been described above to run parallel to the posterior aspect of Heschl's gyrus, extending along the lateral half of the gyrus and onto the superior temporal gyrus immediately lateral to Heschl's gyrus. Region 5, located 14.5 mm antero-lateral (and inferior) of the center of LA (PaAi), could represent the antero-lateral end of this auditory area. STA (PaAe) was described above to run parallel to LA (PaAi) along its extent. Region 5, located inferiorly ($z = +2.4$ mm) is located 13 mm anterior of the center of STA (PaAe) and could mark the anterior extent of this inferiorly located ($z = +4$ mm) auditory area. Region 5 is unlikely to represent a higher-frequency response in AA (PaAr). AA (PaAr) is observed to extend anteriorly from the antero-lateral aspect

of Heschl's gyrus onto the superior temporal gyrus, but not to extend posteriorly onto the postero-lateral aspect of Heschl's gyrus [29].

We propose that Region 6, located on or immediately lateral to the superior, postero-lateral aspect of Heschl's gyrus, is wholly contained in LA (PaAi). Region 6 is located 11 mm antero-lateral of the center of LA (PaAi), 14 mm antero-medial and superior of the center of STA (PaAe) and 16 mm antero-lateral of the center of AI (KAm and KAlt). Region 6 is positioned appropriately to be contained within the extent of LA (PaAi), following along the posterior aspect of Heschl's gyrus. Therefore, Region 6 is at least partly attributed to LA (PaAi). Region 6 is located near the lateral one-third of Heschl's gyrus, outside the extent of koniocortex, precluding attribution of this classified region to AI (KAm and KAlt). STA (PaAe) is adjacent to LA (PaAi), posteriorly and laterally, along the length of LA (PaAi). It is possible for Region 6 to be shared with STA (PaAe) on this basis. However, our attribution of Region 5—7 mm inferior to Region 6 and only 3 mm lateral—to STA (PaAe), coupled with the inclusion of Region 6 in this anatomical area, would indicate that STA (PaAe) progresses from its center of mass anteriorly in the superior temporal plane prior to moving laterally and inferiorly onto the superior temporal gyrus. This description is inconsistent with the reports in the literature [29]. Region 6 is also unlikely to correspond to a portion of AA (PaAr) because of its location posterior to or on the postero-lateral aspect of Heschl's gyrus. Therefore, we hypothesize that Region 6 is only contained within LA (PaAi).

Region 7, located on or just anterior to the antero-lateral aspect of Heschl's gyrus, is proposed to represent a shared border between AA (PaAr) and MA (ProA). The activation focus of Region 7 is located only 3 mm lateral of the reported center of AA (PaAr), suggesting that Region 7 represents a lower-frequency response in this anatomical area. Because this frequency sensitive region is not in the vicinity of the medial two-thirds of Heschl's gyrus, it cannot be attributed to AI (KAm and KAlt). Region 7 may, however, represent a lateral, lower-frequency portion of MA (ProA), an anatomical area that runs along the inferior, anterior aspect of Heschl's gyrus to border, laterally, with AA (PaAr). Therefore, under the assumption of mirror frequency organization, Region 7 may be shared by these two anatomical areas. However, the interposition of the center of AA (PaAr) between Region 7 and MA (ProA) makes this proposal tenuous.

Region 8, located postero-lateral to Heschl's gyrus, on the superior temporal gyrus, is

hypothesized to represent a shared lower-frequency border between STA (PaAe) and LA (PaAi). Region 8 is located 5 mm postero-lateral of the center of mass of LA (PaAi) and 8 mm (4.8 mm postero-medial and 6 mm superior) from the center of STA (PaAe). Such close proximity to both areas suggests that Region 8 is partly contained in each, representing a lower-frequency sensitive portion of the postero-lateral border of LA (PaAi) with STA (PaAe). This suggestion is consistent with our knowledge that the posterior portion of STA (PaAe) abuts the posterior portion of LA (PaAi) [29].

2.4.3 Proposed Frequency Organization of Cytoarchitectural Areas

We first propose that koniocortex (AI; KAm and KAlt) contains two tonotopic maps, one corresponding to each of the two divisions proposed by Galaburda and Sanides (KAm and KAlt). Assuming that a characteristic frequency may be defined for most of the neurons in auditory cortex, and given our previously established correspondence of Regions 1 and 2 to portions of medial AI (KAm), our data suggest that this auditory area has a tonotopic map of lower- to higher-frequencies running across the superior surface of Heschl's gyrus from Region 1 to Region 2. Given our assumption that neighboring tonotopic maps may share a higher- or lower-frequency border, and our correspondence of Regions 1 and 3 to lateral AI (KAlt), we propose that the lateral division of koniocortex is tonotopically organized with lower- to higher-frequency sensitivity progressing from Region 1 to Region 3.

We propose that at least three non-primary auditory areas may exhibit a tonotopic organization. Auditory area LA (PaAi) may possess a tonotopic map progressing from lower-frequencies in Region 6 to higher-frequencies in Region 3, sharing this higher-frequency border with lateral AI (KAlt). LA (PaAi) may also exhibit a second tonotopic map in an anterior division—between Regions 5 and 6—organized as a mirror of the map between Regions 3 and 6. It is further possible that a third tonotopic map connects Region 3 to Region 8. We have previously proposed that both of these areas could be partly assigned to both LA (PaAi) and STA (PaAe). The interposition of the center of LA (PaAi) between Region 3 and Region 8 argues for this map to be assigned to this anatomical area. However, the largely lateral-to-medial orientation of this proposed tonotopic map would not be entirely consistent with the physical orientation of LA (PaAi), running parallel to the posterior portion of Heschl's gyrus and anteriorly on the superior temporal gyrus [29]. It is possible that Regions 6 and 8 could represent ends of iso-frequency contours in the proposed tonotopic

map between Regions 3 and 6, within LA (PaAi). It may be more likely, however, that the map between Regions 3 and 8 is contained within STA (PaAe), an anatomical area that extends along the superior temporal gyrus lateral to Heschl's gyrus and medially onto the superior temporal plane, posterior to LA (PaAi) [29]. A second possible tonotopic map, connecting lower-frequency Region 8 to higher-frequency Region 5, can also be proposed for STA (PaAe). This possible tonotopic map follows the expected course of STA (PaAe) along the lateral edge of the superior temporal plane. Last, we propose that cytoarchitectural area MA (ProA), situated on the anterior aspect of Heschl's gyrus, is tonotopically organized with lower-frequencies represented in Region 7 and higher-frequencies represented in Region 2.

The locations of our eight classified frequency sensitive regions do not support the proposal of a tonotopic maps within the two remaining cytoarchitectural areas—PA (PaAc/d) and AA (PaAr). While higher-frequency Region 4 seems likely to represent responses within PA (PaAc/d), no lower-frequency sensitive region was consistently (five sessions or more) observed near the medial end of Heschl's gyrus, precluding the assignment of a tonotopic organization to this auditory area. AA (PaAr) likely encompasses the activation focus of Region 7, but no classified higher-frequency sensitive regions were observed anterior to, or on, the antero-lateral aspect of Heschl's gyrus. Region 5, located on the inferior, posterolateral aspect of Heschl's gyrus, is unlikely to be connected to Region 7 by a tonotopic map because AA (PaAr) is not reported to extend so far posteriorly on Heschl's gyrus [29, 82].

2.4.4 Comparison to Human Functional Studies

Attempts to map tonotopic progressions in human auditory cortex using evoked magnetic fields (e.g. [10, 66, 67, 84]), evoked potentials (e.g. [5, 97]), a combination of these two techniques [65], positron emission tomography [45] and fMRI [98] have yielded mixed results regarding the presence, location and orientation of such progressions. Despite the variability in the observed organization of frequency sensitivity, we may still find correspondences between our proposed tonotopic maps and some of the maps that have been sampled in these other studies.

The estimated depth from the surface of the scalp of our proposed tonotopic organization for medial AI (KAm), taken from Figure 2-4, is in general agreement with the depth of the tonotopic progression observed for the sustained field (SF) of Pantev et al. [66], obtained

via magnetoencephalography and postulated to correspond to primary auditory cortex (AI). The depth from the scalp of the sustained field response generator was observed to increase from 3 cm for the lowest frequency presented (250 Hz) to 4 cm for the highest frequency presented (4000 Hz). These distances are in reasonable correspondence to the observed depths of Region 1 (approximately 3 cm) and Region 2 (approximately 5 cm) from the surface of the scalp.

The lateral tonotopic map from the evoked potential (N100) and evoked magnetic field (M100) literature coincides with our prediction of a tonotopic organization for cytoarchitectural area LA (PaAi). Analyses using M50 and N/M100 components to sample tonotopic progressions have suggested the presence of a map on or just posterior to Heschl's gyrus running from lower-frequencies, at a depth of 2 cm from the scalp, to higher-frequencies, at a depth of 3 cm from the scalp [5, 10, 65–67, 84, 97]. The location of this more lateral tonotopic progression is most nearly coincident with our proposed tonotopic mapping of the posterior portion of anatomical area LA (PaAi) in which lower-frequency sensitivity is represented by Region 6 (approximately 2 cm from the scalp) and higher-frequency sensitivity is represented by Region 3 (approximately 3.5 cm from the scalp). This argument is supported by the observation that the M100 response was generally parallel to and located approximately 1 cm more lateral than the MEG sustained field map [66] corresponding to AI, an orientation and position that roughly describes the position of this proposed map for LA (PaAi) relative to the map of medial AI (KAm).

The MEG observation of a 6 mm separation between generators for responses to frequencies two octaves apart was slightly smaller than the separation suggested by our fMRI responses to higher- and lower-frequency stimuli. The separation observed with MEG was derived from studies of the M100 response [10, 66, 67, 84, 101] that we have proposed to correspond to area LA (PaAi). The activation foci of Regions 3 and 6 were separated by 1.4 cm while our stimuli were separated by 2–4 octaves. These values suggest that the spatial representation of an octave may be as small as 3.5 mm or as large as 7 mm in this auditory area. A firm conclusion may not be drawn from these values, however, due to the coarse spatial resolution of our data (at least 3 mm due to reslicing), the variable center-frequencies of the higher- and lower-frequency stimuli, and the fact that we have not accounted for any spatial shift in the focus of activation due to the bandwidth of the instrumental music and noise stimuli used in four of the imaging sessions. Further, our distances

are computed between locations of statistical maxima, but the fMRI signal changes may not necessarily be proportional to changes in metabolic activity (e.g. [9]).

Our eight classified regions extend the picture of the spatial organization of frequency sensitivity in the superior temporal plane begun with PET and continued with fMRI. The fMRI study of Wessinger et al. [98] used two stimulus frequencies below 1 kHz, separated by four octaves, to observe separations of activation foci ranging from 0.0–15.7 mm. The response to the lower stimulus (55 Hz) was typically observed to be located more laterally than the response to the higher stimulus (880 Hz). This relationship between lower and higher frequency responses is consistent with that of Lauter et al. [45]. In this PET study, responses to two frequencies were sampled and it was observed that the response focus for the lower frequency stimulus (500 Hz) was more lateral on Heschl’s gyrus than the response focus for the higher frequency stimulus (4000 Hz). The gap between these two foci was 2.7 cm, a value that seems large compared to the MEG results (3 mm per octave [84]). Our findings are similar to those of the MEG and fMRI studies in that the low- and high-frequency regions separated by 2–4 octaves are typically less than 2 cm apart, suggesting that the regions from the PET study belong to different auditory areas. The medial high frequency response in the PET work appears to coincide well with Region 2, the higher-frequency sensitive end of primary auditory cortex (medial AI; KAm), but the location of the lateral low frequency response appears to be more consistent with the location of Region 6 than Region 1.

2.4.5 Comparison to Animal Studies

Results of fMRI studies on humans may be compared to electrophysiological studies of animals if we account for differences in the techniques. One difference is that an fMRI response results from a blood oxygenation level dependent (BOLD) process [44, 61] that may not be directly proportional to changes in neural firing rates [9, 20, 49, 50]. Further, fMRI responses are obtained by observing changes in blood flow, blood volume, and oxygen consumption that occur over the span of seconds [9, 38, 44, 51, 61], leading to a coarse temporal resolution. Combined with the coarse spatial resolution of fMRI (mm) compared to single unit recordings, the potential exists for fMRI to yield substantially different physiological assessments of a region of cortex than are obtained by single unit recordings. Also, fMRI studies are conducted on awake humans rather than anesthetized animals. While we have controlled for

arousal in our studies, the performance of a task is likely to change the underlying neuronal response compared to the passive state.

Despite these many differences, fMRI studies of the retinotopic organization of human visual cortex (e.g. [89,96]) have yielded maps that are similar to those obtained in monkey visual cortex by electrophysiological means. This suggests that we may use fMRI to obtain meaningful information about cortex that is related to the underlying neural activity, even if we are not able to make a point-by-point comparison between an fMRI map of physiological behavior and an electrophysiological map.

In our study of human auditory cortex, the number of proposed tonotopic maps compares well with the number of tonotopic maps in the auditory cortex of non-human primates and in the cat. We have observed what may be as many as seven tonotopic maps in the auditory cortex of the human. This number is comparable to the reported observation of four tonotopic maps in auditory areas of the cat (AI, A, P, VP) [40] along with some weakly tonotopic areas (e.g. AII). As many as four tonotopic maps have been observed in owl and rhesus monkeys. Two auditory areas (AI and RL or R) [41, 43, 52, 57] have been reported to be strongly tonotopic, while two more (AL and PL) [43, 58] were observed to be tonotopic over the extent they were mapped. While we have not assessed frequency sensitivity at threshold (characteristic frequency), moderate stimulus levels were utilized in these experiments to limit the response of a region of cortex to those frequencies contained in the tips of the tuning curves. Therefore, we anticipate that our observed organization of higher- and lower-frequency sensitivity will not differ significantly from that which would be observed using threshold stimulation levels.

2.4.6 Implications of Tonotopy

One implication of multiple tonotopically organized auditory areas is that these areas perform frequency-specific processing. This implication is well supported by the effect of the ablation of tonotopically organized primary auditory cortex on the sound-localization capabilities of cats [42]. In this study, cats were trained to walk to one of seven speakers from which a short duration tone or noise burst was emitted. Ablation of frequency-specific regions of the upper four layers of primary auditory cortex, while sparing all (tonotopic and non-tonotopic) secondary auditory areas, impaired the ability of the cats to localize tone bursts only for the frequency range ablated. This suggests that some information relevant

to the identification of the sound source is coded by place within the primary auditory cortex. Therefore, frequency specific function is demonstrated for primary auditory cortex.

Another implication of multiple tonotopically organized auditory areas is that these areas are functionally distinct. Again, the results of Jenkins and Merzenich [42] support this implication. Ablation of the upper layers in all (tonotopic and non-tonotopic) non-primary auditory areas, except for some portions of tonotopically organized VP, did not affect the ability to localize sound at any tested frequency. This finding is in contrast with the frequency-specific impairment resulting from localized lesions in primary auditory cortex. The observation of a behavioral deficit when primary auditory cortex was lesioned, but not when secondary auditory cortex was lesioned and primary auditory cortex spared, demonstrates a functional differentiation between the primary auditory area and the remainder of auditory cortex. These results are consistent with other studies in which sound localization deficits were observed in both cats and monkeys after lesions were induced in large portions of both primary and secondary auditory cortex [22, 36, 59].

Anatomical distinctions between the multiple auditory areas in monkeys further argue for functional differentiation of multiple tonotopically organized cortical areas. The auditory cortex of the macaque may be divided into three anterior-to-posterior groupings of anatomical areas: a central koniocortical “core,” a lateral “belt,” and a medial “root” [30]. Each of these divisions consists of four anatomical areas (“stages”) that are arranged in parallel across the three divisions. Corticocortical projections between these divisions indicate that the forward flow of information runs laterally, primarily from the core to the belt. The projections within each division suggest that the forward flow of information between stages within each division is from the posterior to the anterior. The three divisions (core, belt and root) may reflect the segregation of thalamocortical projections. From anatomical studies of both owl and rhesus monkeys, it is known that the koniocortical core receives inputs primarily from the ventral division (MGv) of the medial geniculate nucleus (MGN) while the belt and root regions receive thalamic inputs primarily from the magnocellular (MGmc) and dorsal (MGd) divisions of the MGN [57, 58]. The different stages within each of the parallel divisions also appear to receive different inputs, with the anterior anatomical areas receiving a greater proportion of inputs from the MGv, and the posterior anatomical areas receiving more inputs from the MGd [64]. The variable inputs to each of the auditory areas in the auditory cortex of the macaque make it seem likely that each area is func-

tionally distinct. Studies in the macaque suggest that the ablation of the anterior auditory areas results in greater impairment of both hearing thresholds [32] and the interpretation and retention of auditory stimuli [14] than ablation of the posterior auditory areas. This may illustrate a functional differentiation of secondary auditory areas.

It is likely that an organization of cytoarchitecture, connectivity and function similar to that observed in the macaque exists in the human auditory cortex. If so, the complex connectivity could indicate that tonotopic areas are organized in a hierarchical structure [39, 55], akin to that proposed for visual cortical areas [24], while the functional differentiation suggests that tonotopic areas are organized in a parallel processing structure (e.g. [78]) or a combination of both organizations.

Other animal studies, and the effects of strokes and lesions in the temporal lobes of humans, suggest that auditory cortex is critical for the temporal analysis of complex acoustic stimuli (e.g. [46]). Cats can still detect auditory stimuli and make gross frequency discriminations when much of auditory cortex has been ablated, but they are no longer able to discriminate between temporal patterns of stimulation [22, 60]. Similar findings exist in non-human primates, in which ablation of much of the superior temporal plane, including primary auditory cortex, hinders the ability to recognize and interpret complex stimuli (e.g. vocalizations) [31, 33, 34] and also impairs retention (memory) of acoustic stimuli [14]. The lesion-induced deficits in the recognition of vocalizations are consistent with the variable receptive language deficits reported in some human cases involving strokes or lesions of the temporal lobe (e.g. [15, 48, 81]). The deficits observed as a result of temporal lobe lesions suggest that complex temporal analysis of acoustic stimuli is performed at or above the level of auditory cortex. The preserved ability to detect the presence of a stimulus and to make gross frequency differences even after much of auditory cortex is ablated suggest that detection and basic frequency analysis are performed somewhere other than the primary auditory cortex and surrounding auditory areas.

The role of auditory cortex in the detection of acoustic stimuli could be partly elucidated for the human by examining whether abnormal activation in the superior temporal plane induces auditory hallucinations—a finding that would suggest that perception happens in or downstream from auditory cortical areas. A study by David et al. [19] of activity in sensory cortex during periods with and without auditory hallucinations (modulated by antipsychotic drugs) observed suppressed activation in response to speech stimuli during periods involving

auditory hallucinations. While not directly examining cortex, preliminary data from the study of patients with a maskable, unilateral tinnitus [91] reveals suppressed activation in the inferior colliculus, contralateral to the ear in which the tinnitus is perceived, during binaural presentation of white noise. Both of these studies indicate that the perception of a stimulus which is not physically present is coincident with abnormal metabolic activity in the auditory pathway.

In the case of the human, one area of great interest is the extent of the role of the primary and secondary areas in the processing of language. Intra-operative cortical stimulation has demonstrated the involvement of the auditory cortex in linguistic function (e.g. [62, 63]). However, whether the primary and secondary auditory areas perform processing specific to linguistic stimuli, or if lesions in these areas that produce language deficits (e.g. [15, 48, 81]) simply interrupt the pathway by which information reaches linguistic processing areas is uncertain.

The study of the tonotopic organization of the left vs. the right hemisphere may permit us to assess which regions in auditory cortex are most crucial to language. It is feasible to observe hemispheric differences in linguistic function by imaging the cortical response to the presentation of speech stimuli (e.g. [4, 6, 7, 21, 25]). Auditory cortical areas that exhibit hemispheric asymmetries are assumed to be specialized for linguistic processing in the hemisphere in which greater activation is observed. The study of the tonotopic organization of both hemispheres may reveal some aspect of the specializations that lead to the observed asymmetry in the response to speech stimuli. The capability for the right hemisphere to compensate for some lost linguistic abilities in humans with left hemisphere damage [1, 17] makes this investigation more complex, however. For example, areas in the right hemisphere may be capable of linguistic function but this capability may remain latent until the left hemisphere is disabled. It is uncertain if such areas would behave comparably under fMRI examination of the organization of frequency sensitivity. The majority of the data presented in this study (seven of eight sessions) were only from the left hemisphere. Experiments similar to those in this study could be conducted using our bilateral surface coils (Section 2.2.4) to obtain information from both hemispheres, permitting direct inter-hemispheric comparisons.

Chapter 3

Progressions of Frequency Sensitivity

3.1 Introduction

In the preceding chapter we demonstrated the presence of eight regions within the human auditory cortex that consistently exhibit sensitivity for either higher- or lower-frequency stimulation. We proposed a correspondence between these “frequency sensitive regions” and specific anatomically defined auditory areas. Certain pairs of higher- and lower-frequency sensitive regions may represent responses from different portions of the same auditory areas, suggesting that frequency sensitivity is spatially segregated within these areas. We argued that the spatial segregation of cortical frequency sensitivity observed with fMRI is consistent with an underlying tonotopic organization.

In this study, we used fMRI to assess whether the frequency sensitivity in auditory cortex varies continuously as a function of position. Specifically we measured activation in the superior temporal plane in response to repeated presentation of moderate intensity, bandlimited, swept stimuli in which the center-frequency and bandwidth co-varied exponentially as functions of time, examining whether regions of cortex exhibited a consistent time of response to each presentation of the swept stimulus. Any regions that did exhibit a consistent time of response were said to exhibit frequency sensitivity. The time of response was compared across regions of cortex and the order of response times was related to the order of center-frequency presentation within the swept stimulus. This relationship yields a

measure of “relative frequency sensitivity,” with earlier (later) responses indicating greater sensitivity for center-frequencies presented earlier (later) in the swept stimulus. The positional variation of the relative frequency sensitivity in the cortex was examined using a flat map of auditory cortex [18] to assess the continuity of the variation across the surface. We will argue that there is a tonotopic organization in those portions of cortex over which the relative frequency sensitivity varies continuously from higher- to lower-frequencies.

We have identified seven spatial progressions of frequency sensitivity. The endpoints of these spatial progressions correspond to seven of the eight frequency sensitive regions identified in the previous chapter. Our data, combined with previous anatomical work, lead us to suggest that five cytoarchitecturally defined auditory areas are tonotopically organized.

3.2 Materials and Methods

3.2.1 Subjects

Seven adult subjects (5 male, 2 female), ages 22–35, were imaged in 17 sessions. All subjects had normal hearing in the range from 100 Hz to 8000 Hz. Functional imaging was performed in two or more sessions on six of the subjects to assess the test-retest reliability of the experimental paradigm. Informed consent was obtained from the subjects prior to each imaging session. Experimental protocols were approved by human studies committees at the Massachusetts Institute of Technology, Massachusetts Eye and Ear Infirmary and the Massachusetts General Hospital.

3.2.2 Acoustic Stimulation

In each session, subjects were repeatedly stimulated monaurally in the right ear (16 sessions) or binaurally (1 session) with a narrow bandwidth, amplitude-modulated noise sweep. The center-frequency of the noise was varied exponentially over the course of 64 s between end frequencies of 125 Hz and 8000 Hz. The bandwidth of the stimulus co-varied with the center-frequency, being 0.3 octaves. A bandwidth proportional to the center-frequency was used based on evidence that the progression of characteristic frequencies is approximately logarithmic as a function of linear distance in the cortex of mammals [53]. Amplitude-modulation was at 8 Hz with a modulation index of 0.7. Eight sweeps were presented in

each functional imaging “run.” Within each run, the center-frequency in all eight sweeps was directed “Up” from 125 Hz to 8000 Hz or “Down” from 8000 Hz to 125 Hz. Between three and eight runs of a particular sweep were performed in each imaging session. Results focus on the six subjects (1–6) on whom both Up and Down sweep runs were performed.

Stimulus presentation levels were set at 35 (9 sessions) or 40 dB (8 sessions) above behavioral hearing thresholds measured under the same acoustic conditions as those present during functional imaging. Prior to the first imaging session for each of the subjects, hearing thresholds were obtained for 0.3 octave bandwidth, amplitude-modulated (8 Hz) noise for eight center-frequencies (100, 200, 500, 1000, 2000, 4000, 8000 and 10000 Hz) using a standard up-down method. Hearing threshold measurements were conducted during the acquisition of functional images to account for any masking due to imaging noise. The sweeps to be used for each subject were then generated on a Unix platform such that the intensity of the stimulus was a function of the center-frequency, following an interpolated (log-linear) threshold curve for the subject. All stimuli were played through LabVIEW on a Macintosh Quadra computer outfitted with a D/A board (National Instruments A2100), and presented via the pneumatic delivery system described in Section 2.2.2.

In 16 of the 17 sessions, subject attention to the stimulus was maintained by an intensity change detection task. Subjects were requested to attend to the stimulus and to raise their right index finger when they detected small (± 3 dB) intensity changes of 2 s duration that were incorporated into the sweep at random intervals (5–10 per 64 s sweep). These intensity changes were often difficult to detect because the intensity of the stimulus followed the subject’s interpolated audiogram, as described above. Subject performance was monitored by the experimenter. A run was discarded if the subject failed to detect at least 50% of the intensity changes. Subject motion was limited in all sessions through the use a dental bite bar made prior to each imaging session.

3.2.3 Imaging

Anatomical Imaging

High-resolution (1 mm \times 1 mm \times 1.2 mm) T₁-weighted “reference” anatomical images with high gray matter-white matter contrast were obtained in one imaging session for each of the seven subjects. Images were acquired for five subjects on a 1.5 T Siemens (Erlangen,

Germany) Vision imager and for two subjects on a 1.5 T General Electric (Milwaukee, WI) Signa imager. These high contrast images, acquired for the entire brain (128 slices), were required for the subsequent cortical flattening process (see Section 3.2.4) [18].

Functional Imaging

Each functional imaging session consisted of the same five segments of data collection as described in Section 2.2.3. All images were acquired on a General Electric 1.5 T Signa imager, equipped for echo-planar imaging by ANMR, Inc. (Wilmington, MA). For functional imaging, an asymmetric spin-echo acquisition sequence ($TE = 70$ ms, $\tau = -25$ ms, 128×64 acquisition matrix, in-plane resolution = 3.1 mm \times 3.1 mm, $TR = 2$ s) was used to acquire 256 images of each of eight (14 sessions) six (1 session) or five (2 sessions) axial oblique slices (3 mm thick with a 1 mm inter-slice gap). The imaged slices were selected to encompass Heschl's gyrus and much of the superior temporal plane. Images were acquired using the surface coils developed for the previous study (Section 2.2.4).

3.2.4 Data Processing

Cortical Flattening

The high-resolution T_1 -weighted "reference" anatomical image set obtained for each subject was used to generate a patch of flattened cortex containing much of the superior temporal plane, including Heschl's gyrus, Heschl's sulcus, and the superior temporal gyrus. The flattened cortex was generated using the procedure of Dale and Sereno [18] and is outlined here. First, the high contrast between gray matter and white matter in the reference images permitted the automated detection of the outline of the white matter in each slice. The slices were combined into a single three-dimensional volume and the surface of the white matter was constructed by "shrink-wrapping" the brain. This surface (Figure 3-1, part a) was then inflated, with minimized distortion, to eliminate the folding of the gyri and sulci (Figure 3-1, part b). In order to study the auditory cortex more effectively, a patch enclosing the superior temporal plane (black outline in Figure 3-1, part b) was computationally "cut" from the three-dimensional representation of the cortical surface. The patch was always selected to include Heschl's gyrus (HG), Heschl's sulcus (HS) and the superior temporal gyrus (STG). The remaining curvature of this patch was then removed, computationally,

to yield a flat patch of auditory cortex (Figure 3-1, patch c).

Functional Imaging Analysis

For the purpose of displaying responses on the patch of flattened cortex generated above, data from each functional session were registered to the reference anatomical images. First, the high-resolution T₁-weighted images acquired in each session immediately prior to the functional imaging runs were manually registered to the higher-resolution reference anatomical image set. Data from the functional runs were then aligned (SPM95 [28]) to the first images of the first functional run. The close temporal proximity of the first functional run to the T₁-weighted imaging segment should limit the amount of misregistration between maps of cortical responses and the underlying cortical anatomy from the higher-resolution reference images.

Functional imaging data were combined across runs and sessions to improve the detectability of responses to the stimulus. First, all runs of a single stimulus type (Up or Down sweep) conducted within each imaging session were averaged together. Each of these averaged data sets (one or two per imaging session) was analyzed in the Fourier domain to determine the magnitude and phase angle of the response of each voxel at the period of sweep presentation (once every 64 s) [89]. The Fourier magnitude and phase angle comprise the “average response vector” for each voxel. The phase angle is related to the average time of response during the sweep presentation,

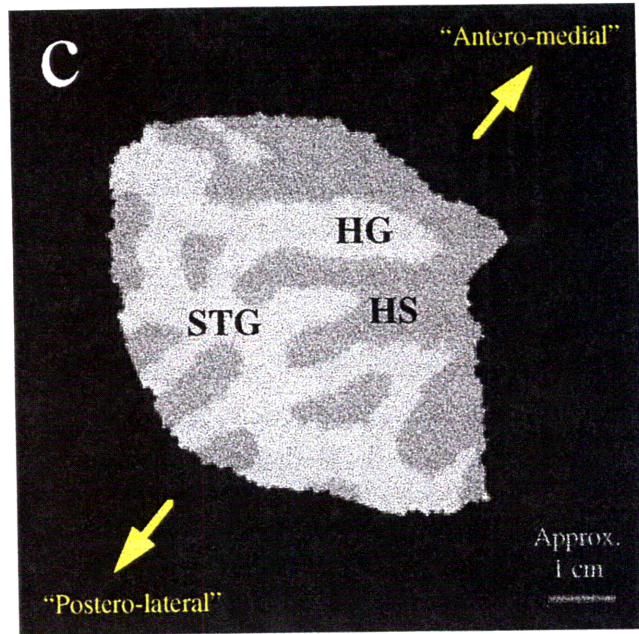
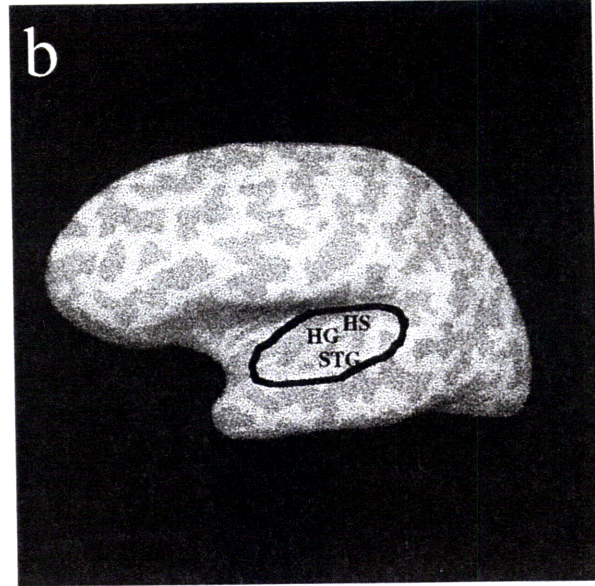
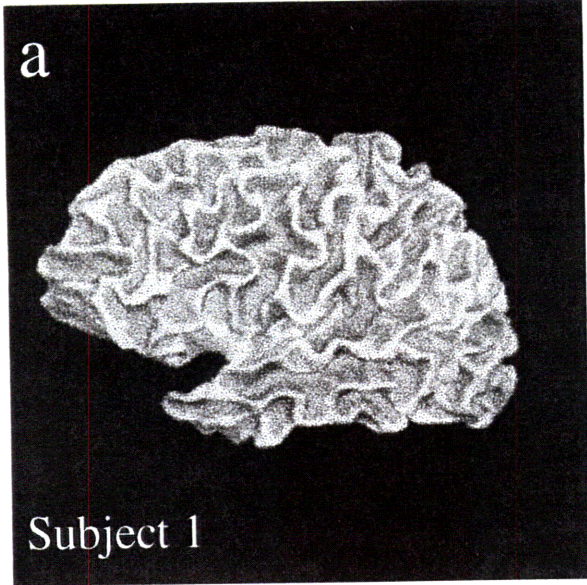
$$\text{average time of response} = \angle(\text{average response vector}) \times \text{sweep duration}$$

where the phase angle of the response vector is given as a fraction of one cycle. The average response vectors for the Down and Up sweeps were then mapped onto a three-dimensional representation of the cortical surface prior to inflation (e.g. Figure 3-1, part a). A “net response vector” was generated by adding, on the cortical surface representation, the responses to both Up and Down sweep stimulation:

$$\text{net response vector} = \frac{\sum_m(\text{Down response vector})}{m} + \frac{\sum_n(\text{Up response vector})^*}{n}$$

where * indicates the complex conjugate, m is the number of sessions in which Down sweeps were presented, and n is the number of sessions in which Up sweeps were presented. The

Figure 3-1: Generation of a flat patch of left auditory cortex (Subject 1) [18]. (a) Surface of white matter constructed from high-resolution (voxel size = $1 \text{ mm} \times 1 \text{ mm} \times 1.2 \text{ mm}$) anatomical images with high gray matter-white matter contrast. (b) Surface of white matter inflated and computationally area corrected to yield a smooth surface. Tops of gyri (defined by outward curvature) are colored light gray while sulci (defined by inward curvature) are colored a darker gray. Patch of the left superior temporal plane (black outline) is selected to contain Heschl's gyrus (HG), Heschl's sulcus (HS) and the superior temporal gyrus (STG). (c) The outlined patch in (b) is detached from the inflated surface, further flattened, and rotated to more closely resemble an axial image of the left superior temporal plane. After inflation and flattening, some spatial relationships are distorted. In general, however, a progression along the surface toward the upper right of the patch is antero-medial while a progression toward the lower left is postero-lateral.



conjugation takes into account the fact that the higher-frequencies presented early in a Down sweep are presented late in an Up sweep. The phase angle resulting from the presentation of an Up sweep should theoretically be complementary to the phase angle resulting from the presentation of a Down sweep. However, due to the onset and offset delays of the blood oxygenation level dependent (BOLD) fMRI response [2, 44] the responses to Up and Down sweeps are not ideal reversals of one another. When the Up sweep is conjugated for addition to the Down sweep, the BOLD response delays produce a phase angle mismatch, reducing the overall magnitude of the response and yielding a weighted-average measurement of the observed times of response. The Down sweep reference frame was selected because this stimulus was used in more imaging sessions (16 sessions) than the Up sweep (9 sessions). A preference for the Down sweep was based upon a desire to minimize any phase angle compression resulting from the lower-frequency bias of the tuning curves in the peripheral auditory system, but both sweep directions are required to determine if a region of cortex exhibits a progression of frequency sensitivity.

The net response vectors were analyzed using a Fourier f -test to compute the statistical significance of the response. If a region of cortex does not respond to the same frequency range for both Up and Down sweeps, the phase angles of the two responses will not be complements of one another and, after conjugation, will not add maximally. After sufficient averaging, response vectors in regions of cortex that are not frequency sensitive should have a magnitude approaching zero, a random phase angle, and thus no statistical significance.

Based upon the order of presentation of center-frequencies in the Down sweep, a correspondence may be established between phase angle (proportional to average time of response) and relative frequency sensitivity. If we compare two arbitrary locations on the cortical surface, the location with the lower phase angle (earlier response) is more sensitive to a higher band of frequencies than the location with the higher phase angle (later response). Conversely, the location with the higher phase angle (later response) is more sensitive to a lower band of frequencies than the location with the lower phase angle (earlier response). Therefore, the phase angle for cortical regions exhibiting statistically significant ($p < 0.01$, f -test) responses was indicated in color on the flattened cortical patch, with the particular color serving as an indication of relative frequency sensitivity.

The relative nature of the assessment of sensitivity precludes the assignment of absolute frequency sensitivity (e.g. 1 kHz) to any portion of cortex. However, over the entire surface

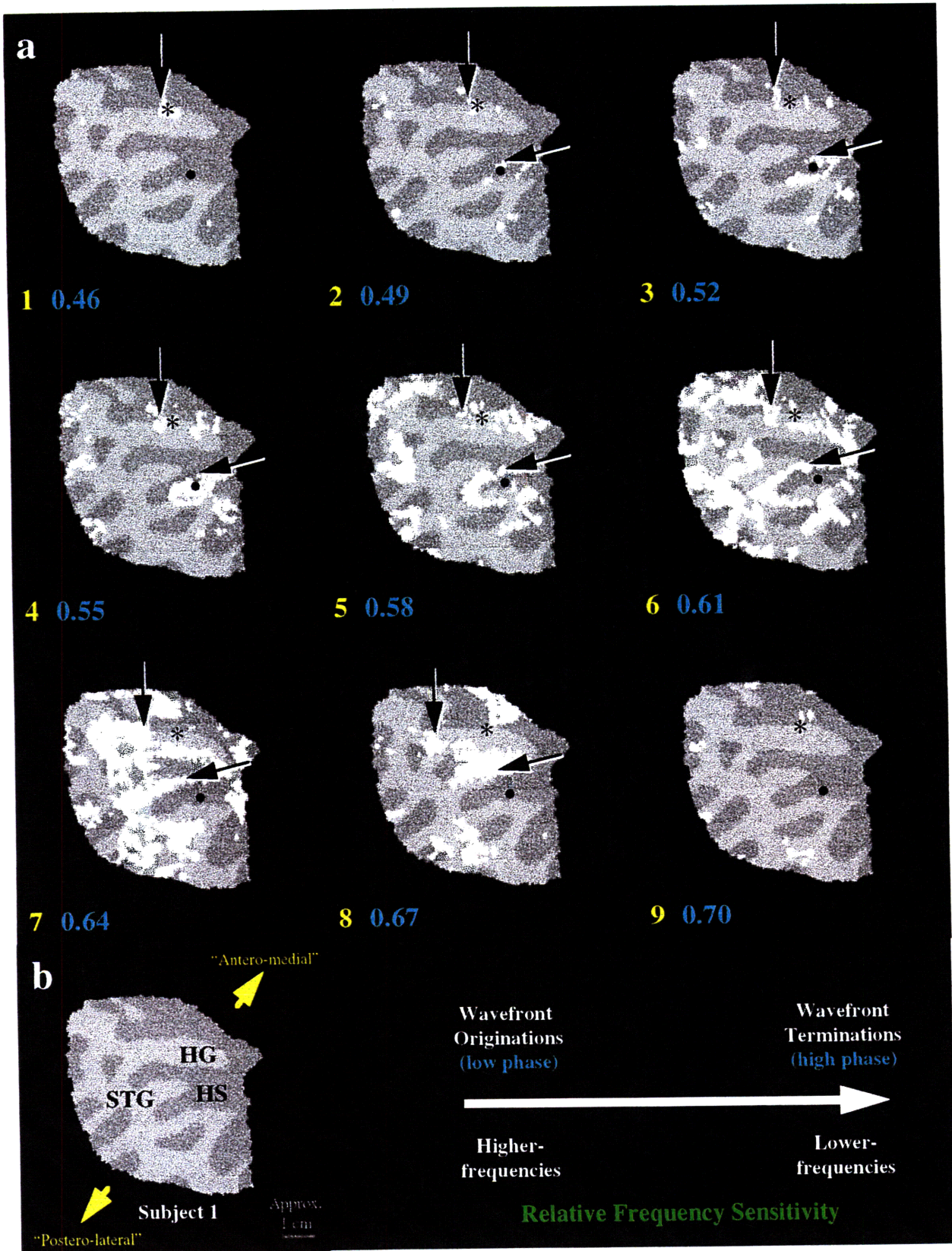
of the auditory cortex, those portions that exhibit lower phase angles than the remainder of the cortex are the most sensitive to higher-frequency stimulation (“higher-frequency regions”). Similarly, those portions of the cortex that exhibit higher phase angles than the remainder of the cortex are the most sensitive to lower-frequency stimulation (“lower-frequency regions”). This classification permits us to examine progressions of frequency sensitivity (as measured in Chapter 2) without assigning an absolute frequency sensitivity to any portion of the cortex.

3.3 Experimental Results

3.3.1 Identification of Frequency Sensitivity in Response to Swept Stimuli

“Wavefronts”—contours of voxels exhibiting the same average time of response (iso-angle contours)—of statistically significant activation ($p < 0.01$, f -test) were observed to move across the auditory cortex in response to stimuli that were swept in frequency (Figure 3-2). The nine panels (1–9, yellow numerals) in part a of Figure 3-2 display, on the flattened cortex of Subject 1 (Figure 3-2, part b), nine sequential wavefronts (white) progressing from earlier responses (phase angle = 0.46, blue numerals) in panel 1 to later responses (phase angle = 0.70) in panel 9. The movement of the wavefronts across the surface of the cortex may be observed by comparison of the position of two of the wavefronts (down and left arrows) to their sites of origin—the locations of earliest response (star and dot, respectively). The star and dot in each panel of Figure 3-2 are in fixed anatomical positions. The star is located on the antero-medial aspect of Heschl’s gyrus (HG in Figure 3-2, part b), and the dot is located in the posterior portion of Heschl’s sulcus (HS in Figure 3-2, part b). Two wavefronts have been indicated by the arrows to demonstrate the manner in which the wavefronts move across the surface of the cortex. First, observe that the wavefront anterior to Heschl’s gyrus (down arrow) “originates” at the location indicated by the star in panel 1 and moves laterally (left in Figure 3-2) in panels 2–7. In panel 8, the wavefront merges with other wavefronts and “terminates” on the lateral aspect of Heschl’s gyrus. The second highlighted wavefront (left arrow) “originates” at the location indicated by the dot in Heschl’s sulcus, in panel 2 of Figure 3-2. This wavefront progresses antero-laterally (toward the top left of the figure) in panels 2–7, before it “terminates” just posterior to Heschl’s gyrus in panel 8. Other wavefronts may be observed in this figure, but a description of their movement will wait

Figure 3-2: Spatial progression of iso-angle contour “wavefronts” on flattened patch of the left superior temporal plane for Subject 1. (a) Wavefronts (indicated in white) for nine phase angles (blue numerals). The earliest responses are shown in panel 1 (phase = 0.46) and the latest responses are in panel 9 (phase = 0.70). Observe the continuous spatial progression of the wavefronts across the surface of the cortex from their origination (panels 1–4) to their termination (panels 7–9). Two example wavefronts have been indicated by the down and left arrows. The wavefront indicated by the down arrow originates in panel 1 on the antero-medial aspect of Heschl’s gyrus (star), moves laterally (left) in panels 2–7, and terminates on the antero-lateral aspect of Heschl’s gyrus in panel 8. The second example wavefront (left arrow) originates in the posterior portion of Heschl’s sulcus (dot) in panel 2, moves antero-laterally (toward the top left) in panels 3–7, and terminates just posterior to Heschl’s gyrus in panel 8. A correspondence may be made between the time of presentation of center-frequencies within each repeated Down sweep and the average time of response (proportional to phase angle). Earlier response times (lower phase angles) indicate greater sensitivity to higher-frequency stimulation (“higher-frequency regions”) than later response times (higher phase angles) that, in turn, indicate greater sensitivity to lower-frequency stimulation (“lower-frequency regions”). (b) Anatomy of left superior temporal plane patch for Subject 1 (HG—Heschl’s gyrus; HS—Heschl’s sulcus; STG—superior temporal gyrus).



until Section 3.3.4. Phase angle values are in the Down sweep reference frame (Section 3.2.4) so regions of cortex exhibiting an earlier response (lower phase angle) are responding to higher frequencies than regions of cortex exhibiting a later response (higher phase angle). Therefore, the locations from which the wavefronts originate are “higher-frequency regions” and the locations at which the wavefronts terminate are “lower-frequency regions.”

In order to more easily examine the spatial organization of frequency sensitivity across our subjects, the data of all nine panels of Figure 3-2, part a, is summarized in a single image (Figure 3-3, part b). In Figure 3-3, the time of response (phase angle) is indicated for all locations achieving the $p < 0.01$ significance level (f -test) by a color overlay on the (grayscale) patch of flattened cortex. The correspondence between pseudo-color and phase angle is illustrated in Figure 3-3, part a, in which the wavefront progressions of Figure 3-2 have been reproduced in white overlaid on the pseudo-color map that depicts the phase angle at each point on the flattened cortical surface. Note that Figure 3-3 does not utilize the full dynamic range of the pseudo-color map (colorbar at bottom of Figure 3-3) due to the relatively narrow (0.35 cycles) range of phase angles observed in the cortex for this subject. The compression of the range of the full pseudo-color map into this range of phase angles would create an image with sharper color contrast, making it more difficult to observe the smooth positional variation of phase angle. In Figure 3-3, part b, earlier responses are colored red and purple, later responses are colored cyan, and intermediate responses are blue. Observe that the highlighted wavefronts of Figure 3-2 (down and left arrow) originate in red regions in Figure 3-3 (panels 1 and 2, star and dot) and terminate in cyan regions (panel 8). Using our previously established correspondence between the time of response and frequency sensitivity, higher-frequency regions in Figure 3-3 are colored red and purple while lower-frequency regions are colored cyan. If the full dynamic range of the pseudo-color map (colorbar at bottom of Figure 3-3) is utilized, the visual representation of an ordered progression of frequency sensitivity (tonotopic map) is a color gradient that varies from red and purple to blue to cyan and green as the frequency sensitivity varies from higher- to lower-frequency.

3.3.2 Intra-Subject Comparison of Frequency Sensitive Regions

For two subjects, the relative frequency sensitivity revealed by the swept stimuli will be compared to the frequency sensitive regions observed in response to the non-swept stimuli

Figure 3-3: Spatial progression of iso-angle contour “wavefronts” and pseudo-color map of phase angle overlaid on left superior temporal plane patch for Subject 1. (a) Wavefronts (indicated in white) for the same nine phase angles (blue numerals) as in Figure 3-2, overlaid on pseudo-color map of phase angle (relative frequency sensitivity). The pseudo-color map has, in turn, been overlaid on the (grayscale) flattened patch of the left superior temporal plane of Figure 3-1, part c. The earliest responses are shown in panel 1 (phase = 0.46) and the latest responses are in panel 9 (phase = 0.70). Observe the continuous spatial progression of the wavefronts across the surface of the cortex from their origination (panels 1–4) to their termination (panels 7–9). The two example wavefronts (down and left arrows) of Figure 3-2 have been reproduced in this figure. Earlier response times (lower phase angles) indicate greater sensitivity to higher-frequency stimulation (“higher-frequency regions”) than later response times (higher phase angles) that, in turn, indicate greater sensitivity to lower-frequency stimulation (“lower-frequency regions”). Observe that wavefronts “originate” in regions colored red and purple (e.g. locations of star and dot), and “terminate” in regions colored cyan. This figure does not utilize the full dynamic range of the pseudo-color map (colorbar, bottom) due to the relatively narrow (0.35 cycles) range of phase angles observed in the cortex. The compression of the range of the full pseudo-color map into this range of phase angles would create an image with sharper color contrast, making it more difficult to observe the smooth positional variation of phase angle. (b) Left superior temporal plane patch (grayscale) for Subject 1 overlaid with pseudo-color map of phase angle (relative frequency sensitivity) and outline of cortical anatomy (white). Anatomical landmarks are same as in Figure 3-2. Earlier response times (higher-frequencies) are colored red and purple, intermediate response times are colored blue, and later response times (lower-frequencies) are colored cyan.

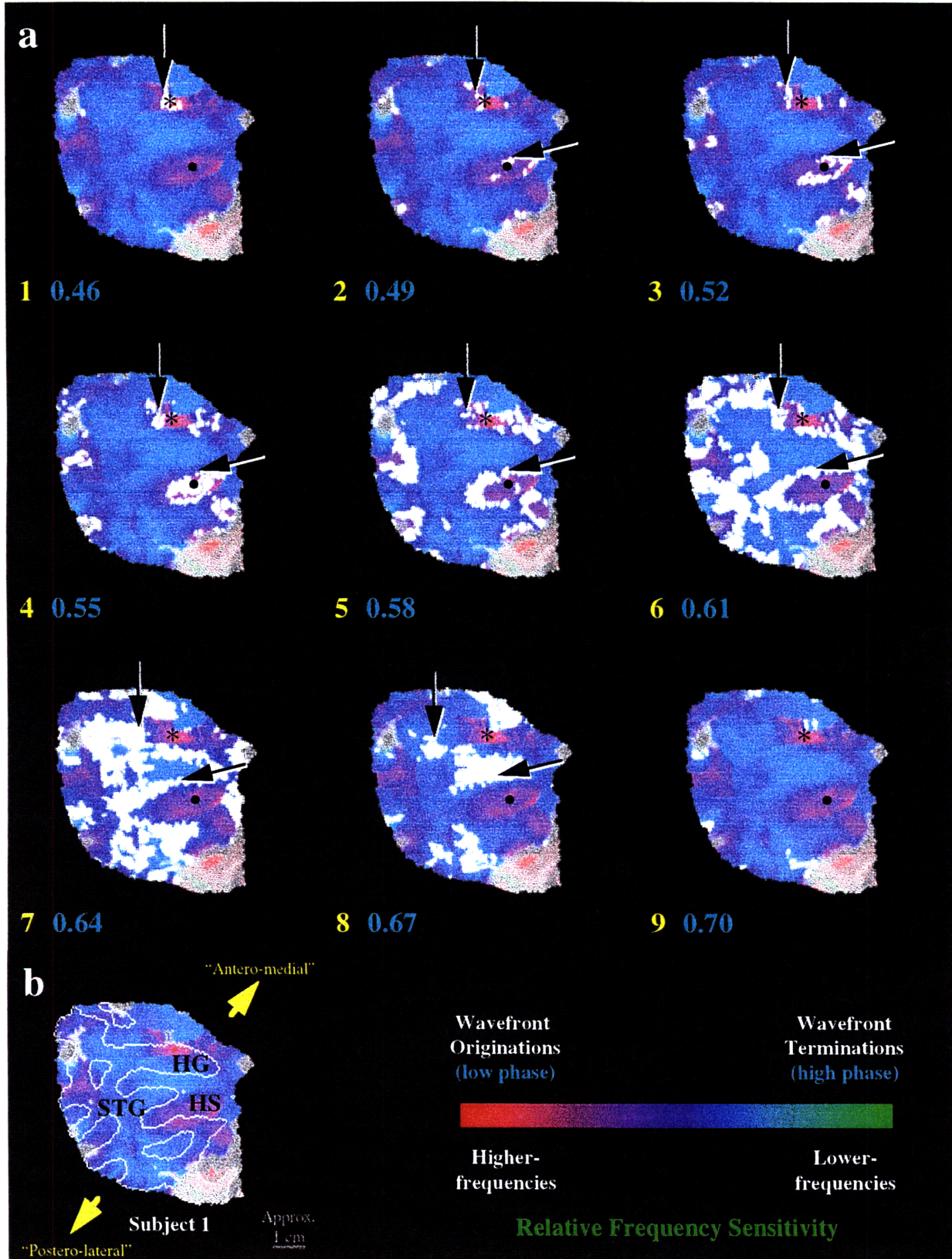
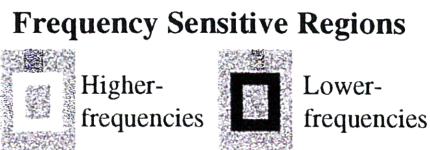
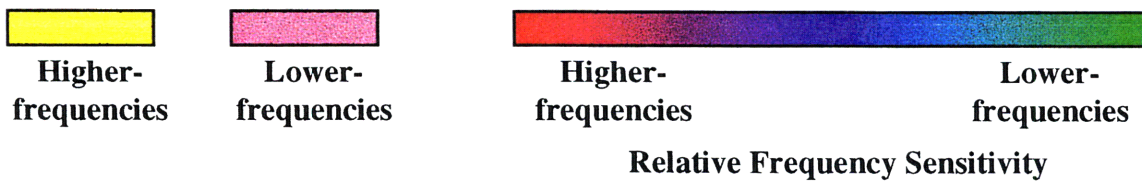
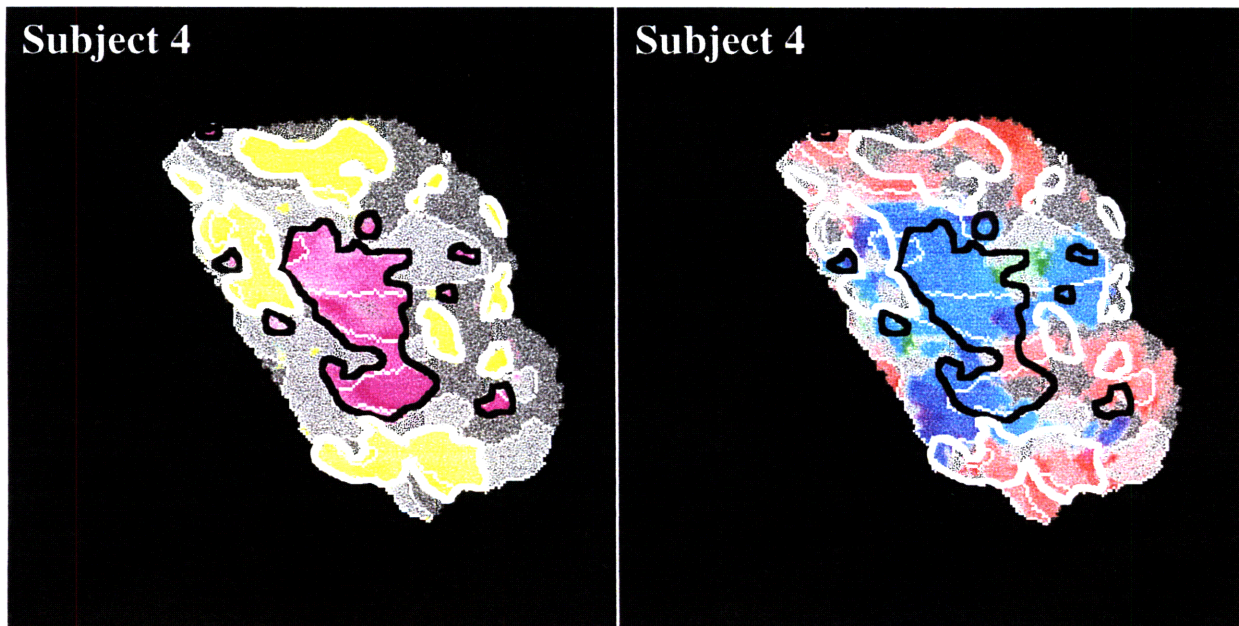
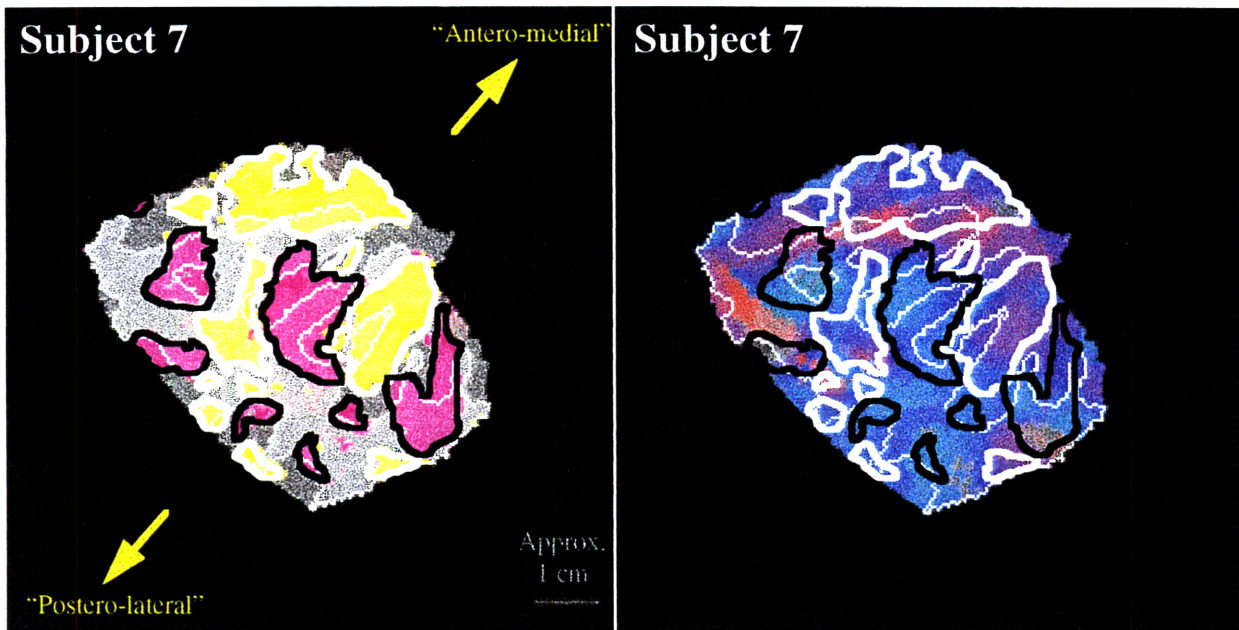


Figure 3-4: Comparison of frequency sensitivity in the left superior temporal plane as assessed by (left) presentation of two sustained, non-swept stimuli with different center-frequencies and (right) average time of response to swept stimuli. *Left*: Statistically significant ($p < 0.05$, normalized t -statistic) data from session 6 (top, Subject 7) and session 8 (bottom, Subject 4) of Chapter 2 have been displayed on (grayscale) flat patches of auditory cortex for the two subjects. Higher-frequency (Lower-frequency) response regions are colored yellow (magenta). Thick white (black) outlines indicate the spatial extent of the higher-frequency (lower-frequency) sensitive regions for comparison at right. *Right*: Pseudo-color map of frequency sensitivity of statistically significant ($p < 0.01$, f -test) responses to swept stimuli overlaid on (grayscale) flat patches of auditory cortex for the same subjects as at left. The relationship between color and relative frequency sensitivity in the swept stimulus results at right is the same as in Figure 3-3. Results for Subject 7 are from one session of Down sweeps; results for Subject 4 are from two sessions of Down sweeps and two sessions of Up sweeps. Outlines of regions of higher- and lower-frequency sensitivity as determined in Chapter 2 (left) have been reproduced on the maps of relative frequency sensitivity (right). Observe that the black outlines largely enclose blue, cyan and green colored regions, indicating intermediate- and lower-frequency sensitivity for these portions of cortex when responding to swept stimuli. The white outlines, in contrast, mostly encompass red, purple and blue regions indicating intermediate- and higher-frequency sensitivity for these portions of cortex when responding to swept stimuli. Some of the higher-frequency sensitive regions at left (white outlines) encompass mostly blue or cyan regions at right, particularly in Subject 7 (top). This demonstrates that the relative frequency sensitivity revealed by the swept stimuli is different in some portions of cortex than the frequency sensitivity revealed by non-swept stimuli. Careful examination reveals, however, that the frequency sensitivity within most of the white outlines (higher-frequency regions) is, in fact, higher than that within nearby black outlines (lower-frequency regions). This indicates that the positional variation of relative frequency sensitivity is consistent between the two studies. The thin lines in all parts of the figure are the outline of the cortical anatomy.

Response to Non-Swept Stimulus

Response to Swept Stimulus



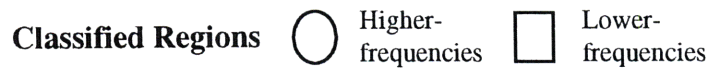
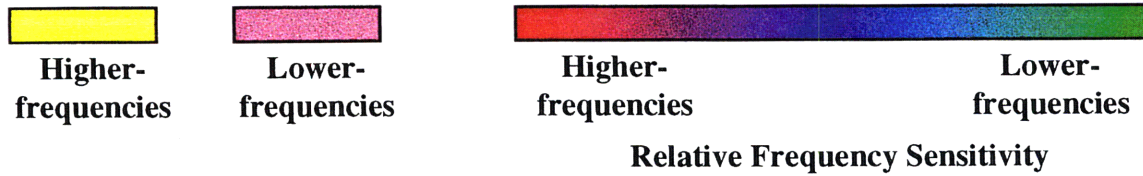
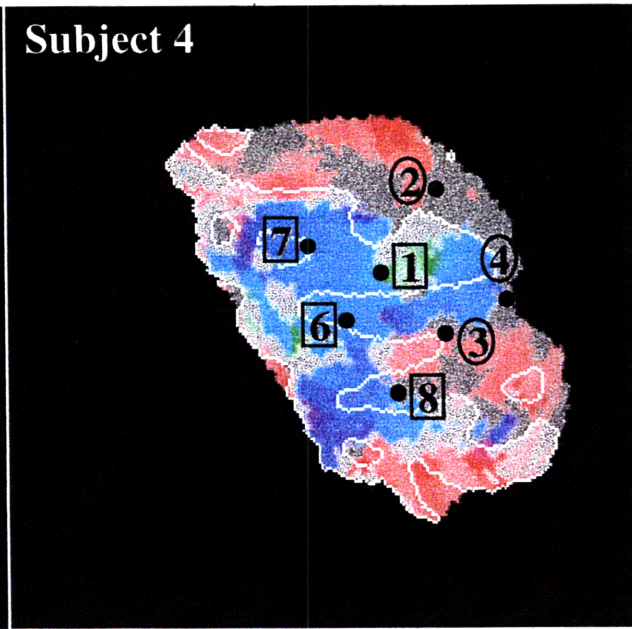
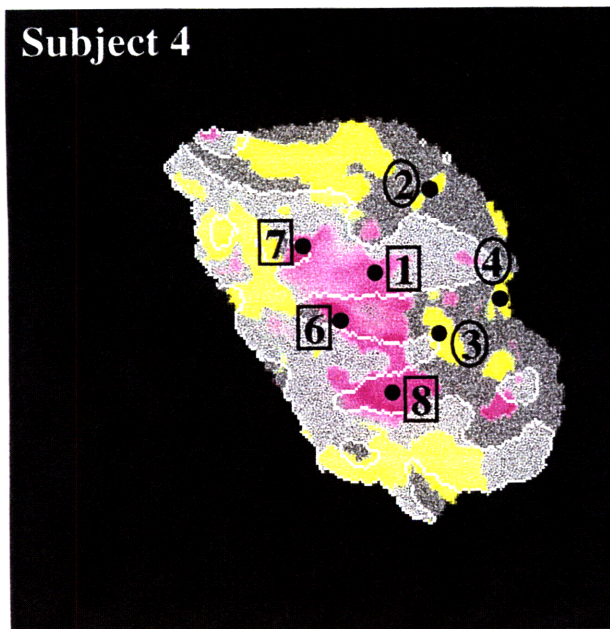
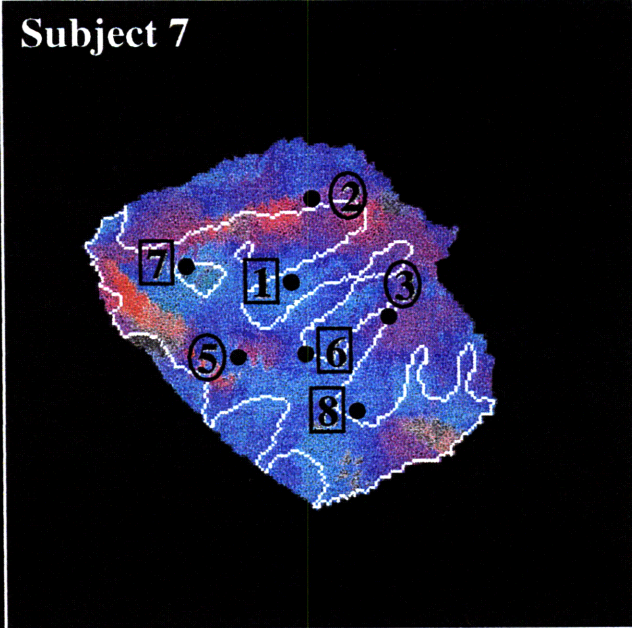
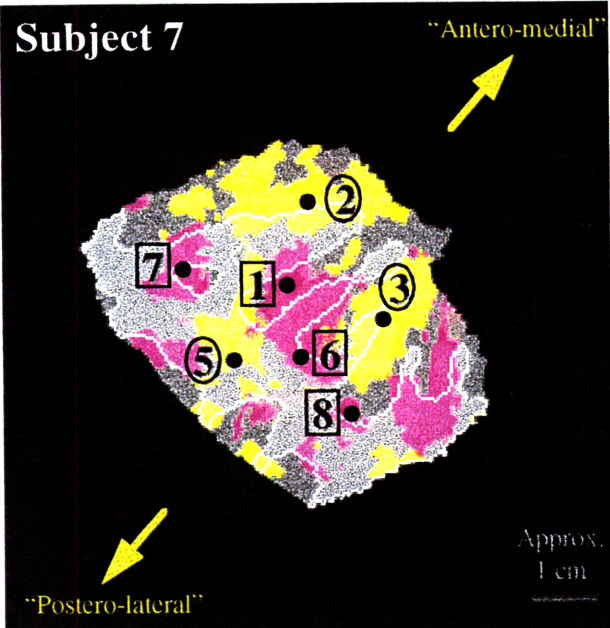
of the previous study (Chapter 2). In Figure 3-4, results for Subjects 4 and 7 from imaging sessions conducted using (left) non-swept and (right) swept stimuli are presented. The non-swept data at left were presented in Chapter 2 as (top, Subject 7) session 6 and (bottom, Subject 4) session 8. In Figure 3-4, left, the full spatial extents of the (classified and unclassified) higher- and lower-frequency sensitive regions achieving the normalized significance level of $p < 0.05$ (t -test) have been displayed on (grayscale) flat patches of auditory cortex. At right the pseudo-color maps of relative frequency sensitivity have been overlaid on the same (grayscale) flat patches of auditory cortex as at left. The outlines of the observed frequency sensitive regions at left are reproduced at right. Observe that most of the lower-frequency regions at left (thick, black outlines) enclose blue, cyan and green colored regions at right. Some black outlines do, however, contain some red and purple regions. From our previously determined correspondence of color to frequency sensitivity, the blue, cyan and green regions indicate that the swept stimulus paradigm has revealed the majority of these “lower-frequency sensitive” regions to be most sensitive to intermediate- and lower-frequency stimulation. The higher-frequency regions from the non-swept sessions (thick, white outlines at left) tend to enclose red, purple and blue regions at right. Note that some of the white outlines do not contain any red or purple regions, particularly in Subject 7. Therefore the swept stimulus paradigm has revealed the majority of the “higher-frequency sensitive regions” at left to be most sensitive to both intermediate- and higher-frequency stimulation.

The activation foci of seven of the eight classified frequency sensitive regions of Chapter 2 (Table 2.1) are observed to exhibit the same (lower- or higher-frequency) sensitivity in response to both swept and non-swept stimuli (Figure 3-5). The Talairach locations of the activation foci of each of the seven regions observed in sessions 6 and 8 (Subjects 7 and 4, left) were identified and indicated on the flat patches of auditory cortex by a dot, with the black numerals corresponding to the number of each region. Observe that the activation foci of lower-frequency Regions 1 and 6–8 are located in magenta regions while the activation foci of higher-frequency Regions 2–5 are located in yellow regions. Note that multiple activation foci (e.g. Regions 1, 6 and 8) may be observed within a single region of statistically significant activation ($p < 0.05$, normalized t -statistic). In the pseudo-color maps of relative frequency sensitivity at right, note that the activation foci of lower-frequency Regions 1 and 6–8 are located in regions that are colored blue, cyan or green, while the activation

Figure 3-5: Comparison of frequency sensitivity at the locations of the eight classified frequency sensitive regions (Regions 1–8) from Chapter 2. Dots indicate the Talairach locations of the activation foci for the classified frequency sensitive regions observed in session 6 (top left, Subject 7) and session 8 (bottom left, Subject 4) from the previous study. The numbers of the classified regions are indicated by black numerals, with the type of region indicated by the surrounding square (lower-frequency) or circle (higher-frequency). Region 4 was not observed in session 6 (Subject 7) and Region 5 was not observed in session 8 (Subject 4). Observe at right that the foci of the lower-frequency sensitive regions (Regions 1, 6–8) are located in blue, cyan or green regions, while the foci of three of the higher-frequency regions (Regions 2, 3 and 5) are located in or in the immediate vicinity of red or purple regions. Regions 2 and 4 in Subject 4 (bottom right) are the only exceptions, with no significant ($p < 0.01$, f -test) activation observed at the corresponding Talairach location in response to the swept stimuli. For Region 2, the coloration of the nearest statistically significant activation (red) is consistent with the expected higher-frequency sensitivity. For Region 4, however, the coloration of the nearest statistically significant activation (blue) is not consistent with the higher-frequency sensitivity predicted from Chapter 2. For a description of the underlying color images, see Figure 3-4.

Response to Non-Swept Stimulus

Response to Swept Stimulus



foci of higher-frequency Regions 2, 3 and 5 are located in or in the immediate vicinity of regions that are colored red or purple. In Subject 4, the activation foci of Regions 2 and 4 were not located in regions that exhibited statistically significant activation in response to the swept stimuli. For Region 2 the coloration of the nearest significant activation (red) is consistent with the higher-frequency sensitivity observed in Chapter 2. This is not the case for Region 4, for which the coloration of the nearest significant activation (blue) is more consistent with a region of lower-frequency sensitivity. The correspondence between the coloration and frequency sensitivity indicates that the cortex in the immediate vicinity of the activation foci of Regions 2, 3 and 5 is sensitive to higher frequencies than the cortex surrounding the activation foci of Regions 1 and 6–8. These results are in agreement with the classification of frequency sensitivity from Chapter 2.

Note also in Figure 3-5 that the activation foci observed for the non-swept stimuli are not necessarily located at the precise points of origination or termination of wavefronts (earliest or latest responses) observed for the swept stimuli. In contrast, the full spatial extents of the higher- and lower-frequency sensitive regions (Figure 3-4) often encompassed portions of red and green regions. These observations support our previous assumption (Section 2.4) that an fMRI response would be observed from the cortical regions tuned to the highest and lowest CFs even though the probable CFs in these regions were not contained in the spectra of the non-swept stimuli.

3.3.3 Inter-Subject Comparison of Frequency Sensitive Regions

The frequency sensitive organizations revealed by presentation of the swept and non-swept stimuli were compared across subjects by examining the frequency sensitivity indicated by the swept stimulus at the average locations of the eight classified frequency sensitive regions (Regions 1–8, Table 2.1). The average Talairach co-ordinates were examined because runs of the stimulus paradigm from Chapter 2 were not conducted on all subjects. Dots located at the average Talairach co-ordinates of the corresponding activation foci were overlaid, in Figure 3-6, on the pseudo-color maps of frequency sensitivity for all six subjects on whom both Down and Up sweep runs were conducted. The numerals next to the dots and surrounding square (lower-frequency) or circle (higher-frequency) indicate the classification of each activation focus. The underlying anatomy of each of the flat patches (Figure 3-7) is outlined in white. In Figure 3-7 HG denotes Heschl's gyrus, HS denotes Heschl's sulcus, and

STG denotes the superior temporal gyrus. Note that, in Subjects 2 and 3, Heschl's gyrus is bisected by the intermediate transverse sulcus, leading to the identification of first (HG-1) and second (HG-2) Heschl's gyri, anterior to Heschl's sulcus [76]. Consistent localization of an activation focus in a region of higher- or lower-frequency sensitivity permits us to establish a correspondence between the two.

The frequency sensitivity of seven of the eight frequency sensitive regions (Regions 1–3, 5–8) identified in the previous study was found to be consistent between the swept and non-swept stimuli. For all six subjects (Figure 3-6), the average Talairach co-ordinates of the foci of these seven regions were located within one standard error of regions of appropriate frequency sensitivity. An assessment of the standard error may be obtained from a comparison of the location of the average activation foci depicted on Subject 4 in Figure 3-6 with the exact location of the activation foci for Subject 4 in Figure 3-5. The activation focus of Region 4 was only observed to be located in a higher-frequency sensitive region in four subjects in this study (Subjects 1, 3, 5 and 6), though it was located within one standard error of higher-frequency regions (red) in Subjects 2 and 4.

Lower-Frequency Sensitive Regions

The average Talairach co-ordinates of the activation foci of all four classified lower-frequency sensitive regions from Chapter 2 (Regions 1, 6–8; Table 2.1) were observed to be located in regions of lower-frequency sensitivity (cyan and green regions) in at least five of the six subjects of Figure 3-6. The activation focus of Region 1 was, in all six subjects, encompassed by a lower-frequency region located (Subjects 1, 4–6) on the posterior portion of Heschl's gyrus (HG) or (Subjects 2–3) in the intermediate transverse sulcus between the first and second Heschl's gyri (HG-1 and HG-2). The activation focus of Region 6 was always located within a lower-frequency region that was postero-lateral to Heschl's gyrus. This focus was located just lateral to (Subjects 1, 2 and 4), or in (Subject 5), the intermediate transverse sulcus. In Subjects 3 and 6, the focus of Region 6 was located laterally on the superior temporal gyrus, just posterior to the intermediate transverse sulcus. The activation focus of Region 7 was observed in a lower-frequency region on (Subjects 2, 4–6), or just anterior to (Subjects 1 and 3), the antero-lateral end of Heschl's gyrus. This lower-frequency region always extended onto the main body of Heschl's gyrus and encompassed Region 1. The lower-frequency region also extended to include Region 6 in Subjects 1–4 and 6. In four

Figure 3-6: Flattened cortical patches of the left superior temporal plane for Subjects 1–6 overlaid with pseudo-color maps of relative frequency sensitivity. Pseudo-color overlay is of statistically significant ($p < 0.01$, f -test) responses to repeated presentation of the swept stimuli. Early responses (higher-frequency sensitivity) are colored red and purple, later responses (lower-frequency sensitivity) are colored cyan and green, and intermediate responses are colored blue. The underlying anatomical landmarks from Figure 3-7 are outlined in white. The pseudo-color map varies between subjects depending upon the range of observed phase angle values (from 0.25 cycles for Subject 5 up to 0.8 cycles for Subject 6). This method precludes assignment of absolute frequency sensitivity to any point on the cortex. Black dots are located at the average Talairach co-ordinates of the eight classified frequency sensitive regions (Regions 1–8; Table 2.1) from Chapter 2, with the classification of each activation focus indicated by the nearby number and its surrounding square (lower-frequency) or circle (higher-frequency). Approximate antero-medial to postero-lateral axis runs from the upper right of each patch to the lower left.

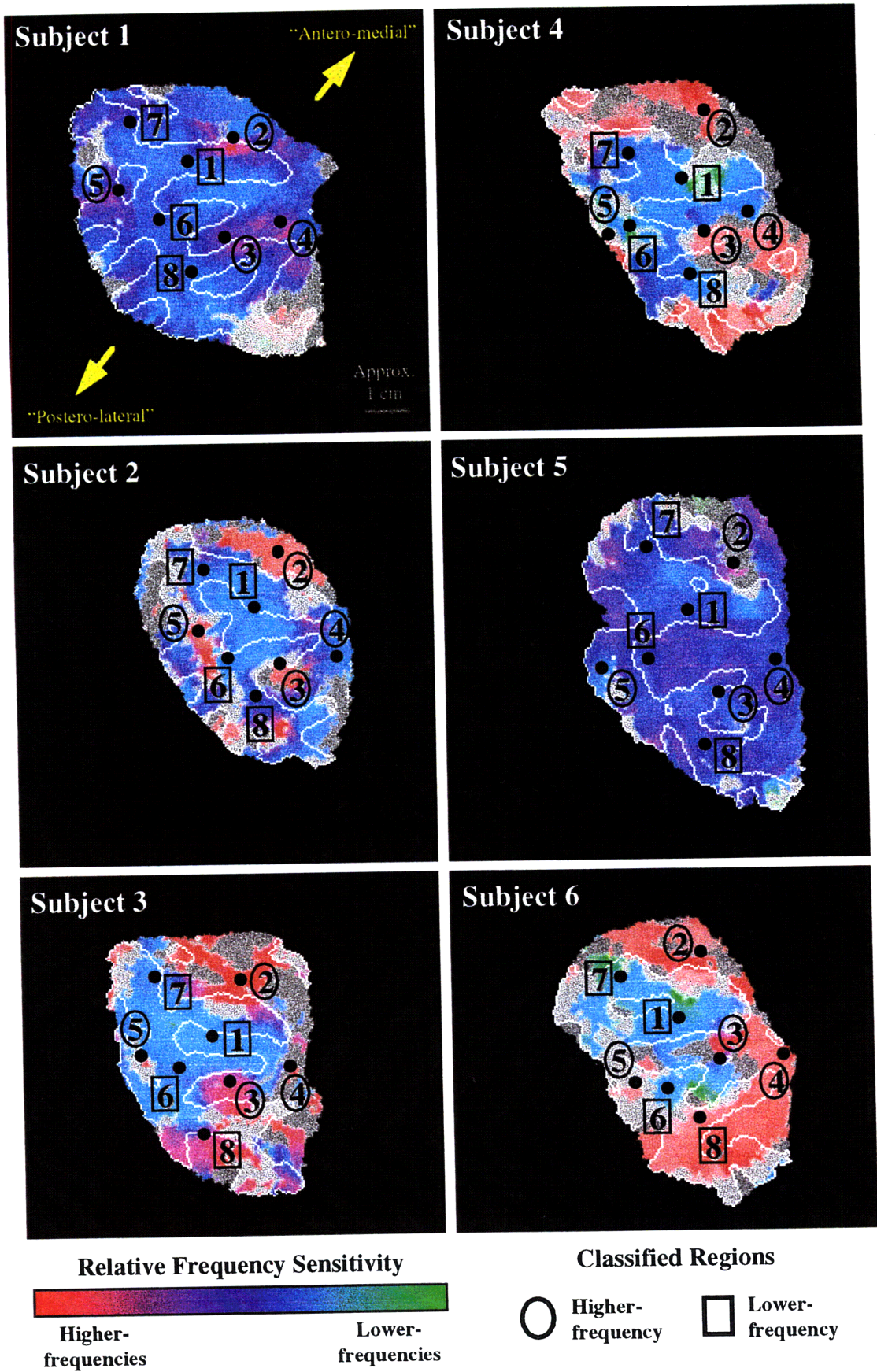
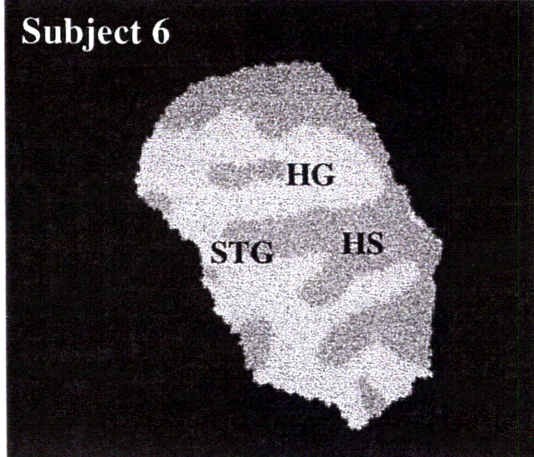
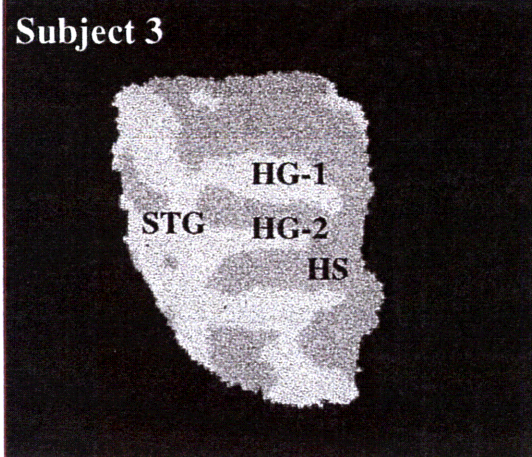
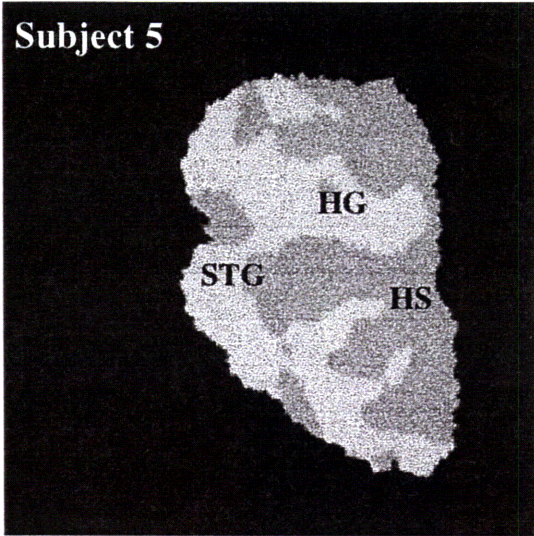
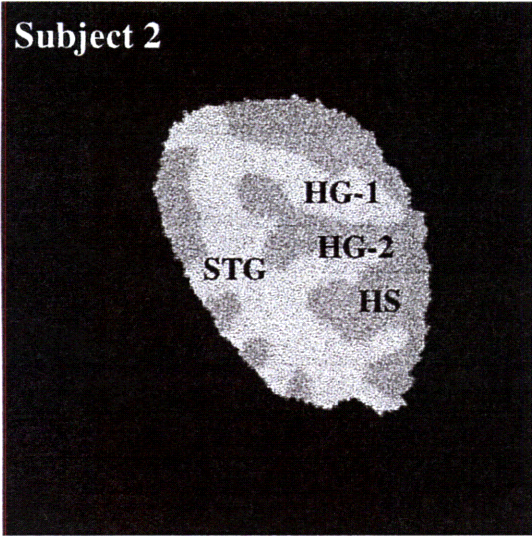
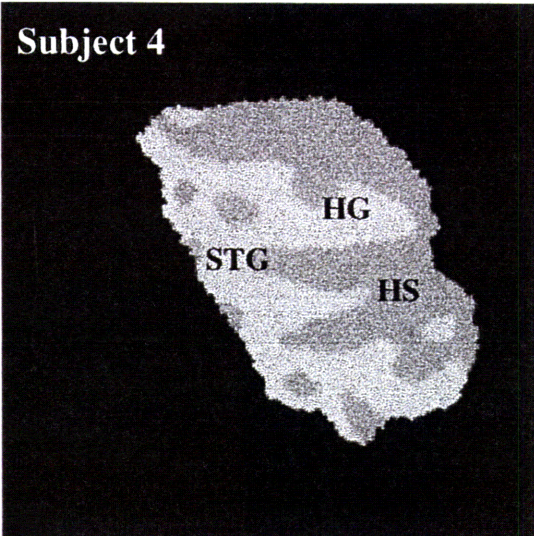
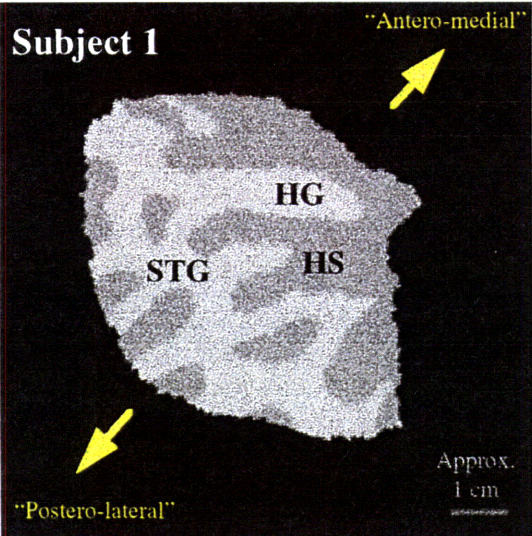


Figure 3-7: Flattened cortical patches of the left superior temporal plane for Subjects 1–6. Tops of gyri (defined by outward curvature) are shown as light gray, while sulci (defined by negative curvature) are shown as a darker gray [18]. Patches were selected to include Heschl’s gyrus (HG), Heschl’s sulcus (HS) and the superior temporal gyrus (STG), along with the posterior portion of the superior temporal plane. In Subjects 2 and 3 the intermediate transverse sulcus divides Heschl’s gyrus into the first (HG-1) and second (HG-2) Heschl’s gyri. Patches are oriented to resemble axial images of the left superior temporal plane, as shown in Chapter 2. Approximate antero-medial to postero-lateral axis runs from the upper right of each patch to the lower left.



of six subjects (Subjects 1, 2, 4 and 5) the activation focus of Region 8 was located in a lower-frequency region on the superior temporal gyrus, postero-lateral to Heschl's sulcus. In Subject 3 the focus of Region 8 was located at the posterior edge of a lower-frequency region situated postero-lateral to Heschl's sulcus. Region 8 was located in a higher-frequency region postero-lateral to Heschl's sulcus in Subject 6, within one standard error of a lower-frequency region in the postero-lateral portion of Heschl's sulcus.

Higher-Frequency Sensitive Regions

The average Talairach co-ordinates of the activation foci of three of the four classified higher-frequency sensitive regions (Regions 2, 3 and 5; Table 2.1) were observed in at least five subjects to be located in higher-frequency sensitive regions (red and purple regions) in Figure 3-6. In all six subjects the activation focus of Region 2 was observed to be located within a higher-frequency region on the antero-medial aspect of Heschl's gyrus. In Subjects 1, 3 and 6 this higher-frequency region extended onto the surface of the gyrus (defined by outward curvature). The activation focus of Region 3 was found to be encompassed by a higher-frequency region in the posterior portion of Heschl's sulcus in Subjects 1-4. In Subject 6 the focus of Region 3 was just at the postero-lateral edge of a higher-frequency region in a similar location. In Subject 5 the focus of Region 3 was encompassed by a lower-frequency region located on the posterior aspect of the gyrus posterior to Heschl's sulcus. This focus was observed to be within one standard error of an antero-medially located higher-frequency (purple) region. For Subjects 1, 2 and 6, the activation focus of Region 5 was found to be encompassed by a higher-frequency region located on the inferior portion of the superior temporal gyrus, postero-lateral to Heschl's gyrus (Subjects 1 and 6) or the first Heschl's gyrus (Subject 2). In Subjects 3 and 4 the focus of Region 5 was located just anterior to a (small) higher-frequency region in a location similar to that of Subjects 1, 2 and 6—postero-lateral to the first Heschl's gyrus for Subject 3, postero-lateral to Heschl's gyrus for Subject 4. The focus of Region 5 was encompassed by a lower-frequency region in Subject 5, but a higher-frequency (purple) region was observed to be located anteriorly, within one standard error.

3.3.4 Observed Frequency Sensitive Progressions

Seven wavefronts (e.g. Figure 3-3, down arrow) were observed that moved across the cortical surface between higher- and lower-frequency region endpoints in at least three of six subjects. These “progressions” (A–G, Table 3.1; Figure 3-8) were identified in each subject by visually identifying the location of statistically significant ($p < 0.01$, f -test) higher- (red and purple) and lower-frequency (cyan and green) regions in Figure 3-6, and examining the wavefronts for continuity as they moved between these regions using images of the wavefront positions at equally spaced phase angles (e.g. Figure 3-3). It should be noted that the stepped progression of wavefronts in Figure 3-3, part a, and the pseudo-color map of frequency sensitivity in Figure 3-3, part b, contain precisely the same information. Therefore, all described progressions may be observed, for appropriate subjects, in Figure 3-6, though the continuity of the frequency sensitivity is acknowledged to be more readily observed in the stepped progressions. When describing the progressions of frequency sensitivity we shall use the convention that higher-frequency regions (earlier response times) are where wavefronts “originate” and that lower-frequency regions (later response times) are where wavefronts “terminate.”

Progression	Number of Subjects in which Progression was Observed
A	6/6
B	5/6
C	5/6
D	5/6
E	4/6
F	4/6
G	3/6

Table 3.1: Rate of occurrence of progressions of frequency sensitivity

Progression A was observed in all six subjects in Figure 3-6. This progression originated in the higher-frequency region containing the activation focus of Region 2 and terminated in the lower-frequency region corresponding to Region 1. The trajectory of this wavefront progression is illustrated in Figure 3-8 by a line connecting these two classified regions.

Progression B (Subjects 1–4, 6) originated in the higher-frequency region corresponding to Region 3 and terminated in the same lower-frequency region as Progression A (Region 1). The left arrow in Figures 3-2 and 3-3 followed the course of this progression. A line

connecting Region 3 to Region 1 in Figure 3-8 summarizes this progression.

Progression C (Subjects 1–3, 5 and 6) originated in the same higher-frequency region as Progression A (Region 2) and terminated in the lower-frequency region that contained the focus of Region 7. The down arrow in Figures 3-2 and 3-3 followed this progression. The trajectory of Progression C is illustrated by a line from Region 2 to Region 7 in Figure 3-8.

Progression D (Subjects 1–4, 6) was observed to originate in the same higher-frequency region as Progression B (Region 3) and to terminate in the lower-frequency region containing the focus of Region 8 in Subjects 1–4, and just antero-medial to the focus of Region 8 in Subject 6. Therefore, Progression D is illustrated in Figure 3-8 by a line connecting Region 3 to Region 8.

Progression E (Subjects 1–4) originated in the same higher-frequency region as Progressions B and D (Region 3) and terminated in the lower-frequency region that contained the activation focus of Region 6. Progression E is summarized in Figure 3-8 by a line originating in Region 3 and terminating in Region 6.

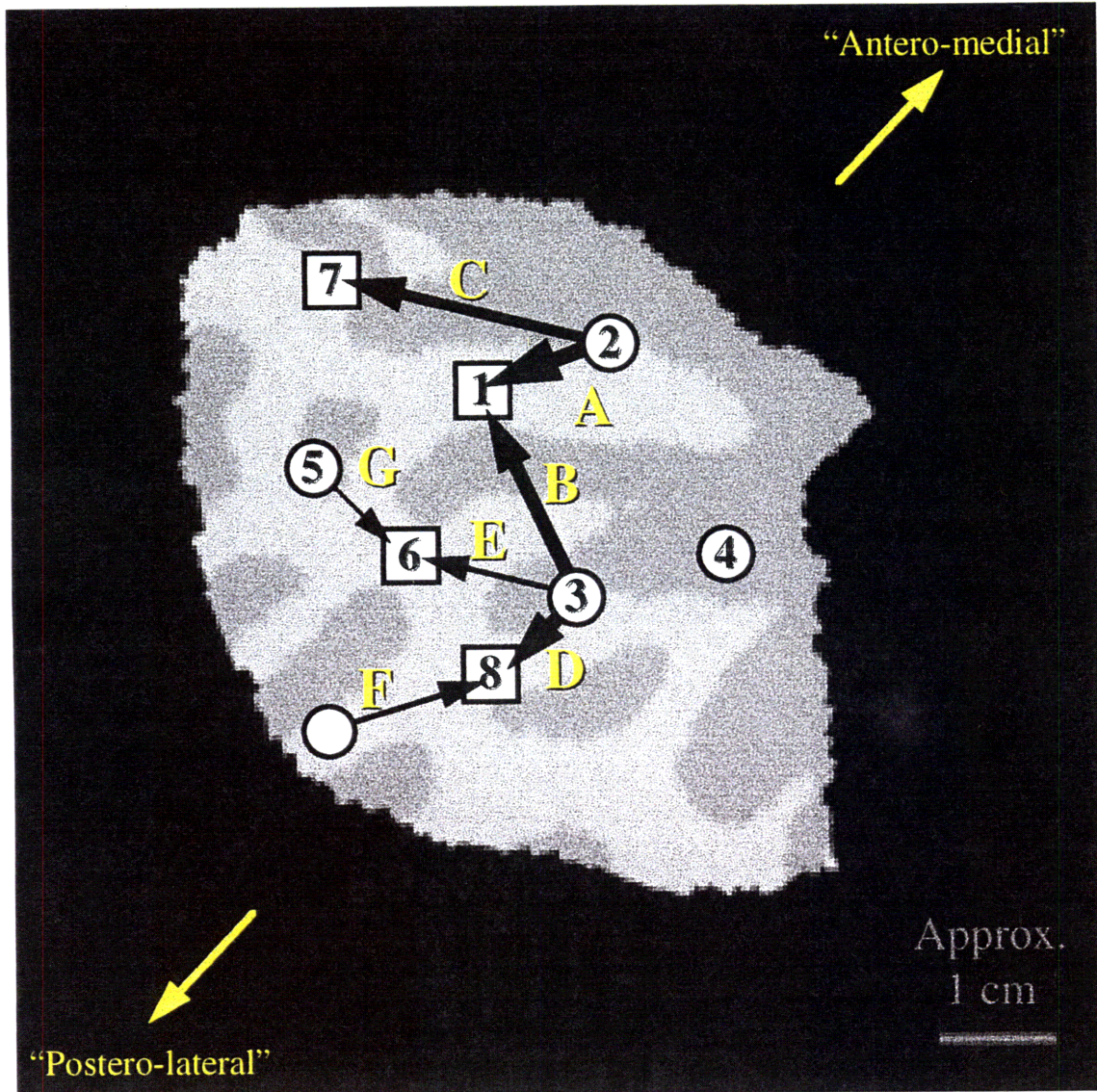
Progression F (Subjects 1–4) originated in a higher-frequency region located posterolateral and inferior to Heschl's sulcus, and terminated in the same lower-frequency region as Progression D (Region 8). The higher-frequency region in which Progression F originated was not classified in Chapter 2 because a higher-frequency sensitive region was not observed in at least five of the eight sessions near this location—Talairach co-ordinates $(x,y,z) = (-57.3 \pm 2.3, -31.0 \pm 1.0, 6.8 \pm 1.7)$. This (unlabeled) higher-frequency region has been indicated in Figure 3-8 along with a line indicating the trajectory of Progression F, terminating in Region 8.

Progression G (Subjects 1, 2 and 4) was observed to originate in the higher-frequency region corresponding to Region 5, and to terminate in the same lower-frequency region as Progression E (Region 6). Progression G is summarized in Figure 3-8 by a line connecting these two classified regions.

3.4 Discussion

Seven progressions (A–G) of frequency sensitivity were observed in this study and are summarized in Figure 3-8. The progressions effectively interconnect seven of the eight frequency sensitive regions classified in Chapter 2. In the previous chapter we proposed a correspon-

Figure 3-8: Summary of wavefront progressions (A–G) in Subject 1 that were observed in the left superior temporal plane in at least three of six subjects. Arrows illustrate the trajectory of wavefront progressions, originating in higher-frequency regions (circles) and terminating in lower-frequency regions (squares). The thickness of each arrow is related to the number of subjects in whom the progression was observed (A: six subjects; B, C, D: five subjects; E, F: four subjects; G: three subjects). Progressions B and C were indicated the left and down arrows, respectively, in Figures 3-2 and 3-3. Classified frequency sensitive regions (Regions 1–8) have been placed at the average Talairach co-ordinates of the corresponding activation foci from the previous chapter (Table 2.1). The unlabeled higher-frequency sensitive region on the postero-lateral superior temporal gyrus indicates the average origin of Progression F on the lateral to inferior surface of the superior temporal gyrus. This region was not observed in at least five sessions in the previous study (Chapter 2). Note that the wavefronts do not necessarily originate or terminate at the precise location of the classified frequency sensitive regions. Rather, Regions 1–8 serve as convenient landmarks to describe the spatial extent of the wavefront progressions.



Lower-frequency Sensitive Region ← Progression of Frequency Sensitivity → Higher-frequency Sensitive Region

dence between the eight frequency sensitive regions and the underlying anatomical auditory areas. We also proposed the existence of seven tonotopic maps where pairs of higher- and lower-frequency regions apparently correspond to particular anatomical areas. We may now use the established relationship between our observed progressions and the seven spatially distinct frequency sensitive regions to test and extend our previous hypotheses regarding the tonotopic organization within human auditory cortex.

3.4.1 Tonotopic Organizations in Human Auditory Cortex

We propose that both medial AI (KAm) and lateral AI (KAlt) are tonotopically organized. In the previous chapter we established a correspondence between medial AI (KAm) and Regions 1 (lower-frequency) and 2 (higher-frequency) based upon their proximity to the center of Rivier and Clarke's AI [82] (Figure 2-4) and their positions on Heschl's gyrus, relative to the reported extent of koniocortex [29,76]. In this study we have observed that Progression A (Figure 3-8) originated in the higher-frequency region corresponding to Region 2 and terminated in the lower-frequency region corresponding to Region 1. Therefore, we propose that Progression A connects lower- to higher-frequency sensitivity in cytoarchitectural area medial AI (KAm)—a tonotopic map. In the previous chapter lateral AI (KAlt) was hypothesized to include portions of Regions 1 and 3, the foci of which were typically contained within the lower- and higher-frequency regions at the origination and termination endpoints of Progression B (Figure 3-3, left arrow). Therefore, we propose that lateral AI (KAlt) is also tonotopically organized.

We propose that three of the non-koniocortical auditory areas—MA (ProA), LA (PaAi) and STA (PaAe)—are tonotopically organized, as hypothesized in Chapter 2. In the previous study we established a correspondence of MA (ProA) to higher-frequency Region 2 and also, though more tentatively, lower-frequency Region 7. We then proposed a possible tonotopic map connecting Region 2 to Region 7 in MA (ProA). Progression C (Figure 3-3, down arrow) was observed to connect the higher-frequency region corresponding to Region 2 to the lower-frequency region corresponding to Region 7 (Figure 3-8), suggesting that MA (ProA) does, indeed, possess a tonotopic map. Regions 3 and 6, the endpoints of Progression E (Figure 3-8), were related to portions of LA (PaAi) in the previous study based upon proximity to the center of LA (PaAi) and the anatomical extent of this auditory area. The observation of Progression E is in agreement with our previously hypothesized tonotopic

organization for LA (PaAi), connecting lower-frequency Region 6 to higher-frequency Region 3. Frequency-sensitive regions corresponding to Regions 3 and 8 were found to be the endpoints of Progression D, suggesting the presence of a tonotopic map connecting these two regions. Region 8 was previously proposed to be located at the border between LA (PaAi) and the posterior portion of STA (PaAe) while Region 3 was proposed to represent the shared boundary of lateral AI (KAlt), LA (PaAi), PA (PaAc/d) and STA (PaAe). We have already proposed a tonotopic organization within LA (PaAi) originating at Region 3 and terminating at Region 6 (Progression E), and suggested in Chapter 2 that it was possible that Regions 6 and 8 might represent the ends of iso-frequency contours in LA (PaAi). This hypothesis is unlikely to be true, because the wavefronts for Progressions D and E diverge in order to terminate in Regions 6 and 8 (Figures 3-3 and 3-6). The rejection of this hypothesis suggests that Progression D is an independent tonotopic map. In Chapter 2 we concluded that the orientation of this proposed map was not consistent with the known anatomical extent of LA (PaAi), and chose to attribute this possible map to STA (PaAe). Therefore, we propose that Progression D represents a separate tonotopic map from Progression E, and that this map is contained within a postero-medial division of STA (PaAe).

We propose that LA (PaAi) contains a second tonotopic map, as hypothesized in Chapter 2. LA (PaAi) runs parallel to the lateral half of the posterior aspect of Heschl's gyrus and antero-laterally onto the superior temporal gyrus [29]. Higher-frequency sensitive Region 5 was attributed, in part, to the anterior end of LA (PaAi), where it proceeds onto the superior temporal gyrus, lateral to Heschl's gyrus. We predicted a possible tonotopic organization in this anterior division of LA (PaAi), connecting higher-frequency Region 5 to lower-frequency Region 6. Progression G was observed to originate in the higher-frequency region corresponding to Region 5 and to terminate superiorly on the superior temporal gyrus in the lower-frequency region corresponding to Region 6. Therefore, our data suggest that LA (PaAi) possesses two tonotopic maps that "mirror" each other across the lower-frequency region containing the focus of Region 6 (Figure 3-8).

We hypothesize that STA (PaAe), like LA (PaAi), possesses multiple tonotopic maps. We had previously proposed a second tonotopic organization for STA (PaAe) with Regions 8 and 5 forming the lower- and higher-frequency ends of the map, respectively. However, wavefronts originating in the higher-frequency region corresponding to Region 5 were not

observed to terminate in the lower-frequency region that corresponded to Region 8. Instead, Region 8 was consistently observed to be the termination endpoint of a wavefront (Progression F) that originated infero-laterally on the superior temporal gyrus (unlabeled higher-frequency region in Figure 3-8). This unlabeled higher-frequency region is observed to be in close proximity (8 mm) to the average Talairach location of the center of STA (PaAe) reported by Rivier and Clarke [82], inferior and lateral to Region 8. We therefore attribute this unlabeled region to STA (PaAe) and propose that Progression F represents a tonotopic map in a second, more lateral division of this auditory area.

The data obtained in this study do not support the proposal of a tonotopic map within AA (PaAr) or PA (PaAc/d). AA (PaAr) is reported to be located antero-lateral to Heschl's gyrus, on the superior temporal gyrus, and to extend onto the antero-lateral aspect of Heschl's gyrus [29, 82]. We previously (Chapter 2) attributed only one classified frequency sensitive Region to AA (PaAr)—Region 7. No wavefronts were consistently observed to connect the lower-frequency region encompassing the activation focus of Region 7 to any higher-frequency regions located along the superior temporal gyrus or on the antero-lateral surface of Heschl's gyrus. We therefore conclude that we have not observed a tonotopic organization in AA (PaAr). PA (PaAc/d) has been observed to cover an area posterior to the medial half of Heschl's gyrus and, sometimes, to extend across the medial end of Heschl's gyrus onto its antero-medial aspect [29]. In Chapter 2, it was noted that three classified higher-frequency sensitive regions (Regions 2–4) could represent portions of this auditory area. The failure to observe a spatially distinct higher-frequency region containing the focus of Region 4 in at least five subjects precludes the proposal of any tonotopic organization for PA (PaAc/d) that includes this classified region. The other two classified frequency sensitive regions attributed to PA (PaAc/d)—Regions 2 and 3—were not observed to be the origins of wavefronts that terminated in lower-frequency regions at the medial end of, or medial to Heschl's gyrus. Therefore, we have not observed a tonotopic organization within PA (PaAc/d).

3.4.2 Comparison to Non-human Primate Auditory Cortex

Further insight into the organization of frequency sensitivity in the human auditory cortex may be gained by comparison to the frequency sensitivity in the auditory cortex of owl and rhesus monkeys. Two components will be examined: (1) the physical location of poten-

tially homologous cytoarchitectural areas in humans and monkeys, and (2) the orientation of tonotopic maps within these possibly homologous cytoarchitectural areas. From the orientations of tonotopic organizations that have been related to cytoarchitectural auditory areas in the human cortex, we may propose analogies between the human and monkey auditory areas.

The anatomical organization of auditory areas in the human may be almost identical to that observed in owl and rhesus monkeys, although the orientations may differ somewhat. Auditory cortex in monkeys is located on the superior surface of the temporal lobe with a core of koniocortex running along an anterior-posterior axis, surrounded by belts of para- and prokoniocortical regions [30, 43, 57]. This organization is similar to that revealed by cytoarchitectural study of the human [29, 82]. Many of the cytoarchitectural belt areas identified in the human are believed to be homologous to those in the monkey, with specific correlations proposed between human AA (PaAr) and monkey PaAr [41], human LA (PaAi) and monkey PaAlt [29, 30, 41], and human PA (PaAc/d) and monkey PaAc [29]. Non-koniocortical areas in the human are distributed relative to koniocortex in a pattern that is similar, but not identical, to that observed in the monkey. For example, prokoniocortex (Pro) was found in the macaque to be located medial to koniocortex (KA) by Galaburda and Pandya [30], but MA (ProA) is found to be antero-medial to koniocortex in the human [29]. This reorientation suggests that the formation of the transverse temporal gyrus (Heschl's gyrus) has caused posterior portions of auditory cortex to be pulled medially. The unchanged location of AA (PaAr), anterior and lateral to koniocortex, is consistent with this reorganization, as is the position and extent of LA (PaAi), following the lateral border of koniocortex on the superior temporal gyrus and into the superior temporal plane.

Human and monkey koniocortical areas also appear to be tonotopically organized in an analogous manner. Both monkey and human koniocortical areas (human: KAm and KAlt; monkey: R and AI) exhibit a reversal in the progression of frequency sensitivity at their common (low frequency) border. The human anatomical areas KAm and KAlt are proposed to be represented by Progressions A and B, respectively, providing a mirror relationship at the location corresponding to lower-frequency sensitive Region 1 (Figure 3-8). In the macaque, AI and R have been observed to be tonotopically organized and to share a low frequency border in the middle of their combined anterior-posterior extent [43,57]. Because the koniocortical region defined in Galaburda and Pandya [30] appears to correspond largely

to the rostral area (R) [57], human medial AI (KAm) may be homologous to R in the monkey. The location of prokoniocortex would be consistent with this homology if the postero-medial end of R had been pulled medially by the development of Heschl's gyrus. This homology is also supported by the anterior-posterior orientation of the tonotopic map in macaque AI, similar to that observed in lateral AI (KAlt) of the human in this study (Figure 3-8, Progression B).

The proposed organization of the two divisions of LA (PaAi) is consistent with the proposed homology between LA (PaAi) in the human and PaAlt in the monkey. LA (PaAi) is proposed to contain two tonotopic maps (Progressions E and G) that share a lower-frequency border (Region 6) just lateral to the lower-frequency border between the two koniocortical regions (Region 1). Monkey PaAlt contains at least a portion of both the antero-lateral (AL) and postero-lateral (PL) anatomical areas [57]. These two areas have been observed in the macaque and owl monkey to contain mirrored tonotopic maps, sharing a lower-frequency region that is located just lateral to the lower-frequency border of areas R and AI [43, 58]. This would argue for a potential homology between monkey AL and the anterior division LA (PaAi) in the human, and between PL and the posterior division of LA (PaAi), though the physical separation of the higher-frequency regions of anterior LA (PaAi) and medial AI (KAm)—Regions 5 and 2, respectively—is not consistent with the adjacency of the higher-frequency representations in monkey areas AL and R [43].

The two tonotopic maps proposed to be located in STA (PaAe) do not have obvious homologous relationships with tonotopic areas described in the monkey. The medial division (Progression D) of STA (PaAe) may be the equivalent of the caudal area (C) in the rhesus monkey [57], possibly a portion of the temporoparietal cortex (Tpt) [30]. Tpt is a region of cortex believed to be related to speech processing in the human and demonstrated, in the macaque, to be used in the analysis of the temporal pattern of sounds [46]. Progression F, the more lateral map in STA (PaAe), may correspond to a portion of area Ts3 of the monkey [30] or to a lateral portion of Tpt. While the parabelt region of the monkey cortex to which these two divisions of STA (PaAe) probably correspond has not been well-mapped in the monkey, the mirror tonotopic organization about a lower-frequency border (Region 8) is consistent with the organization of the two divisions of both AI (KAm and KAlt) and LA (PaAi).

We are unable to draw any conclusions regarding the similarity of tonotopic organization

in human and monkey prokoniocortex due to a lack of physiological information for the monkey. MA (ProA) was observed to be tonotopically organized with a progression of frequency sensitivity (Progression C) running almost parallel to that of medial AI (KAm, Progression A). The corresponding monkey region, likely included in the rostro-medial auditory area (RM) of Morel et al. [57, 58], has not been thoroughly examined due to the difficulty of making depth electrode penetrations in this region [41, 52].

The seven tonotopic maps observed in the human may be assigned to parallel divisions of tonotopic areas, similar to those described in the macaque [30] based upon corticocortical and thalamocortical connections (Section 2.4.6). Based upon the parallel connectional organization of auditory areas in the macaque cortex [30] and our presumed homologies between the human and monkey auditory cortex, we may assign the two divisions of STA (PaAe) to a parabelt region, the two divisions of LA (PaAi) to the lateral belt, medial AI (KAm) and lateral AI (KAlt) to the koniocortical core, and MA (ProA) to the medially located root division. The resulting parallel organization of tonotopic maps is similar to that observed by Kosaki et al. [43] in the macaque, in which a large lower-frequency region was centrally located, with higher-frequencies represented both anteriorly and posteriorly. This organization may arise from the segregation of thalamocortical inputs to the cortex [57, 58, 64]. The parallel organization of tonotopic maps may also arise in part from the connections between divisions within the same stage (e.g. KA in the core to PaAlt in the belt division) or between stages within the same division (e.g. from PaAc to KA within the core). Such local connectivity may preserve tonotopic organization between areas.

In this study, regions of cortex that are observed more frequently may correspond to anatomical auditory areas that possess “stronger” tonotopic maps. Among other things, “stronger” tonotopic maps may mean sharper tuning (leading to finer spatial resolution for the BOLD response), greater density of tuned cells (leading to greater magnitude of metabolic demand), lesser gradient of positional variation in CF (longer duration of responses within a voxel, resulting in stronger statistics) or lower thresholds (more cells responding to the moderate intensity stimulus). For example, Progression A, observed in all six subjects, is hypothesized to be primary auditory cortex (medial AI; KAm), an anatomical area with a high density of sharply tuned neurons that receives strongly tonotopic inputs from the ventral division of the medial geniculate nucleus (MGv) [58]. The stronger tonotopic organization of thalamic inputs to the core regions (primarily from MGv) [58],

coupled with the forward projections from the core to the lateral belt [30] may explain why we observed the majority of our tonotopic maps (Progressions A, B, D–G) in the core and belt areas rather than in root areas, medial to the koniocortex, such as PA (PaAc/d).

3.4.3 Extensions and Applications

Alternative methods of elucidating progressions of frequency sensitivity may yield further information regarding the functional specialization of human auditory cortical areas. For example, anatomical auditory areas may respond differently to different acoustic stimuli. While the tonotopic organization of human auditory cortex has been examined in this study using narrow bandwidth noise, the choice of this stimulus was based upon evidence from animal studies that non-tonal stimuli can produce stronger responses in non-primary auditory cortex [77]. Attempts to examine the tonotopic organization of human cortex using pure tones could further elucidate functional specializations in auditory areas. Differential responses to stimuli would be evidenced if only a subset of the proposed tonotopic organizations were observed in a pure tone study, or, conversely, if progressions of frequency sensitivity not described herein were observed.

Two technical improvements could also reveal more useful detail in the tonotopic organization of the human auditory cortex. First is the use of a higher magnetic field (e.g. 3 T) to obtain greater spatial resolution. Finer resolution could permit more accurate assessment of the origination and termination endpoints of the wavefronts and also provide stronger evidence of the monotonicity of the observed progressions. The second improvement is the use of a less acoustically hostile imaging sequence (see Appendix A [23]) to reduce the magnitude of the cortical response to the noise of the imaging procedure (see Appendix B [94]). A reduction in the magnitude of the response to the imager could lead to greater signal changes being observed in response to the swept stimuli, leading to greater statistical significance. The reduction in the background noise could also lead to cortical responses that more truly reflect the content of the swept stimulus, leading to more accurate phase angle measurements and thus more accurate measures of relative frequency sensitivity in the auditory cortex.

Our initial assessment of the frequency sensitivity of the human auditory cortex (Chapter 2) primarily examined the left hemisphere response to binaural stimulation whereas this study concentrated upon the left hemisphere response to contralateral stimulation. We

have observed generally good, but not complete agreement in the results of these two studies (e.g. Region 4 in Figure 3-5). It is possible that some of the differences in the observed frequency sensitivity may be a consequence of cortical selectivity for stimulus laterality (e.g. [13, 56]). We have developed a set of bilateral surface coils (Section 2.2.4) that permit the simultaneous acquisition of high signal-to-noise ratio data from both hemispheres. Preliminary investigations in one subject (Subject 4) suggest that the tonotopic organization of the right hemisphere (ipsilateral response) is similar to that of the left hemisphere (contralateral response), but we do not have sufficient data to draw firm conclusions. Tonotopic mapping of both hemispheres in response to ipsi- and contralateral stimulation, as well as binaural stimulation, could reveal hemispheric differences at the level of individual auditory areas. As noted in Chapter 2, further information regarding the functionality of auditory cortex could be gained through the study of the tonotopic organization of the right hemisphere. Any differences that may be observed between the tonotopic organizations of the two hemispheres could reflect differences in the processing of acoustic stimuli, including specializations for the processing of linguistic stimuli.

The ability to map the tonotopic organization of the auditory cortex has implications for the study of both functionality and connectivity in the cortex. For example, cortical reorganization of frequency sensitivity is known to occur after frequency-specific injury of the peripheral auditory system [83, 99]. Knowledge of the tonotopic organization of human auditory cortex can be used as a basis for the study of cortical reorganization following damage to the peripheral auditory system. Long-term partial recovery of auditory function lost through unilateral injury or lesion, presumably by cortical compensation of the contralateral hemisphere, has been observed in the human [17] and the macaque [32, 35, 37]. Some changes in cortical function observed in pathological cases (e.g. [87]) may be due to cortical compensation or simply a result of changes in the input to these regions of cortex. Identification of possible cortical reorganizations could reveal information about the connectivity of the auditory cortex to other cortical regions and subcortical structures. It is possible that changes in the tonotopic organization of human auditory cortex may result from central lesions and be dependent upon the localization of the lesion. The use of fMRI to study both the extent and time-course of the development of organizational changes after cortical injury could help to answer such questions.

Appendix A

Improved Auditory Cortex Imaging Using Clustered Volume Acquisitions

W.B. Edmister, T.M. Talavage, P.J. Ledden, R.M. Weisskoff

A.1 Abstract

The effects of the noise of echo-planar functional magnetic resonance imaging on auditory cortex responses were compared for two methods of acquiring functional MR data. Responses observed with a distributed volume acquisition sequence were compared to those obtained with a clustered volume acquisition sequence. In the former case, slices from the volume were acquired at equal intervals within the repetition time, whereas the latter acquired all slices in rapid succession at the end of the imaging period. The clustered volume acquisition provides a period of quiet during which a stimulus may be presented uninterrupted and uncontaminated by the noise of echo-planar imaging. Both sequences were implemented on a General Electric Signa imager retrofitted for echo-planar imaging by Advanced NMR Systems, Inc. The sequences were used to acquire 60 images per slice of a fixed volume of cerebral cortex while subjects were presented an instrumental music stimulus in an On vs. Off paradigm. Data were acquired for both sequences using TR values of 2, 3, 4, 6 and 8 s. The clustered volume acquisition sequence was found to yield greater measures of dynamic range (percent signal change, mean statistical power per unit

imaging time) across the tested range of TR values. Observations of more consistent spatial extent of responses, greater mean signal changes, and higher and more consistent values of mean t -statistic per unit imaging time demonstrate the efficacy of using a clustered volume acquisition for fMRI of auditory cortex.

A.2 Introduction

Acoustic contamination of functional MRI (fMRI) data is of great concern to those members of the scientific community attempting to elucidate the function of the auditory pathway (brainstem and cortex). The acoustic noise inherent in the process of echo-planar fMRI is a short duration (32–50 ms) burst of a tone complex (a “beep”) that is certain to generate responses throughout the auditory pathway. The presence of a cortical fMRI response was demonstrated by Bandettini et al. [3], raising the possibility that the response will limit the dynamic range of responses to the desired stimuli, reducing the sensitivity of the fMRI technique. The cortical response to the beeps may also change the spatial distribution of the stimulus-induced fMRI response, reducing the accuracy of traditional stimulus vs. no stimulus paradigms. This accuracy may be further degraded by the changed perception of the stimulus due to acoustic masking and a reduction in the ability of the subject to attend to the desired stimulus. The latter could yield a changed cortical response in both sensory [88, 100] and higher order cortical areas. This work was undertaken to assess the experimental effect of the fMRI measurement process on the activation observed in response to a stimulus known to yield strong activation in auditory cortex, instrumental music.

Peak noise levels generated by the echo-planar imaging (EPI) beep at our facility range from 117 dB Sound Pressure Level (SPL) on a 1.5 T machine to 133 dB SPL on a 3.0 T imager [79]. These values are consistent with other measurements on similar machines [16]. Noise levels are typically reduced through the use of passive attenuation measures such as earmuffs and earplugs. These reductions are generally on the order of 30–35 dB, bringing the beep level down to 85–90 dB SPL at 1.5 T [79]. This level is still loud enough to mask a desired auditory stimulus both simultaneous with and immediately following the imaging beep. Such simultaneous and non-simultaneous masking will be most evident under fMRI echo-planar sequences in which the beeps are present throughout auditory stimulation.

In most conventional and echo-planar techniques on General Electric/Advanced NMR

Systems, Inc. (GE/ANMR) systems, slices are acquired at equal intervals within the repetition time (TR) of the imaging experiment (distributed volume acquisition, DVA). This is in contrast to the typical imaging sequence on other fMRI systems (e.g. Siemens) in which the volume is acquired at the end of the TR, with one slice acquired approximately every 100–200 ms (clustered volume acquisition, CVA).

The regular pulsing of the echo-planar gradients on the GE/ANMR system can lead to a consistent pattern of masking of the desired stimulus. Under typical functional imaging conditions, eight to sixteen slices are imaged every two seconds, producing four to eight beeps per second (one per slice acquisition). For the GE/ANMR system, each gradient readout sequence is 32 ms in duration. The beep associated with the readout lasts for approximately 50 ms, including reverberation [79]. With less than 250 ms between beeps, a significant fraction of the auditory stimulus is being masked by the imaging noise. Such masking is likely to have an effect on the functional response dependent upon the measures taken to compensate for the imager noise background. Measurements at our facility indicate approximately 30 dB of masking of continuous, amplitude modulated noise (0.3 octave bandwidth) centered at the 1 kHz fundamental switching frequency of the 1.5 T machine EPI gradients. This masking drops to less than 5 dB for center frequencies more than two octaves from 1 kHz.

While the investigator can compensate for masking produced by the imaging noise, the effects of the beeps are not readily eliminated through modification of experimental parameters. For example, a simple measurement of the subject's behavioral hearing thresholds in the presence of imaging noise may be used to present stimuli at a fixed level above hearing threshold, but this will not eliminate the auditory cortex response induced by the beeps. The net fMRI response in cortex is probably a non-linear combination of responses to the background noise and the auditory stimulus. A related effect is that the stimulus being perceived by the subject is certainly different from the stimulus which would be perceived under the quiet conditions typical of other functional imaging modalities such as positron emission tomography (PET) and magnetoencephalography (MEG), making direct comparisons of results across these modalities difficult. Therefore, it is desirable that functional MRI is performed in an environment as free of imaging noise as is possible.

In CVA sequences the stimulus may be presented, uninterrupted, for most of the TR with the beeps occurring as rapidly as possible at the end of the TR. If the total duration

of a volume acquisition is shorter than the onset of the fMRI-observable blood-oxygenation level dependent (BOLD) response to the beeps associated with that volume acquisition, the inclusion of cortical responses to the beeps is avoided. With selection of a long TR it should be possible for the cortical response to the beeps to decay prior to the next volume acquisition, providing volumetric fMRI data with greater dynamic range. In the case of TRs greater than 10 s, and perhaps at shorter TR values in conjunction with small imaging volumes, this data should be free of the responses induced by the imaging noise. Accordingly, it becomes possible to use typical TR values to obtain data more consistent with a stimulus-only response than obtained using a distributed volume acquisition (DVA) imaging sequence.

In this paper we use fMRI equivalent CVA and DVA sequences, both implemented on a 1.5 T GE/ANMR EPI system, to compare auditory cortex responses to complex acoustic stimuli, and discuss the advantages inherent in the use of CVA sequences in this and other fMRI applications.

A.3 Methods

A.3.1 Imaging Sequence

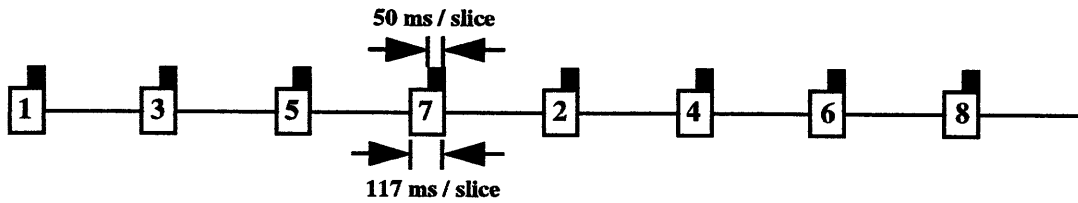
The CVA pulse sequence was implemented on a General Electric (Milwaukee, WI) 1.5 T Signa imager, retrofitted for echo-planar imaging (EPI) by Advanced NMR Systems, Inc. (Wilmington, MA). An asymmetric spin-echo (ASE) echo-planar sequence with slice acquisitions distributed equally throughout the repetition time (TR) was modified to perform the clustered multi-slice imaging. Both the DVA and CVA sequences are illustrated, with their accompanying beeps, in Figure A-1 for the example of eight slices acquired with TR = 4 s. Observe that the CVA sequence provides a block of time when no slices are acquired and during which the stimulus may be presented without significant distraction.

Due to slice profile imperfections, acquisition of all slices within one T_1 can lead to significant crosstalk between adjacent slices. Assume that we are acquiring a volume of eight slices clustered at the end of each TR. Further assume that the slice acquisitions are interleaved such that the odd slices (1, 3, 5 and 7) are acquired in the first half of the cluster and the even slices (2, 4, 6 and 8) in the second half. Overlapping of the slice profiles results in the acquisition of one slice perturbing some fraction of the spins in the

Figure A-1: Comparison of temporal acquisition of eight slices with $TR = 4$ s for (a) distributed volume acquisition (DVA) sequence and (b) clustered volume acquisition (CVA) sequence. Each slice acquisition (open box) is 117 ms in duration, producing a burst of imager noise (black box) that is 50 ms in duration, including reverberation. A typical axial slice ordering, inferior (slice 1) to superior (slice 8), is shown at bottom. Note that in the interleaved DVA sequence, adjacent slices are imaged much further apart in time than in the centric CVA sequence.

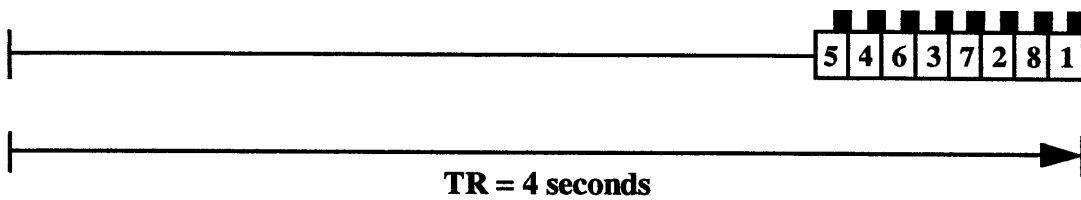
Distributed Volume Acquisition (DVA)

a



Clustered Volume Acquisition (CVA)

b



slice #

8	superior
7	
6	
5	
4	
3	
2	
1	inferior

Imaged Volume

neighboring slices (e.g. acquisition of slice 4 perturbs the spins in slices 3 and 5). In a clustered volume acquisition with normal interleaving the odd slices are imaged almost a full TR after being perturbed and signal levels for these slices are comparable to those obtained in a single-slice acquisition. The acquisition of the odd slices perturbs some of the spins in the even slices (2, 4, 6 and 8) that are imaged just 500 ms later, resulting in signal levels that may be significantly reduced from those obtained in a single-slice acquisition. The multi-slice signal-to-noise ratio (SNR) in the even slices was reduced by as much as 60% from the single-slice acquisition SNR when using the default GE/ANMR slice excitation pulses. The SNR loss was reduced to below 5% by sharpening the profile of the acquired slices by the following modifications. First, the Hamming-windowed 90- and 180-degree sinc pulses were widened from 3.2 ms with a single side lobe to 6.4 ms with two side lobes. Then the corresponding slice-select gradient amplitudes and transmit frequencies were rescaled to maximize the slice width with minimal crosstalk between adjacent slices. This optimization was performed using a phantom containing a wide range of T_1 values, including those of fat, white matter and gray matter. The 90- and 180-degree pulses of the DVA sequence were modified to use slice profiles identical to the CVA sequence.

A.3.2 Imaging Parameters

Data acquisition for all experiments described in this paper was performed on the 1.5 T system using asymmetric spin-echo (ASE) echo-planar imaging ($TE = 70$ ms, $\tau = -25$ ms, 128×64 collection matrix, 40 cm \times 20 cm FOV). Slices were 4 mm thick and contiguous. The in-plane resolution for all studies described was 3.1 mm \times 3.1 mm. A surface receive coil positioned around the left ear was used to maximize signal from Heschl's gyrus (site of primary auditory cortex) and the rest of the auditory cortex. This coil is integrated into a passive attenuation system used to reduce the level of the EPI noise by 30 dB to approximately 85–90 dB SPL [79]. The body coils of the magnet were used for transmit. Functional images were acquired with the coolant compressor turned off to eliminate the dominant, periodic component of the non-EPI background noise, effectively producing a condition of quiet for periods which required no auditory stimulation.

A.3.3 Experiments

Four subjects (ages 22–26; three male, one female) were imaged using both the CVA (clustered volume acquisition) and the DVA (distributed volume acquisition) sequences for TR values of 2, 3, 4, 6 and 8 s to acquire 60 images of eight (axial) oblique slices. Images of the left auditory cortex were acquired during right monaural presentation of an instrumental music stimulus in an On vs. Off paradigm with 24 s epochs. Music stimulation was continuous for the entire 24 s period. The TR values were chosen to cover the typical experimental usage at our facility, and range from the shortest to longest TRs that are experimentally practical due to duty cycle requirements and total imaging time limitations. Two subjects were exposed to the five TR values in an increasing order, and two in a random order. Multiple presentation orders were used to prevent bias resulting from habituation.

The primary goal of this study was to plot percent signal change against TR for both CVA and DVA sequences to determine if the auditory cortex response to a consistent paradigm would be dependent upon the volume acquisition sequence. Therefore, runs of the paradigm obtaining equal numbers of images, rather than utilizing equal imaging time, were chosen so that the percent signal changes, *t*-statistics, and activation maps could be directly compared across TR values and volume acquisition sequences with consistent error bars. As a consequence of this decision, the duration of each imaging session remained less than two hours because runs using shorter TR values required less time than runs using longer TR values. The two hour imaging session duration was desired to prevent boredom or discomfort from distracting the subjects from the presented stimuli.

A.3.4 Data Analysis

Prior to statistical analysis, images were motion corrected using SPM95 [28], spatially smoothed by a 3-point Hamming filter and drift corrected using a minimum mean square error fit for each individual voxel. Computation of percent signal change and Student's *t*-statistic for all voxels meeting a minimum signal threshold requirement was performed using in-house software. A boxcar paradigm waveform was shifted by one (TR = 3 and 4 s) or two images (TR = 2 s) to account for the approximately 3 s onset delay of the BOLD response. The waveform was not shifted for the cases of TR = 6 and 8 s.

Indicators of the dynamic range of auditory cortex, percent signal change and Student's

t -statistic, were computed to determine the optimal TR that minimizes the stimulation of auditory cortex by the beeps while maximizing the number of images per unit time. Auditory cortex was defined for this study as a volume including Heschl's gyrus, the planum temporale and extending inferiorly to the superior temporal sulcus. Areas of functional activation were defined as regions achieving statistical significance of $p < 0.01$ (uncorrected t -statistic, $t > 2.66$ for 30 time points in each condition) in at least 3 of the 10 runs of the music paradigm. The 3 in 10 criterion was selected to reduce the false positive rate to approximately one in one million. For each subject, all voxels that met the 3 in 10 criterion were combined to form a single region of interest (ROI).

To assess variations in dynamic range as the TR was changed for each sequence, mean values of both percent signal change and t -statistic were computed using each subject's ROI. Ninety-five percent confidence intervals were computed for both mean quantities. Statistical power per unit imaging time was computed for each run by dividing the mean t -statistic in the ROI by the square root of the TR. Assuming that the image noise (non-acoustic) is stationary and uncorrelated across runs, this quotient weights the mean t -statistic by the number of points that are acquired per unit imaging time. Comparison of values of statistical power per unit imaging time indicates at which TR the strongest responses would have been observed given a fixed total imaging time, rather than a fixed number of image acquisitions. A fixed total imaging time is a more common constraint when planning fMRI experiments.

A.4 Results

Activation maps obtained with the CVA sequence were directly compared to DVA sequence maps obtained under identical conditions. Measures of dynamic range (percent signal change) and statistical power were compared for the two sequences. Increases in both dynamic range and statistical power were found to occur when using the CVA sequence with long TR values, with improvement over the DVA sequence maintained at shorter TRs.

A.4.1 Spatial Extent of Responses

Figure A-2 compares, for all subjects, the spatial extent of activation for the CVA and DVA sequences during auditory functional studies. In these images, the color-coded p -value is overlaid on a T_1 -weighted anatomic image (grayscale), with p -value magnitudes indicated

on the colorbar. The slices presented for both the CVA and DVA sequences contained the sites of strongest responses over the range of TR values. These slices include Heschl’s gyrus, much of the planum temporale and other secondary auditory areas. The left side of the figures depicts the responses obtained with the CVA sequence while the right side presents those obtained using DVA. For each of the subjects, the images in the top row are results for TR = 8 s and the bottom row consists of the maps for TR = 3 s. Because each run consisted of a constant number of images, the low-level cutoff for statistical significance was fixed, at $p < 0.01$ (uncorrected t -statistic, $t > 2.66$). For both displayed TR values, the CVA responses were always greater in both spatial extent and statistical significance than the DVA results. This was generally true across the set of TRs (Table A.1).

Subject (ROI Points)	Imaging Sequence	TR (s)				
		2	3	4	6	8
1 (223 points)	CVA	96	186	144	144	164
	DVA	130	142	108	130	66
2 (356 points)	CVA	195	283	301	200	328
	DVA	193	281	285	160	33
3 (506 points)	CVA	281	436	445	346	348
	DVA	63	287	362	165	148
4 (280 points)	CVA	158	190	152	143	272
	DVA	130	175	167	157	203

Table A.1: Spatial extent (number of voxels) of activation ($p < 0.01$) in auditory cortex

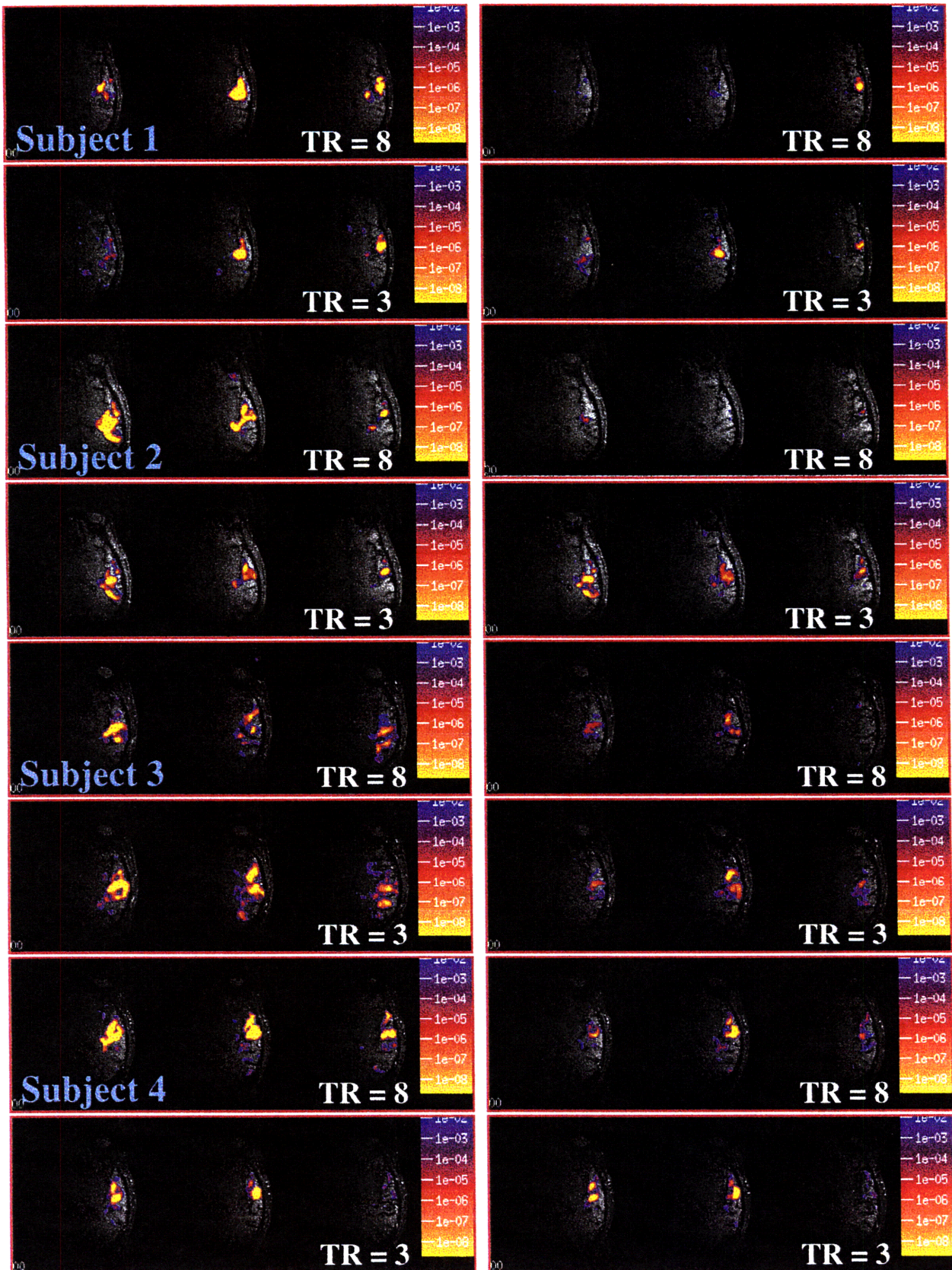
A.4.2 Strength of Responses

In Figure A-3, the averages of all activated voxels in the four subjects for (a) percent signal change and (b) statistical power per unit imaging time are plotted as a function of TR for both sequences. The results for mean t -statistic paralleled those of percent signal change. The statistical power per unit imaging time, achieved by dividing by the square root of TR, provides an assessment of the mean statistical power achieved for each TR under the more practical assumption of constant imaging time, rather than constant number of images. Statistically significant differences ($p < 0.05$, t -test) between CVA and DVA percent signal changes were observed at each TR value. The mean statistical power per unit imaging time exhibited a statistically significant difference ($p < 0.05$, t -test) between CVA and DVA sequences for TR values of 2, 3, 6 and 8 s. At a TR of 4 s, the improvement in statistical

Figure A-2: Comparison of the spatial extent and statistical significance of auditory cortex activation, in response to instrumental music, as a function of imaging sequence (CVA left, DVA right) and TR. Activation (t -test, $p < 0.01$) is displayed as a colormap overlaid on T_1 -weighted images (grayscale). All parts depict three slices (inferior to superior, left to right) containing the majority of auditory cortex. For each subject, responses obtained using TR = 8 s are displayed in the top row, and responses obtained using TR = 3 s are displayed in the bottom row. The CVA sequence responses are consistent across TR in both location and spatial extent while the DVA results vary in both of these respects, sometimes considerably. The DVA variation is most apparent in the most inferior (left) slice where activation may be observed to consistently increase in extent and strength with decreasing TR.

Clustered Volume Acquisition (CVA)

Distributed Volume Acquisition (DVA)



power for the CVA sequence over the DVA sequence did not achieve significance.

A.5 Discussion

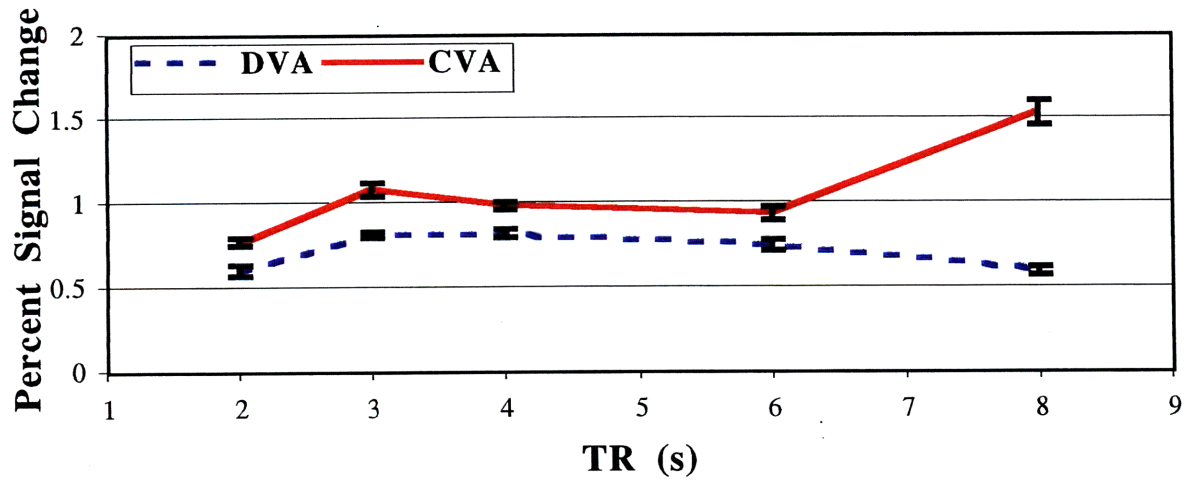
The BOLD response due to neuronal activation in auditory cortex has both a time constant for activation and a time constant for recovery to the initial baseline. In visual cortex, the rise time from stimulus onset to 90% maximum activation and the recovery time from stimulus cessation to 10% above baseline have been measured to be between 4–10 s [2, 8, 44, 86]. These values suggest rise and recovery time constants on the order of 3–4 s, but such values may be different for auditory cortex.

If a DVA sequence is used with a TR longer than the rise time, the beep associated with the initial slice acquisition for the volume may produce an observable fMRI response in the latter slices acquired. After the initial BOLD response develops, because the time between slice acquisitions is shorter than the duration of the response to the imaging noise, all subsequent slice acquisitions are contaminated by responses to imager noise. Elimination of this effect would require the use of very long (e.g. 10 s per slice) and experimentally impractical TR values.

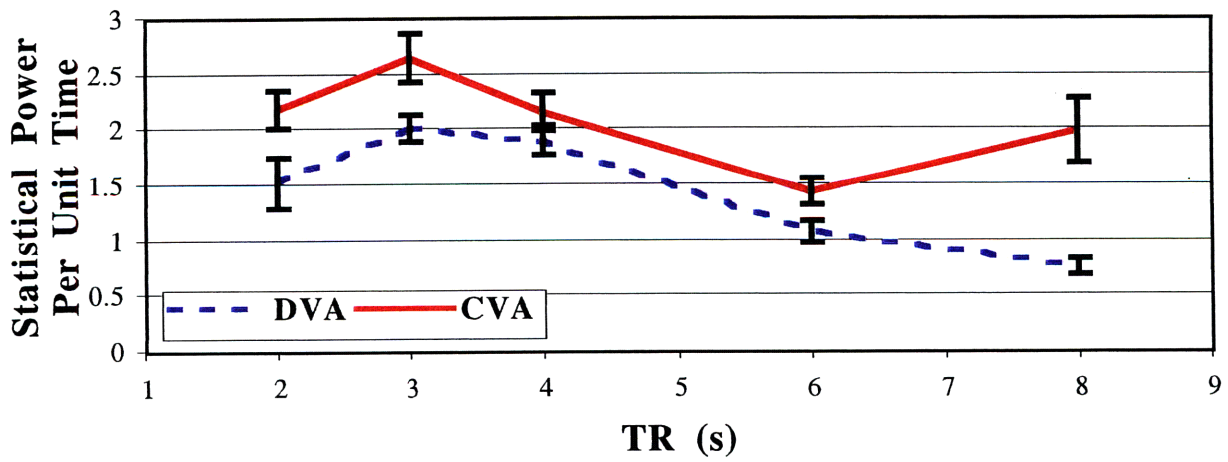
A CVA sequence simplifies this problem by allowing the separation of within-acquisition responses from between-acquisition responses due to the quiet period between volume acquisitions. The music activation maps generated using a CVA sequence with TR = 8 s for eight slices should be largely free from imager noise contamination. The CVA sequence should, in general, be free of direct, slice acquisition-to-slice acquisition contamination because the readout time for up to eight slices is less than one second in duration. There will be a long-term BOLD response to the noise of the CVA volume acquisition, but the use of a long TR (e.g. 8 s) will permit this response to decay prior to the subsequent volume acquisition. At shorter TR values, the response to previous acquisitions does not achieve full recovery to baseline, thereby limiting the dynamic range of responses to auditory stimuli. This will lead to partial saturation of the signal in auditory cortex, with saturation increasing with decreasing TR. It is unknown if this is saturation of the neuronal response, the BOLD response, or due to a limitation of the sensitivity of the fMRI technique to hemodynamic changes.

Figure A-3: Graphs of (a) mean percent signal change and (b) mean statistical power per unit imaging time. Values were computed by pooling data of all subjects from ROIs of those voxels achieving $p < 0.01$ (uncorrected t -statistic, $t > 2.66$) in at least 3 of the 10 runs of the instrumental music paradigm. Error bars indicate ninety-five percent confidence intervals. Mean percent signal changes were significantly higher ($p < 0.05$, t -test) for the CVA sequence at all TR values. Power per unit imaging time was also significantly higher ($p < 0.05$, t -test) for the CVA sequence than for the DVA sequence (TR = 2, 3, 6 and 8 s).

a



b



A.5.1 Analysis of Functional Effect

Both CVA and DVA sequences yield similar areas of cortical activation for $TR = 3$ s, but the CVA activation appears to be more robust in spatial extent across TR values (Figure A-2 and Table A.1). At shorter TR values, e.g. 2–4 s, the DVA maps differ from longer TR data in both the spatial extent and location of foci of greatest statistical significance. The changes in DVA activation at long TRs, though consistent across the four subjects, were particularly large for Subjects 1 and 2. Both subjects reported difficulty attending to the stimulus at $TR = 8$ s due to interaction of the music tempo with the 1 Hz rate of the beeps. The reduction of such stimulus-specific interactions by the introduction of a quiet period into the TR interval is an advantage of CVA sequences.

The response strength differences between CVA and DVA seen in the activation maps of Figure A-2 are reflected in the graph of percent signal change in Figure A-3, part a. The mean percent signal change for the CVA sequence was reasonably constant from 3–6 s. The increase in percent signal change at $TR = 8$ s may be a consequence of our reduced sampling of the onset of the response to the stimulus and thus may be artificially high. The increase in percent signal change when the TR was increased from 6 s to 8 s could also indicate that, for at least some portions of auditory cortex, the beep-induced response may persist longer than our maximum measured TR of 8 s. The percent signal change for the DVA sequence remained relatively constant, and lower than for the CVA sequence, across all TR values.

The statistical power per unit imaging time (Figure A-3, part b) was higher across TR values for the CVA sequence than the DVA sequence. The relatively constant percent signal changes observed between 3 and 6 s for both sequences imply that there should be no statistical gain from using a longer TR value. This is confirmed by the linear decrease observed in power per unit imaging time over this range. The large drop in percent signal change at a TR of 2 s is not compensated for by the increased number of images for a given experimental duration. As previously stated, this analysis assumes that all non-acoustic noise across experiments is uncorrelated and stationary. Because some sources of physiologic noise in the fMRI experiments are correlated (e.g. cardiac, respiratory), this analysis leads to a small bias in favor of the lower-TR experiments.

For these experiments, in which eight slices were acquired (1 s duration of 8 Hz beeps

for CVA), the optimal TR for the use of the clustered volume acquisition sequence was 3 s. A TR value of 3 s selects the peak statistical power per unit time (Figure A-3, part b) and results in a statistically significant improvement in percent signal change over the DVA sequence at all TRs (Figure A-3, part a). This value strikes a good balance between temporal resolution and experimental duration along with the subject's ability to track and respond to the stimulus prior to image acquisition. Subjectively, for TR values greater than 2 s, subjects expressed a preference for the CVA sequence over the DVA sequence. Subjects reported that it was easier to concentrate on the stimulus during the CVA quiet periods and to block out the periodic trains of beeps than to concentrate on a stimulus which is "constantly" being masked.

We wish to emphasize that the optimal TR will vary with the duration of the volume acquisition. Changes in the duration of the volume acquisition will need to be offset by changes in the inter-acquisition delay. This delay appears to serve three purposes. First, the subject is permitted a period of time to recover from masking effects from the beeps. Second, the BOLD response to the imager beeps is allowed to rise and decay during these non-imaging periods. Finally, the subject is able to attend to the stimulus alone rather than the stimulus plus beeps. All of these changes in the perception of the stimulus are believed to contribute to the greater percent signal changes observed for the CVA sequence over the DVA sequence.

A.5.2 Benefits of Clustered Volume Acquisition

Clustered volume acquisition sequences have a number of advantages over distributed volume acquisition sequences when used for auditory experiments. CVA does not require prolonged continuous presentation of stimuli in order for all slices in the volume to exhibit a functional response in the short-term. By triggering the stimulus to the beginning of the TR, not only is the time between stimulus and slice readout precisely known for all slices, but the BOLD response in each slice may have time to evolve to detectable levels prior to the first acquisition in a stimulus epoch. This may not occur in a DVA sequence due to the acquisition of slices throughout the TR period, during the onset delay of the BOLD response.

The effect on response latencies is a more general benefit of the imaging sequence, as these will become more uniform across the slices imaged. Under the DVA sequence, adjacent

slices are often collected at widely spaced intervals, potentially leading to response onsets occurring within different volume acquisitions for any two slices in the volume of interest. The clustered, rapid readout of the slices in the CVA sequence reduces this temporal spread and makes it easier to precisely localize the imaging time of a slice relative to the onset of the stimulus.

Use of the CVA sequence should also improve the effectiveness of standard image registration routines. With slices in the volume of interest being acquired as rapidly as possible rather than being interleaved throughout the TR as in the DVA sequence, motion is more likely to occur between, rather than within, volume acquisitions. Therefore, the standard rigid body approximation used in most motion correction algorithms should be more accurate.

A.5.3 Extension of Paradigms

The CVA sequence permits many complex functional paradigms to be explored to a greater degree than the DVA sequence. For example, experiments involving language stimuli, such as word presentation or vocalization, are straightforward to implement and analyze on a trial-by-trial basis, perhaps even separating the perception of the word from the execution of the required activity (e.g. verb generation, repetition). Paradigms that require significant time locking of the stimulus to the imaging, such as an “oddball” paradigm used to elicit the P300 EEG response, should be more easily implemented using a CVA sequence. Event-related fMRI experiments, including those utilizing random order of stimulus presentation, are a logical application of CVA imaging sequences.

Utilization of a flow-compensated gradient-echo sequence rather than the current asymmetric spin-echo technique should permit even more rapid imaging of the cortex, potentially further reducing the acquisition-to-acquisition effect of the imaging noise. This will also permit a greater volume of cortex to be imaged for a given duration of acquisition. Clustered volume acquisitions could also be applied to auditory fMRI using conventional sequences (e.g. FLASH) to realize similar benefits.

A.5.4 Conclusions

The changes in fMRI activation maps across TR values provide evidence that the imaging noise (a beep) does not combine additively with acoustic stimuli, but interferes with the

stimulus and partially saturates the response of auditory cortex. Under the continuous imaging of a DVA sequence, the stimulus perceived by the auditory system may be quite different from the stimulus presented in quiet. The CVA sequence provides this quiet period in which the subject may attend and respond to an uncontaminated stimulus.

When conducting auditory fMRI experiments, a CVA sequence is less affected by beep-induced responses than a DVA sequence. The improved dynamic range of the CVA responses is demonstrated by the observation of greater signal changes at all tested TR values. There also appears to be an optimal ratio between imaging time (acquisition duration) and TR. For a 1 s duration volume acquisition, a TR value of 3 s yielded the highest statistical power per unit imaging time. Use of this sequence for auditory fMRI should improve the ability to observe dynamic signal changes for a minimum amount of imaging time and yield activation maps that are largely free of auditory responses to the noise of the imaging process.

A.6 Acknowledgments

The authors thank Dr. Timothy G. Reese, Dr. Kenneth K. Kwong, Dr. Hans C. Breiter, Dr. Bertrand Delgutte, Dr. John Guinan and Dr. Jennifer R. Melcher for insightful discussions, and Terrance Campbell, R.T. (Technical Manager, MGH-NMR Center) for his gracious assistance in providing time on the imager. Finally, we would like to acknowledge the helpful comments of David B. FitzGerald and Michael P. Harms.

This research was partially funded by NIDA grant P01-DA09467-03, NIH grants P01-DC00119 and T32-DC00038-04, and a NSF Graduate Fellowship in Electrical Engineering.

Appendix B

Quantitative Assessment of Auditory Cortex Responses Induced by Imager Acoustic Noise

T.M. Talavage, W.B. Edmister, P.J. Ledden, R.M. Weisskoff

B.1 Abstract

A clustered volume acquisition functional MRI pulse sequence was modified to assess the response to the acoustic noise of echo-planar imaging in the auditory cortex and to determine whether it is possible to obtain data which is relatively free of acoustic contamination. The spatial location and strength (percent signal change) of cortical responses to the imager noise were examined by introducing extra gradient readouts, without slice excitation, to provide acoustic stimulation immediately prior to acquisition of a cerebral volume. The duration of acoustic stimulation was controlled by varying the number of extra gradient readouts. Slice acquisitions were clustered at the end of the repetition time (TR) period to prevent a response from being induced by the volume acquisition itself (“Intra-Acquisition Response”). The cerebral volumes were acquired using a long TR in order to limit the integration of the cortical response across volume acquisitions (“Inter-Acquisition Response”). Cortical responses were observed to be largest and most significant on the medial two-thirds of Heschl’s gyrus, the location of primary auditory cortex. Mean signal changes induced by the imager noise were observed to be as high as 0.95%. A 2 s delay prior to onset of

the BOLD response was empirically determined. These results demonstrate that clustered volume acquisitions may be utilized for up to 2 s of volume acquisition without inducing an appreciable Intra-Acquisition Response and can be used, with a sufficiently long TR, to provide data which is similarly free of any Inter-Acquisition Response.

B.2 Introduction

Loud acoustic noise levels inherent in the functional MRI echo-planar imaging (EPI) process [16, 79] have been demonstrated to generate responses in the auditory pathway [3], affecting the dynamic range of responses to desired stimuli (Appendix A [23]). The dominant element of echo-planar imaging noise is the rapidly changing gradient during readout of the image. The gradient readout sequence for a GE/ANMR imager is 32 ms in duration, but the transient decay of the resonance along with reverberation of the sound lead to a 50 ms duration burst of imaging noise (beep) associated with each slice acquisition. The readout gradient switches at 1 kHz resulting in a beep that is a tone complex with a fundamental frequency of 1 kHz and significant harmonics out to 8 kHz [79]. The interaction of this beep and the presented stimulus can change the spatial extent of the fMRI-observable response, reducing the accuracy of traditional stimulus vs. no stimulus paradigms [23, 90] (Appendix A). These changes are probably due to the non-linearity of the BOLD response in auditory cortex. The physiological responses in the auditory centers may also be affected by acoustic masking and a reduction in the ability of the subject to attend to the desired stimulus (e.g. [100]).

Direct functional responses to the imaging noise have been qualitatively demonstrated in auditory cortex by Bandettini et al. [3]. Responses to the noise of the imager were observed by comparing the initial images of experiments preceded by gradient readouts without slice excitation (extra beeps) to the initial images of experiments not preceded by gradient readouts (no extra beeps). In this case, the response to the auditory stimulation by the extra beeps is superimposed upon the transient approach to steady-state magnetization. Therefore, quantitative assessment of the strength of the response is non-trivial as the comparison of conditions (extra beeps vs. no extra beeps) assumes that both image noise and signal levels are stationary across experiments.

Representative quantitative measurements of the functional response induced in audi-

tory cortex by the noise of EPI fMRI were obtained in this study through the use of the “Sledgehammer” imaging sequence. Sledgehammer is based on a clustered volume acquisition (CVA) sequence and is used to measure the functional response due to extra beeps inserted prior to a volume acquisition. These additional beeps can effect a change in the cortical BOLD response by changing the duty cycle of the imager noise within a fixed TR. The inclusion of both imaging conditions within a single experiment in the Sledgehammer sequence and the presence of steady-state magnetization in the slices of interest throughout the experiment readily permit accurate quantification of signal changes, something which was not possible in the experiment of Bandettini et al. [3].

The BOLD response to the noise generated by the imager can interfere with stimulus-induced activation in auditory cortex by two mechanisms. The first is a short-term effect in which the beep associated with the acquisition of the first slice in a volume induces a BOLD response that is observed in a slice imaged later within the same volume acquisition. We shall refer to this response as an “Intra-Acquisition Response” in this paper. An Intra-Acquisition Response should be observed when a slice is acquired subsequent to the first slice of a volume acquisition at a delay greater than the onset time of the BOLD response, provided that the time between slice acquisitions is less than the time it takes the BOLD response to return to baseline. The second mechanism that may alter a response is a long-term, integrative effect across volume acquisitions. In this “Inter-Acquisition Response,” the beep train generated by one volume acquisition leads to a BOLD response that does not decay prior to subsequent volume acquisitions and is thus observed as a signal change. An Inter-Acquisition Response should occur when any slice of a given volume acquisition is acquired after the onset, but prior to the decay, of the BOLD response to the slice acquisitions of a preceding volume acquisition.

Given knowledge regarding the time-course of the BOLD response, we may make predictions regarding when both Intra- and Inter-Acquisition Responses will be present in fMRI data. First, we know that the onset delay of the BOLD response is approximately 2 s [8, 44, 86]. Second, we know that the rise and fall times for the BOLD response, as observed in visual and frontal cortex, are 4–10 s [2, 8]. From our previous description of the two noise-induced responses, an Intra-Acquisition Response should be observed when a slice is acquired within a volume acquisition of at least 2 s in duration, and in which the time between slice acquisitions is less than the combined rise and fall times of the BOLD

response—approximately 8–16 s for short duration (1 s) stimuli [2, 8]. The limits on the onset and duration of the BOLD response further imply that an Inter-Acquisition Response may be observed when volume acquisitions are separated by less than 8–16 s.

Clustered volume acquisition sequences (e.g. Siemens EPI) allow for the possibility of acquiring functional data that is free of the effects of the imager noise. A CVA sequence should permit the elimination of the Intra-Acquisition Response by clustering all slices to be acquired into a period of time that is shorter than the 2 s onset delay of the fMRI response to the noise of imaging. The Inter-Acquisition Response may be minimized through appropriate choice of a TR that is sufficiently long (e.g. 8 s or longer) for the response to the imager noise to decay significantly between volume acquisitions.

In this paper we use data obtained with the Sledgehammer sequence to demonstrate that the acoustic noise (beeps) generated by the echo-planar functional MR imaging procedure can effect substantial percent signal changes in particular locations within auditory cortex, specifically primary auditory cortex. The data also suggests that the CVA imaging sequence can be used, for up to 2 s duration volume acquisitions, to yield functional activation maps that are almost free of contamination by the acoustic noise of the imaging procedure.

B.3 Methods

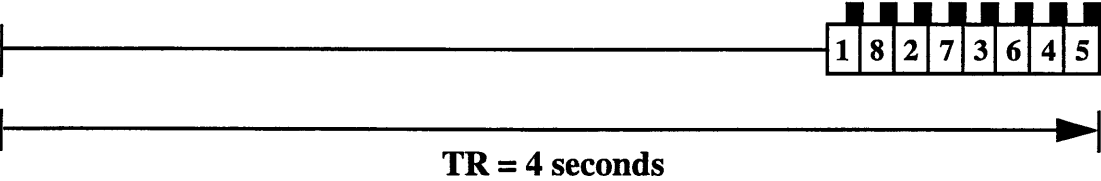
B.3.1 Imaging Sequence

The “Sledgehammer” pulse sequence was implemented on a General Electric (Milwaukee, WI) 1.5 T Signa system retrofitted for echo-planar imaging (EPI) by Advanced NMR Systems, Inc. (Wilmington, MA). The sequence was developed as an extension of a clustered volume acquisition (CVA) imaging sequence (Figure B-1). Sledgehammer alternated stimulus conditions in epochs of three volume acquisitions, maintaining a fixed TR between volume acquisitions. Odd epochs included three clustered volume acquisitions as per a normal CVA sequence. Even epochs likewise included three clustered volume acquisitions, but each volume acquisition was preceded by a fixed number of extra gradient readouts and associated beeps (Figure B-2). Activation was assessed by comparison of selected volume acquisitions from odd and even epochs.

The beep-induced responses in the cortex were not superimposed upon a transient approach to steady-state magnetization as in Bandettini et al. [3], permitting direct statistical

Figure B-1: A clustered volume acquisition (CVA) sequence shown for $TR = 4$ s and using a reverse-centric acquisition order. A typical axial slice ordering, inferior to superior, is shown below the sequence. The period during each slice acquisition (white boxes) in which the imaging noise (beep) occurs is depicted by the black boxes.

Clustered Volume Acquisition (CVA)



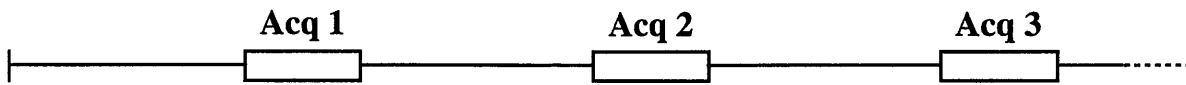
slice #

8	superior
7	
6	
5	
4	
3	
2	
1	inferior

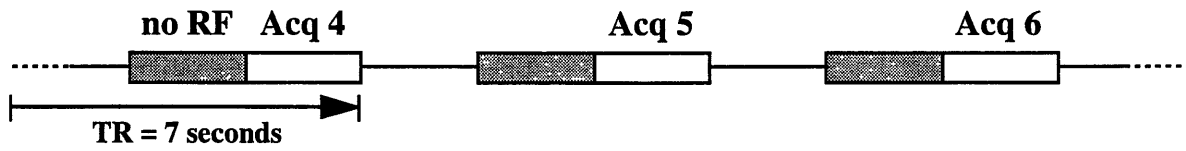
Imaged Volume

Figure B-2: Example of the Sledgehammer sequence ($TR = 7$ s). Odd epochs are identical to a clustered volume acquisition. In even epochs, each clustered volume acquisition is preceded by extra gradient readouts, with no RF transmit, that generate extra acoustic noise (“beeps”) without disturbing the magnetization of the slices. Volume acquisition occurs at the same elapsed time in each TR interval, with or without extra gradient readouts, permitting statistical comparison across epochs. Intra-Acquisition Responses, signal changes observed in a slice that are induced by the beeps associated with the acquisition of slices earlier in the same volume acquisition, are assessed by comparing Acq 3 to Acq 4. Signal increases observed in auditory cortex are responses to the extra beeps associated with the extra gradient readouts (shaded portion of Acq 4). Inter-Acquisition Response differences are computed by comparing Acq 4 to Acq 6, with signal changes due to longer-term, integrative responses of auditory cortex to the extra beeps. For these experiments, 12 or 16 slice volumes were acquired. Between 4 and 20 extra gradient readouts were used in the even epochs to generate total beep train durations of 2–4 s (Table B.1).

Odd Epochs: Regular Volume Acquisition



Even Epochs: Extra Gradients + Volume Acquisition



interpretation of the data obtained in these experiments. The extra gradient readouts used in the even epochs to generate the extra beeps lacked excitation pulses, but otherwise presented gradient patterns and timing identical to those of the gradient readout sequence used to acquire the first slice of the imaged volume. Because these extra gradient readouts lacked slice excitation (i.e. no RF transmit), they did not affect the magnetization of the slices and resulted in steady-state imaging of the desired volume. All experiments also involved the use of at least one volume excitation and readout without data acquisition prior to the commencement of the paradigm. Through the use of these preceding excitations and readouts, steady-state magnetization was achieved in the imaging volume prior to the initial volume acquisition of the experiment. This eliminated the need to discard the initial volume acquisitions prior to data analysis.

B.3.2 Steady-State Imaging Conditions in Sledgehammer

Sledgehammer imaging of a DQA phantom produced consistent patterns of artifactual activation ($t > 2.68$) in the first seven to ten slices of a given volume when acquisitions from even epochs (extra gradient readouts) were compared to acquisitions from odd epochs (no extra gradient readouts). The most significant effects due to the presence of the extra gradient readouts were observed in the first slice, with the effect decaying thereafter. Beyond the tenth slice, the statistical maps ceased to have observable structure relating to the underlying physical structure of the phantom. No significant activation ($t > 2.68$) was observed when a t -test was used to compare volume acquisitions obtained under identical conditions (even or odd epochs) within a single experiment on a phantom. Statistical comparisons were made by randomly assigning each of the 24 images obtained under like conditions to one of two populations and then computing a t -statistic for each voxel in the images. The lack of activation implies that steady-state conditions exist within each epoch type, and indicates that the CVA sequence itself is free of any artifacts.

Signal variations due to the presence or absence of preceding gradient readouts coupled with the internal consistency of the CVA sequence imply that the acquisition of a given slice is dependent upon the history of the volume acquisition (i.e. the gradients are a time-varying system). As an example, let us consider the case of a 16 slice volume acquired with 8 extra gradient readouts in each even epoch. In this case, activation is observed in the first slice because the slice acquisition performed as the first gradient readout of a sequence acquires

information from a different volume than the same slice acquisition performed as the ninth element of a CVA sequence. Similarly, for the second slice, the second readout performed differs from the tenth, the third from the eleventh (slice 3), and so forth. Beyond the 7th–10th slice acquisition, steady-state conditions exist and artifacts cease to be observed (i.e. identically prescribed volumes acquired as the 11th and 19th readouts are equivalent under a t -test).

While there was some day-to-day fluctuation in the number of contaminated slices, this number was found to be independent of both the quantity of extra gradient readouts and the number of slices acquired in the volume. We therefore conclude that Sledgehammer data from slices prior to the 11th should not be used without confirmation of steady-state imaging conditions using a phantom. It is likely that the boundary condition for achievement of steady-state imaging will vary across machines and imaging coils. The issue of steady-state imaging conditions could be avoided by using an acoustic-only reproduction of the gradient readout beep, but this will not lead to measurement of the response to the full character of the beep, including reverberation and physical vibration.

B.3.3 Imaging Parameters

Data acquisition for all experiments described in this paper was performed on the 1.5 T system using asymmetric spin-echo (ASE) echo-planar imaging ($TR = 7$ s, $TE = 70$ ms, $\tau = -25$ ms, 128×64 collection matrix, 40 cm \times 20 cm FOV). Contiguous, (axial) oblique, 4 mm thick slices were obtained such that the central slices passed through the body of Heschl’s gyrus. The in-plane resolution for all studies described was 3.1 mm \times 3.1 mm. A surface receive coil positioned around the left ear was used to maximize signal from Heschl’s gyrus and the rest of the auditory cortex. The body coils of the magnet were used for transmit. Functional images were acquired with the coolant compressor turned off to eliminate the dominant, periodic component of the non-EPI background noise, producing a condition of quiet between clusters of beeps.

Peak noise levels generated in echo-planar imaging (EPI) at our facility range from 117 dB Sound Pressure Level (SPL) on a 1.5 T machine to 133 dB SPL on a 3.0 T imager [79]. These values are consistent with other reports [16]. Such noise levels are typically reduced through the use of passive attenuation measures such as earmuffs and earplugs. Our imaging coil is integrated into a passive attenuation system that reduces the level of the EPI noise

by 30 dB to 85–90 dB SPL [79].

B.3.4 Experiments

Seven volunteers (1 female, 6 male; ages 22–29) were imaged, after providing informed consent, using the Sledgehammer sequence in conditions of quiet. No stimuli were presented to the subject other than the beeps associated with the imaging process. 48 images were acquired of each slice in each experiment (24 images with and without extra beeps) using an epoch duration of three volume acquisitions (21 s). The functional location of auditory cortex in these slices was verified through one run of an On vs. Off paradigm in which instrumental music was presented binaurally to the subject (8 slices, TR = 4 s, CVA sequence).

All seven subjects were imaged using a 16 slice volume with 16 extra beeps in the even epochs (32 beeps vs. 16 beeps). Six subjects were imaged using a 16 slice volume with 8 extra beeps. Five of the volunteers were further imaged using a 12 slice volume preceded by 4, 12, and 20 extra beeps in the even epochs. The additional beeps were selected to compare the response to the imaging noise inherent in the volume acquisition (2 s for 16 slices; 1.5 s for 12 slices) to the response to the extended duration of imaging noise due to the extra beeps (2, 3 or 4 s). The actual durations of the trains of beeps were slightly different from these theoretical values, because the acquisition time for each slice was just less than 118 ms (see Table B.1 for the maximal beep train duration times for each experimental condition). Two subjects were imaged with the 16 slices and 8 extra beeps using TR = 6 s, but all other studies utilized a constant TR = 7 s to permit accurate comparisons of activation levels across imaging noise durations.

In all cases, a reverse-centric slice ordering was used in order to obtain the slices of greatest interest (primary auditory cortex and areas immediately surrounding Heschl’s gyrus) at the end of the acquisition so that they were free of imaging artifact. This ordering also permitted assessment of the effect of the maximal duration of the train of beeps.

B.3.5 Data Analysis

Prior to statistical analysis, the central eight slices of each baseline volume were motion corrected to the first image of the first run of the imaging session using SPM95 [28]. Images were spatially smoothed using a 3-point Hamming filter and drift corrected on an individual

# Slices in Volume	Extra Gradient Readouts	Beep Train Duration (s)	
		Imaged Volume plus Gradient Readouts	Imaged Volume
16	16	3.776	1.888
16	8	2.832	1.888
12	20	3.776	1.416
12	12	2.832	1.416
12	4	1.888	1.416

Table B.1: Duration of imager noise stimulus (beep train) generated by the Sledgehammer sequence

voxel basis using a minimum mean-square error fit.

A t -statistic was computed to compare all volume acquisitions in even epochs (extra beeps) to all volume acquisitions in odd epochs (no extra beeps). Voxels that achieved $t > 2.68$ (uncorrected significance level of $p < 0.01$) and were located on or in the vicinity of Heschl’s gyrus were defined as activated and included in a region of interest (ROI) for subsequent analysis. Separate ROIs were generated for each of the combinations of imaging volume size and extra beeps (e.g. 12 slices with 12 extra beeps). The ROIs generated for the runs using a given slice volume (12 or 16 slices) were combined to maximize the number of voxels analyzed.

The Intra-Acquisition Response was assessed through computation of mean percent signal changes within the composite ROIs. The last acquisition of each odd epoch (e.g. Acq 3 in Figure 2) was compared to the first acquisition of each even epoch (e.g. Acq 4) to examine the immediate effect of the increase in the number of beeps preceding the volume acquisition. Substantial signal changes between these consecutive acquisitions could only be due to the change in the acoustic environment preceding the later acquisition. Analysis involving comparisons of Acq 3 to later acquisitions in the even epoch (e.g. Acq 5 or Acq 6) run the risk of including Inter-Acquisition Responses induced by the first acquisitions within the even epoch. Comparisons involving earlier acquisitions from the odd epoch (e.g. Acq 1 or Acq 2) may not permit recovery of any undershoot resulting from the transition between an even epoch and the subsequent odd epoch.

The integrative Inter-Acquisition Response was analyzed by comparing the first acquisition in each even epoch (e.g. Acq 4) to the last acquisition in each even epoch (e.g.

Acq 6). In this case, signal changes would be due to an accumulation of the increased BOLD response to the longer duration train of beeps. A long TR value (7 s) was selected to maximize the likelihood of observing an Intra-Acquisition Response while minimizing the Inter-Acquisition Response and maintaining a tolerable experimental duration (5:36). It was assumed *a priori* that the Inter-Acquisition Response would be small.

B.4 Results

B.4.1 Noise-Induced Response Localization

Typical auditory cortex activation induced by the alternating duration of beep trains is shown for all seven subjects in Figure B-3. The responses depicted were observed when comparing the auditory cortex response to a 4 s burst of imaging noise (16 slice volume with 16 extra beeps) to the response to a 2 s burst of imaging noise (16 slice volume with no extra beeps). The activation maps were generated using all volume acquisitions (24 per condition). The most significant responses (uncorrected *t*-statistic) are located on the medial two-thirds of Heschl's gyrus, the location of primary auditory cortex [29].

B.4.2 Noise-Induced Response Strength

The percent signal changes observed for both the Intra- and Inter-Acquisition Responses resulting from the variation in beep train duration are listed in Table B.2. Statistically significant differences ($p < 0.05$, *t*-test) were found between the Intra-Acquisition Response to 4 s of beeps (32 beeps) and that observed for 2 and 3 s of beeps (16 and 24 beeps) for both the 12 and 16 slice imaging volumes. The responses to a given maximal duration of the beep train did not differ significantly with respect to the size of the imaging volume (12 or 16 slices). Therefore, the Intra-Acquisition Responses were pooled by the duration of the beep train during even epochs, resulting in statistically significant ($p < 0.05$, *t*-test) signal level differences between all three extended durations of imaging noise. The averaged data for the 12 and 16 slice volumes are shown in Figure B-4 along with the pooled data and associated ninety-five percent confidence intervals.

Inter-Acquisition Responses were not significantly affected by either the volume imaged (12 or 16 slices) or the number of extra beeps preceding the acquisitions (Table B.2). The resulting signal changes were essentially zero for all cases examined in this study.

Figure B-3: Sledgehammer results for seven subjects using odd epoch stimulation of 2 s (16 slice volume) and even epoch stimulation of 4 s (16 slice volume with 16 extra beeps). Statistical overlay (uncorrected t -test, $p < 0.01$ threshold) was computed using all volume acquisitions and represents the complete response (including both Intra- and Inter-Acquisition) to the extra beeps. Underlying T_1 -weighted images were acquired parallel to the Sylvian fissure, cutting through Heschl's gyrus. The strongest (statistical and percent signal change) responses were observed on the medial two-thirds of Heschl's gyrus, location of primary auditory cortex [29]. The white boxes encompass the approximate extent of auditory cortex.

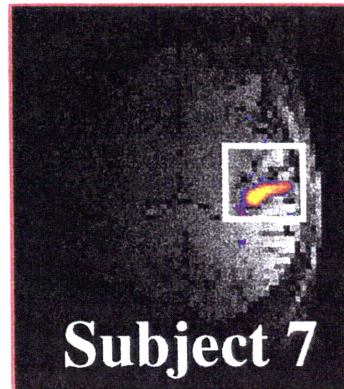
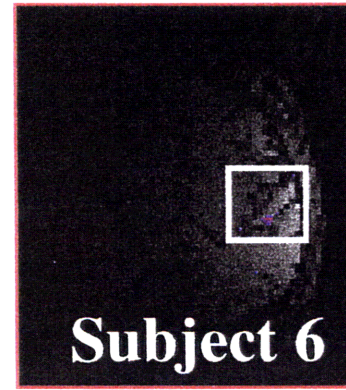
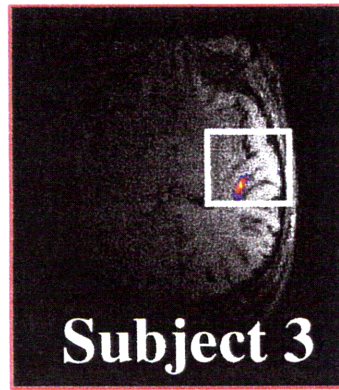
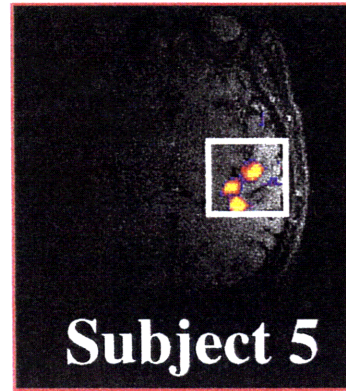
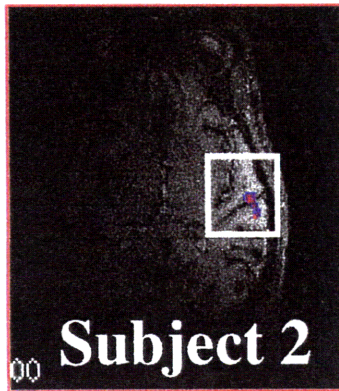
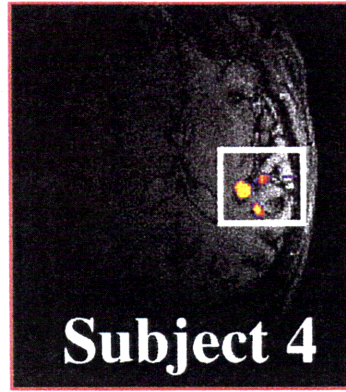
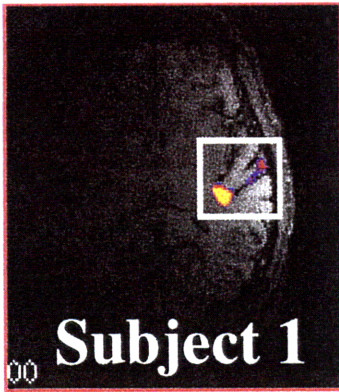
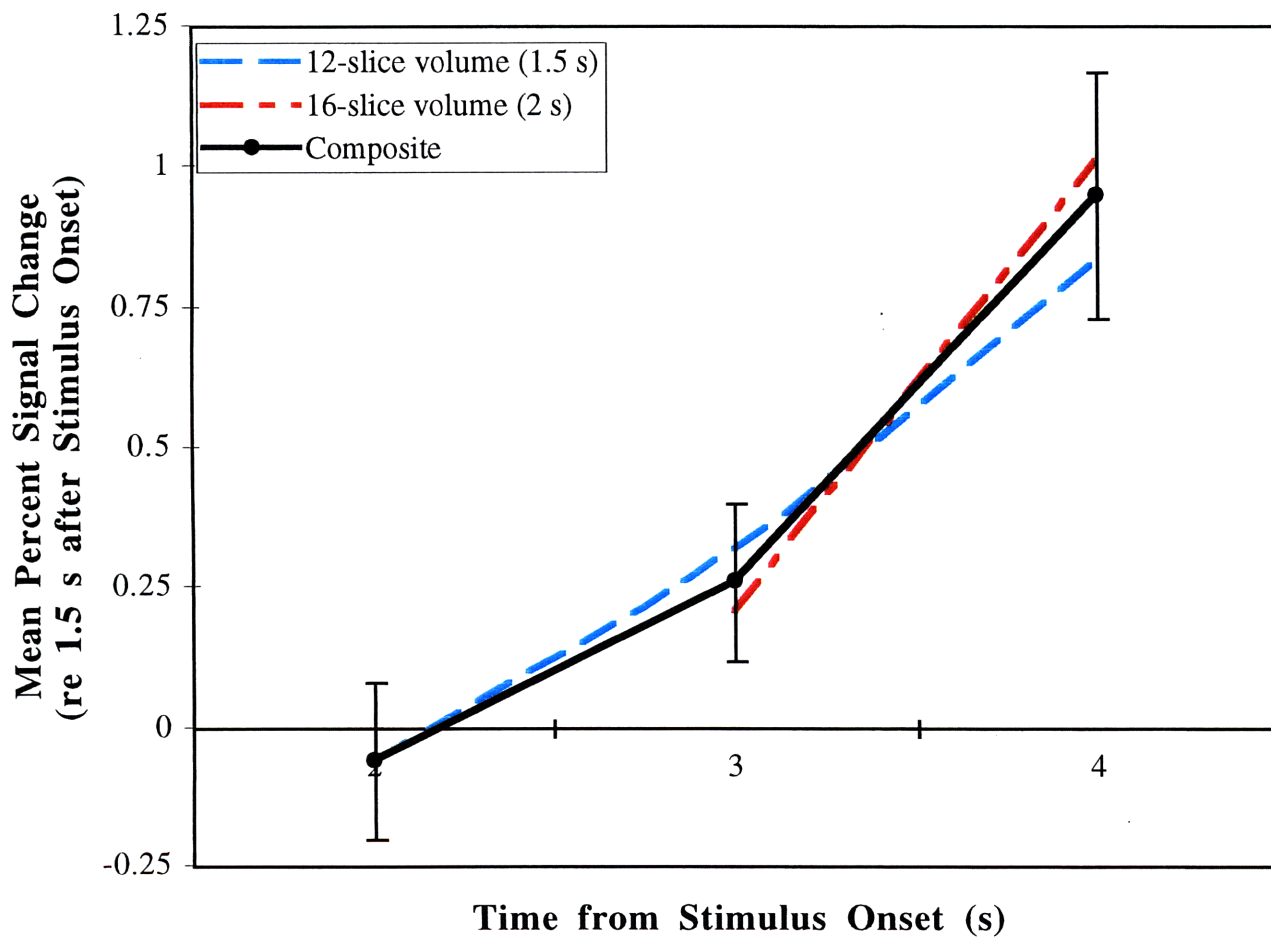


Figure B-4: Graph of Intra-Acquisition Response percent signal changes observed for 12 and 16 slice volumes as a function of the net duration of the beep train (slices plus extra beeps) in the activation condition of the Sledgehammer sequence. Composite values across identical beep train durations are also presented in the graph (solid line). The signal changes at 2, 3 and 4 s after stimulus onset are significantly different (t -statistic, $p < 0.05$) from each other. See Table B.2 for mean and standard error values for 12 and 16 slice volume data.



Subject	Average Percent Signal Change for Slices/Extra Gradient Readout Pairs									
	Intra-Acquisition Response					Inter-Acquisition Response				
	16/16	16/8	12/20	12/12	12/4	16/16	16/8	12/20	12/12	12/4
1	1.19	-0.26	—	—	—	-0.15	-0.73	—	—	—
2	1.11	0.36	—	—	—	0.04	-0.24	—	—	—
3	0.46	0.19	1.03	0.05	0.18	-0.01	0.07	-0.29	0.29	0.22
4	1.19	0.39	0.71	0.52	-0.19	-0.13	-0.31	0.10	-0.26	-0.13
5	0.87	0.04	0.83	0.51	0.02	0.13	-0.37	0.46	0.06	-0.42
6	1.83	—	0.62	0.64	-0.21	-0.37	—	0.10	0.01	0.21
7	0.56	0.55	0.95	0.23	-0.09	0.28	0.00	-0.08	-0.05	0.42
Mean	1.01	0.21	0.83	0.32	-0.06	-0.03	-0.26	0.06	0.01	0.06
S.E.	0.18	0.12	0.08	0.09	0.07	0.08	0.12	0.12	0.09	0.15

Table B.2: Average percent signal changes for Sledgehammer Sequence

B.5 Discussion

B.5.1 Response Characteristics

Maps of auditory cortex activation induced by the noise of echo-planar imaging suggest that the beeps accompanying prolonged acquisition of image data induce substantial amounts of activation in what is probably primary auditory cortex. While other regions of auditory cortex did not exhibit responses that achieved the $p < 0.01$ statistical significance level threshold of Figure B-3, it can not be concluded that secondary auditory cortex did not respond at all to the stimulus. Rather, any responses present were simply sub-threshold based upon our activation criteria.

It has been observed previously [8,44,86] that the onset of the BOLD response exhibits a 2 s delay after the onset of a stimulus. After this delayed onset, the BOLD response is found to peak after approximately 4–10 s [2, 8, 44]. The Intra-Acquisition Response (Figure B-4) induced in auditory cortex by the beep trains was consistent with this *a priori* knowledge. The induced response does not achieve a detectable level (with respect to the level after a 1.5 s duration beep train) until after 2 s of beeps have been presented to the subject. The response is detectable after 3 s (0.25%), but rises sharply to a substantial level (0.95%) by the time the beeps have been present for 4 s.

The lack of significant differences in the percent signal changes observed for the Inter-Acquisition Responses for all Sledgehammer imaging cases indicate that, at a TR of 7 seconds, the Intra-Acquisition Response is the dominant response, as was expected *a priori*.

B.5.2 Implications for Auditory fMRI

The strong dependence upon the duration of the train of beeps exhibited by the Intra-Acquisition Response demonstrates that, for experiments involving frequent slice or volume acquisitions, the activation in auditory cortex is likely to be affected by the noise of the imaging process. This interaction may extend beyond the obvious acoustic masking of the desired stimulus to a reduction either in dynamic range available for cortical BOLD response or in the sensitivity to the stimulus-induced response due to an elevated signal level in Off (baseline) experimental conditions.

The strength of the response after 4 s of beeps is approximately 20-30% of the typical 3-5% signal changes observed in visual cortex. This is potentially a significant reduction in the dynamic range available for a response to the stimulus. We have typically found auditory cortex signal changes, even to robust stimuli such as music or speech, to be smaller (e.g. 1–1.5% in Appendix A [23]) than those values observed in visual cortex. The smaller percent signal changes may be due to reduced dynamic range resulting from the beep-induced response, or the beep-induced response may simply make it more difficult to observe primary auditory cortical responses to auditory stimuli. It should be noted that the beep-induced response might not have saturated after 4 s, implying that longer trains of beeps could lead to greater reductions in dynamic range. This would have serious implications for imaging sequences in which slice acquisitions are distributed equally throughout the TR period (distributed volume acquisition, DVA), particularly when many slices are acquired with a short TR value (e.g. 16 slices with TR = 2 s).

It is important to note that the strength of the beep-induced activation observed in auditory cortex is likely to be dependent upon the effectiveness of passive attenuation measures and the actual sound levels generated by a given imager. These experiments were conducted with the EPI level reduced to approximately 90 dB SPL by earmuffs and foam rubber padding. The coolant compressor noise was removed from the background in an effort to increase the observed percent signal changes. Despite these experiment-specific variables, we would expect the trends apparent in these results to be representative of those obtained under typical imaging conditions.

B.5.3 Implications for Clustered Volume Acquisitions

It should be possible to use up to a 2 s beep train duration (16 slice imaging volume on our imager) for a clustered volume acquisition (CVA) to obtain imaging data that is free of Intra-Acquisition Response contamination. The signal change after 3 s of beeps is significantly different from that at 2 s and indicates that contamination by imager noise is more likely at this delay, though it will not be as detrimental as after 4 s of beeps. After 4 s of beeps images from other slice acquisitions will be significantly contaminated by beep-induced responses (Intra- and/or Inter-Acquisition Responses). The Intra-Acquisition Response curve suggests that the fMRI assessment of activation may be increasingly contaminated by the imager noise as the rate and duration of slice acquisition increases, until the BOLD response in auditory cortex saturates.

The results of these experiments may also be applied to support hypotheses and results of Edmister et al. [23] (Appendix A). The potential degradation due to contamination by the increasing rate of imager beeps with decreasing TR would support the hypothesis that variations in the music response maps observed for both CVA and DVA (distributed volume acquisition) were due to increasing contributions by the integrative (Inter-Acquisition) component of the cortical response. The lack of a significant Inter-Acquisition Response and the probable ability to obtain a 1 s duration volume acquisition (8 slices in this study) without inducing an Intra-Acquisition Response indicate that the CVA music data obtained using $TR = 8$ s was essentially free of noise-induced response contamination. Finally, the sharp rise in the Intra-Acquisition Response between 3 and 4 s (Figure B-4) may help to explain the peak in statistical power per unit imaging time for the CVA sequence at $TR = 3$ s. One hypothesis would be that responses induced by the two prior volume acquisitions (3 and 6 s previous for $TR = 3$ s; 4 and 8 s previous for $TR = 4$ s) are significantly lower for $TR = 3$ s than they are for $TR = 4$ s. Therefore, $TR = 3$ s preserves greater sensitivity to the stimulus-induced response by maintaining a lower steady-state signal level during periods when the stimulus is Off (baseline condition).

B.6 Conclusions

The Sledgehammer data provide quantitative evidence that responses to the beeps associated with the imaging process can interfere with responses to desired stimuli. The

beep-induced response partially saturates primary auditory cortex and thereby reduces the dynamic range available for a stimulus-induced response. We may further view this beep-induced response as leading to an increase in the “baseline” signal level to which a stimulus condition may be compared, reducing sensitivity to subsequent signal changes. Therefore, as postulated by Bandettini et al. [3], a control (Off) period that includes imager noise is quite different from a silent control period because the imager has such a strong stimulatory effect on auditory cortex.

The results obtained across various stimulation conditions indicate that the clustered volume acquisition (CVA) imaging sequence may be used for up to 2 s worth of data acquisition without inducing an Intra-Acquisition Response, as the onset delay of the BOLD response appears to be at least this long. The lack of an Intra-Acquisition Response for such a sizable volume provides strong support for the use of the CVA sequence over a distributed volume acquisition (DVA) sequence in which slices are acquired periodically throughout the TR. The CVA sequence is preferred because the DVA sequence will have contamination from both inter- and intra-acquisition sources when acquiring slices at rates greater than approximately one every two seconds. The Inter-Acquisition Response is easily reduced with the CVA sequence by extending the TR to at least 7 s, though the amount of contamination present at TR = 3 or 4 s may be acceptable for many experiments. There appears to be only a slight penalty in statistical power per unit time (On vs. Off paradigm) for the extended TR values [23] (Appendix A). Therefore, it has been demonstrated that CVA sequences may be used to obtain echo-planar fMRI data that are essentially free of acoustic noise contamination.

B.7 Acknowledgments

The authors thank Dr. Thomas J. Brady, Dr. Timothy G. Reese, Dr. Kenneth K. Kwong, Dr. Bertrand Delgutte, Dr. John Guinan and Dr. Jennifer R. Melcher for helpful discussions and Terrance Campbell, R.T. (Technical Manager, MGH-NMR Center) for his gracious assistance in providing time on the imager. We would also like to acknowledge the helpful comments of David B. FitzGerald, Michael P. Harms, Patrick L. Purdon and Marc A. Burock.

This work was partially funded by NIDA grant P01-DA09467-03, NIH grants P01-

DC00119 and T32-DC00038-04, and an NSF Graduate Fellowship in Electrical Engineering.

Bibliography

- [1] DM Aram and JA Eisele. Limits to a left hemisphere explanation for specific language impairment. *J Speech Hear Res*, 37:824–830, 1994.
- [2] PA Bandettini, A Jesmanowicz, EC Wong, and JS Hyde. Processing strategies for functional MRI of the human brain. *Magn Reson Med*, 30:161–173, 1993.
- [3] PA Bandettini, A Jesmanowicz, J Van Kylen, RM Birn, and JS Hyde. Functional MRI of imager acoustic noise induced brain activation. *Magn Reson Med*, 39:410–416, 1998.
- [4] RR Benson, WJ Logan, GR Cosgrove, AJ Cole, H Jiang, LL LeSuer, RR Buchbinder, BR Rosen, and VS Caviness Jr. Functional MRI localization of language in a 9-year-old child. *Can J Neurol Sci*, 23:213–219, 1996.
- [5] O Bertrand, F Perrin, and J Pernier. Evidence for a tonotopic organization of the auditory cortex observed with auditory evoked potentials. *Acta Otolaryngol Suppl (Stockh)*, 491:116–123, 1991.
- [6] JR Binder, JA Frost, TA Hammeke, RW Cox, SA Rao, and T Prieto. Human brain language areas identified by functional magnetic resonance imaging. *J Neurosci*, 17:353–362, 1997.
- [7] JR Binder, SM Rao, TA Hammeke, FZ Yetkin, A Jesmanowicz, PA Bandettini, EC Wong, LD Estkowski, MD Goldstein, VM Houghton, and JS Hyde. Functional magnetic resonance imaging of human auditory cortex. *Ann Neur*, 35:662–672, 1994.
- [8] RL Buckner, PA Bandettini, KM O’Craven, RL Savoy, SE Petersen, ME Raichle, and BR Rosen. Detection of cortical activation during averaged single trials of a cognitive task using functional magnetic resonance imaging. *Proc Natl Acad Sci USA*, 93:14878–14883, 1996.

- [9] RB Buxton, EC Wong, and LR Frank. Dynamics of blood flow and oxygenation changes during brain activation: the balloon model. *Magn Reson Med*, 39:855–864, 1998.
- [10] S Cansino, SJ Williamson, and D Karron. Tonotopic organization of human auditory association cortex. *Brain Res*, 663:38–50, 1994.
- [11] GG Celesia. Organization of auditory cortical areas in man. *Brain*, 99:403–414, 1976.
- [12] GG Celesia and F Puletti. Auditory cortical areas in man. *Neurology*, 19:211–220, 1969.
- [13] JC Clarey, P Barone, and TJ Imig. Functional organization of sound direction and sound pressure level in primary auditory cortex of the cat. *J Neurophys*, 72:2383–2405, 1994.
- [14] M Colombo, HR Rodman, and CG Gross. The effects of superior temporal cortex lesions on the processing and retention of auditory information in monkeys (*Cebus apella*). *J Neurosci*, 16:4501–4517, 1996.
- [15] HB Coslett, HR Brashear, and KM Heilman. Pure word deafness after bilateral primary auditory cortex infarcts. *Neurology*, 34:347–352, 1984.
- [16] SA Counter, A Olofsson, HF Grahn, and E Borg. MRI acoustic noise: sound pressure and frequency analysis. *J Magn Reson Imaging*, 7:606–611, 1997.
- [17] JL Cummings, DF Benson, MJ Walsh, and HL Levine. Left-to-right transfer of language dominance: a case study. *Neurology*, 29:1547–1550, 1979.
- [18] AM Dale and MI Sereno. Improved localization of cortical activity by combining EEG and MEG with MRI cortical surface reconstruction: A linear approach. *J Cog Neurosci*, 5:162–176, 1993.
- [19] AS David, PW Woodruff, R Howard, JD Mellers, M Brammer, E Bullmore, I Wright, C Andrew, and SC Williams. Auditory hallucinations inhibit exogenous activation of auditory association cortex. *Neuroreport*, 7:932–936, 1996.

- [20] TL Davis, KK Kwong, RM Weisskoff, and BR Rosen. Calibrated functional MRI: Mapping the dynamics of oxidative metabolism. *Proc Natl Acad Sci USA*, 95:1834–1839, 1998.
- [21] JE Desmond, JM Sum, AD Wagner, JB Demb, PK Shear, GH Glover, JD Gabrieli, and MJ Morrell. Functional MRI measurement of language lateralization in Wada-tested patients. *Brain*, 118:1411–1419, 1995.
- [22] IT Diamond and WD Neff. Ablation of temporal cortex and discrimination of auditory patterns. *J Neurophys*, 20:300–314, 1957.
- [23] WB Edmister, TM Talavage, PJ Ledden, and RM Weisskoff. Improved auditory cortex imaging using clustered volume acquisitions. *Hum Brain Map*, In press.
- [24] DJ Felleman and DC Van Essen. Distributed hierarchical processing in the primate cerebral cortex. *Cerebral Cortex*, 1:1–47, 1991.
- [25] DB FitzGerald, GR Cosgrove, S Ronner, H Jiang, BR Buchbinder, JW Belliveau, BR Rosen, and RR Benson. Location of language in the cortex: a comparison between functional MR imaging and electrocortical stimulation. *Am J Neuroradiol*, 18:1529–1539, 1997.
- [26] KA FitzPatrick and TJ Imig. Auditory cortico-cortical connections in the owl monkey. *J Comp Neur*, 192:589–610, 1980.
- [27] PT Fox, MA Mintun, ME Raichle, FM Miezin, JM Allman, and DC Van Essen. Mapping human visual cortex with positron emission tomography. *Nature*, 323:806–809, 1986.
- [28] KJ Friston, J Ashburner, CD Frith, JB Poline, JD Heather, and RSJ Frackowiak. Spatial registration and normalization of images. *Hum Brain Map*, 2:165–189, 1995.
- [29] A Galaburda and F Sanides. Cytoarchitectonic organization of the human auditory cortex. *J Comp Neur*, 190:597–610, 1980.
- [30] AM Galaburda and DN Pandya. The intrinsic architectonic and connectional organization of the superior temporal region of the rhesus monkey. *J Comp Neur*, 221:169–184, 1983.

- [31] HE Heffner and RS Heffner. Effect of unilateral and bilateral auditory cortex lesions on the discrimination of vocalizations by Japanese macaques. *J Neurophys*, 56:683–701, 1986.
- [32] HE Heffner and RS Heffner. Hearing loss in Japanese macaques following bilateral auditory cortex lesions. *J Neurophys*, 55:256–271, 1986.
- [33] HE Heffner and RS Heffner. Cortical deafness cannot account for the inability of Japanese macaques to discriminate species-specific vocalizations. *Brain Lang*, 36:275–285, 1989.
- [34] HE Heffner and RS Heffner. Effect of restricted cortical lesions on absolute thresholds and aphasia-like deficits in Japanese macaques. *Behav Neurosci*, 103:158–169, 1989.
- [35] HE Heffner and RS Heffner. Unilateral auditory cortex ablation in macaques results in contralateral hearing loss. *J Neurophys*, 62:789–801, 1989.
- [36] HE Heffner and RS Heffner. Effect of bilateral auditory cortex lesions on sound localization in Japanese macaques. *J Neurophys*, 64:915–931, 1990.
- [37] HE Heffner and RS Heffner. Effect of bilateral auditory cortical lesions on absolute thresholds in Japanese macaques. *J Neurophys*, 64:191–205, 1990.
- [38] BE Hoppel, RM Weisskoff, KR Thulborn, JB Moore, KK Kwong, and BR Rosen. Measurement of regional blood oxygenation and cerebral hemodynamics. *Magn Reson Med*, 30:715–723, 1993.
- [39] JJ Hutsler and MS Gazzaniga. Acetylcholinesterase staining in human auditory and language cortices: Regional variation of structural features. *Cerebral Cortex*, 6:260–270, 1996.
- [40] TJ Imig and RA Reale. Patterns of cortico-cortical connections related to tonotopic maps in cat auditory cortex. *J Comp Neur*, 192:293–332, 1980.
- [41] TJ Imig, MA Ruggero, LM Kitzes, E Javel, and JF Brugge. Organization of auditory cortex in the owl monkey (*Aotus trivirgatus*). *J Comp Neur*, 171:111–128, 1977.
- [42] WM Jenkins and MM Merzenich. Role of cat primary auditory cortex for sound-localization behavior. *J Neurophys*, 52:819–847, 1984.

- [43] H Kosaki, T Hashikawa, J He, and EG Jones. Tonotopic organization of auditory cortical fields delineated by parvalbumin immunoreactivity in macaque monkeys. *J Comp Neur*, 386:304–316, 1997.
- [44] KK Kwong, JW Belliveau, DA Chesler, IE Goldberg, RM Weisskoff, BP Poncelet, DN Kennedy, BE Hoppel, MS Cohen, R Turner, HM Cheng, TJ Brady, and BR Rosen. Dynamic magnetic resonance imaging of human brain activity during primary sensory stimulation. *Proc Natl Acad Sci USA*, 89:5675–5679, 1992.
- [45] JL Lauter, P Herscovitch, C Formby, and ME Raichle. Tonotopic organization in human auditory cortex revealed by positron emission tomography. *Hear Res*, 20:199–205, 1985.
- [46] L Leinonen, J Hyvärinen, and ARA Sovijärvi. Functional properties of neurons in the temporo-parietal association cortex of awake monkey. *Expr Brain Res*, 39:203–215, 1980.
- [47] C Liegeois-Chauvel, A Musolino, and P Chauvel. Localization of the primary auditory area in man. *Brain*, 114:139–153, 1991.
- [48] CL Ludlow, J Rosenberg, C Fair, D Buck, S Schesselman, and A Salazar. Brain lesions associated with nonfluent aphasia fifteen years following penetrating head injury. *Brain*, 109:55–80, 1986.
- [49] D Malonek, U Dirnagl, U Lindauer, K Yamada, I Kanno, and A Grinvald. Vascular imprints of neuronal activity: relationships between the dynamics of cortical blood flow, oxygenation, and volume changes following sensory stimulation. *Proc Natl Acad Sci USA*, 94:14826–14831, 1997.
- [50] D Malonek and A Grinvald. Interactions between electrical activity and cortical microcirculation revealed by imaging spectroscopy: implications for functional brain mapping. *Science*, 272:551–554, 1996.
- [51] JB Mandeville, JJA Marota, BE Kosofsky, JR Keltner, R Weissleder, BR Rosen, and RM Weisskoff. Dynamic functional imaging of relative cerebral blood volume during rat forepaw stimulation. *Magn Reson Med*, 39:615–624, 1998.

- [52] MM Merzenich and JF Brugge. Representation of the cochlear partition on the superior temporal plane of the macaque monkey. *Brain Res*, 50:275–296, 1973.
- [53] MM Merzenich, JH Kaas, and GL Roth. Auditory cortex in the grey squirrel: tonotopic organization and architectonic fields. *J Comp Neur*, 166:387–402, 1975.
- [54] MM Merzenich, PL Knight, and GL Roth. Representation of cochlea within primary auditory cortex in the cat. *J Neurophys*, 38:231–249, 1975.
- [55] M-M Mesulam and C Geula. Chemoarchitectonics of axonal and perikaryal acetylcholinesterase along information processing systems of the human cerebral cortex. *Brain Res Bull*, 33:137–153, 1994.
- [56] JC Middlebrooks and JD Pettigrew. Functional classes of neurons in primary auditory cortex of the cat distinguished by sensitivity to sound location. *J Neurosci*, 1:107–120, 1981.
- [57] A Morel, PE Garraghty, and JH Kaas. Tonotopic organization, architectonic fields, and connections of auditory cortex in macaque monkeys. *J Comp Neur*, 335:437–459, 1993.
- [58] A Morel and JH Kaas. Subdivisions and connections of auditory cortex in owl monkeys. *J Comp Neur*, 318:27–63, 1992.
- [59] WD Neff and JH Casseday. Effects of unilateral ablation of auditory cortex on monaural cat’s ability to localize sound. *J Neurophys*, 40:44–52, 1977.
- [60] WD Neff, JF Fisher, IT Diamond, and M Yela. Role of auditory cortex in discrimination requiring localization of sound in space. *J Neurophys*, 19:500–512, 1956.
- [61] S Ogawa, DW Tank, R Menon, JM Ellermann, SG Kim, H Merkle, and K Ugurbil. Intrinsic signal changes accompanying sensory stimulation: functional brain mapping using MRI. *Proc Nat Acad Sci USA*, 89:5951–5955, 1992.
- [62] G Ojemann, J Ojemann, E Lettich, and M Berger. Cortical language localization in left, dominant hemisphere. An electrical stimulation mapping investigation in 117 patients. *J Neurosurg*, 71:316–326, 1989.
- [63] GA Ojemann. Cortical organization of language. *J Neurosci*, 11:2281–2287, 1991.

- [64] DN Pandya. Anatomy of the auditory cortex. *Rev Neurol (Paris)*, 151:486–494, 1995.
- [65] C Pantev, O Bertrand, C Eulitz, C Verkindt, S Hampson, G Schuierer, and T Elbert. Specific tonotopic organizations of different areas of human auditory cortex revealed by simultaneous magnetic and electric recordings. *Electroenceph clin Neurophysiol*, 94:26–40, 1995.
- [66] C Pantev, C Eulitz, T Elbert, and M Hoke. The auditory evoked sustained field: origin and frequency dependence. *Electroenceph clin Neurophysiol*, 90:82–90, 1994.
- [67] C Pantev, M Hoke, K Lehnertz, B Lütkenhöner, G Anogianakis, and W Wittkowski. Tonotopic organization of the human auditory cortex revealed by transient auditory evoked magnetic fields. *Electroenceph clin Neurophysiol*, 69:160–170, 1988.
- [68] W Penfield and L Roberts. *Speech and Brain Mechanisms*. Princeton University Press, Princeton, NJ, 1959.
- [69] ME Phelps, DE Kuhl, and JC Mazziota. Metabolic mapping of the brain's response to visual stimulation: studies in humans. *Science*, 211:1445–1448, 1981.
- [70] DP Phillips and DRF Irvine. Responses of single neurons in physiologically defined primary auditory cortex (AI) of the cat: frequency tuning and responses to intensity. *J Neurophys*, 45:48–58, 1981.
- [71] DP Phillips and SS Orman. Responses of single neurons in posterior field of cat auditory cortex to tonal stimulation. *J Neurophys*, 51:147–163, 1984.
- [72] DP Phillips, SS Orman, AD Musicant, and GF Wilson. Neurons in the cat's primary auditory cortex distinguished by their responses to tones and wide-spectrum noise. *Hear Res*, 18:73–86, 1985.
- [73] DP Phillips, MN Semple, and LM Kitzes. Factors shaping the tone level sensitivity of single neurons in posterior field of cat auditory cortex. *J Neurophys*, 73:674–686, 1995.
- [74] J Prichard, D Rothman, E Novotny, O Petroff, T Kuwabara, M Avison, A Howseman, C Hanstock, and R Shulman. Lactate rise detected by 1h nmr in human visual cortex during physiologic stimulation. *Proc Natl Acad Sci USA*, 88:5829–5831, 1991.

- [75] RA Reale and TJ Imig. Tonotopic organization in auditory cortex of the cat. *J Comp Neur*, 192:265–291, 1980.
- [76] J Rademacher, Jr. VS Caviness, H Steinmetz, and AM Galaburda. Topographical variation of the human primary cortices: Implications for neuroimaging, brain mapping, and neurobiology. *Cerebral Cortex*, 3:313–329, 1993.
- [77] JP Rauschecker, B Tian, and M Hauser. Processing of complex sounds in the macaque nonprimary auditory cortex. *Science*, 268:111–114, 1995.
- [78] JP Rauschecker, B Tian, T Pons, and M Mishkin. Serial and parallel processing in rhesus monkey auditory cortex. *J Comp Neur*, 382:89–103, 1997.
- [79] ME Ravicz and JR Melcher. Reducing imager-generated acoustic noise at the ear during functional magnetic resonance imaging: Passive attenuation. In *Abstracts of the Twenty-First Midwinter Research Meeting, Association for Research in Otolaryngology*, page 208, 1998.
- [80] TG Reese, TL Davis, and RM Weisskoff. Automated shimming at 1.5 T using echo-planar image frequency maps. *J Magn Reson Imaging*, 5:739–745, 1995.
- [81] D Riva. Language deficits in a child with omolateral (left) temporo-basal and cerebellar lesions. *Neuropsychologia*, 36:71–75, 1998.
- [82] F Rivier and S Clarke. Cytochrome oxidase, acetylcholinesterase, and NADPH-diaphorase staining in human supratemporal and insular cortex: Evidence for multiple auditory areas. *Neuroimage*, 6:288–304, 1997.
- [83] D Robertson and DRF Irvine. Plasticity of frequency organization in auditory cortex of guinea pigs with partial unilateral deafness. *J Comp Neur*, 282:456–471, 1989.
- [84] GL Romani, SJ Williamson, and L Kaufman. Tonotopic organization of the human auditory cortex. *Science*, 216:1339–1340, 1982.
- [85] GL Romani, SJ Williamson, L Kaufman, and D Brenner. Characterization of the human auditory cortex by the neuromagnetic method. *Expr Brain Res*, 47:381–393, 1982.

- [86] RL Savoy, KM O'Craven, KK Kwong, and RM Weisskoff. Enhancing the effective temporal resolution of functional neuroimaging: Measuring fMRI responses to very brief (100 msec) visual stimuli using computer synchronized stimulus generation and signal averaging. In *Proceedings of the Society of Magnetic Resonance, Second Meeting*, page 667, 1994.
- [87] K Scheffler, D Bilecen, N Schmid, K Tschopp, and J Seelig. Auditory cortical responses in hearing subjects and unilateral deaf patients as detected by functional magnetic resonance imaging. *Cereb Cortex*, 8:156–163, 1998.
- [88] H Scheich, F Baumgart, B Gaschler, C Tempelmann, C Tegeler, D Stiller, and HJ Heinze. Masking of acoustic stimuli produces fMRI activation in a particular human auditory cortex field. In *Abstracts of the Twentieth Midwinter Research Meeting, Association for Research in Otolaryngology*, page 26, 1997.
- [89] MI Sereno, AM Dale, JB Repaas, KK Kwong, JW Belliveau, TJ Brady, BR Rosen, and RBH Tootell. Borders of multiple visual areas in humans revealed by functional magnetic resonance imaging. *Science*, 268:889–893, 1995.
- [90] NJ Shah, L Jäncke, M-L Grösse-Ruyken, S Posse, and H-W Müller-Gärtner. How does acoustic masking noise affect fmri of the auditory cortex during phonetic discrimination? In *Proceedings of the International Society for Magnetic Resonance in Medicine, Fifth Scientific Meeting and Exhibition*, page 360, 1997.
- [91] I Sigalovsky, RA Levine, JR Melcher, JJ Guinan, TM Talavage, ME Ravicz, BR Rosen, RR Benson, and BC Fullerton. Tinnitus studied using functional magnetic resonance imaging: development of methods. In *Abstracts of the Twenty-First Midwinter Research Meeting, Association for Research in Otolaryngology*, page 51, 1998.
- [92] ML Sutter and CE Schreiner. Physiology and topography of neurons with multi-peaked tuning curves in cat primary auditory cortex. *J Neurophys*, 65:1207–1226, 1991.
- [93] J Talairach and P Tournoux. *Co-planar Stereotaxic Atlas of the Human Brain*. Thieme Medical Publishers, Inc., New York, 1988.

- [94] TM Talavage, WB Edmister, PJ Ledden, and RM Weisskoff. Quantitative assessment of auditory cortex response induced by imager acoustic noise. *Hum Brain Map*, In press.
- [95] RBH Tootell, JB Reppas, AM Dale, RB Look, MI Sereno, R Malach, TJ Brady, and BR Rosen. Visual motion aftereffect in human cortical area MT revealed by functional magnetic resonance imaging. *Nature*, 375:139–141, 1995.
- [96] RBH Tootell, JB Reppas, KK Kwong, R Malach, RT Born, TJ Brady, BR Rosen, and JW Belliveau. Functional analysis of human MT and related visual cortical areas using magnetic resonance imaging. *J Neurosci*, 15:3215–3230, 1995.
- [97] C Verkindt, O Bertrand, F Perrin, J-F Echallier, and J Pernier. Tonotopic organization of the human auditory cortex: N100 topography and multiple dipole model analysis. *Electroenceph clin Neurophysiol*, 96:143–156, 1995.
- [98] CM Wessinger, MH Buonocore, CL Kussmaul, and GR Mangun. Tonotopy in human auditory cortex examined with functional magnetic resonance imaging. *Hum Brain Map*, 5:18–25, 1997.
- [99] JF Willot, LM Aitkin, and SL McFadden. Plasticity of auditory cortex associated with sensorineural hearing loss in adult C57BL/6J mice. *J Comp Neur*, 329:402–411, 1993.
- [100] PWR Woodruff, RR Benson, KK Kwong, RJ Howard, T Talavage, J Belliveau, and BR Rosen. Modulation of auditory and visual cortex by selective attention is modality-dependent. *Neuroreport*, 7:1909–1913, 1996.
- [101] T Yamamoto, T Uemura, and R Llinás. Tonotopic organization of human auditory cortex revealed by multi-channel SQUID system. *Acta Otolaryngol (Stockh)*, 112:201–204, 1992.